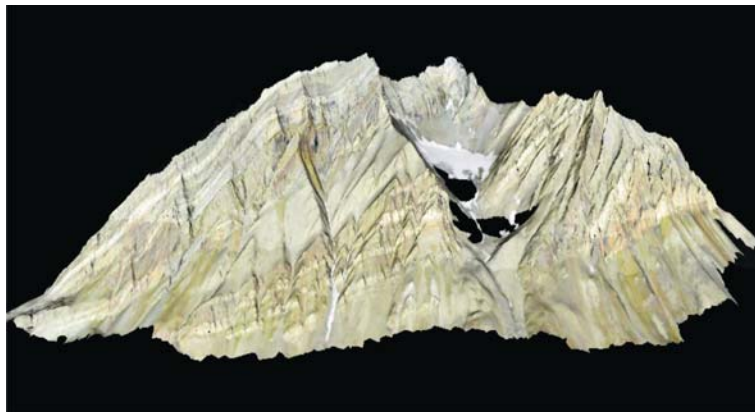




(GEO-3900)

MASTER'S THESIS IN
(STRUCTURAL GEOLOGY)

Fractured carbonates in the Mediumfjellet
thrust-stack in the Tertiary fold-and-thrust belt
of Spitsbergen



Tine Larsen

January, 2009

FACULTY OF SCIENCE
Department of Geology

University of Tromsø

(GEO-3900)
MASTER'S THESIS IN
(STRUCTURAL GEOLOGY)

Fractured carbonates in the Mediumfjellet
thrust-stack in the Tertiary fold-and-thrust belt
of Spitsbergen

Tine Larsen

January, 2009

Abstract

This thesis describes a study that was carried out in the Tertiary fold-and-thrust belt of Svalbard, in the mountain range of Mediumfjellet summer 2007 and 2008. The focuses were on: i) further describing the larger structures of the Mediumfjellet, ii) analyze the fracture distribution in the limestone beds associated with the major structures in the area. Available data sets are based on photo textured Lidar scan and extensive field observations.

The Mediumfjellet thrust stack is situated in the so-called central zone of the Spitsbergen fault-and-thrust belt. The mountain range displays three in-sequence thrusts (M1, M2, and M3) and one out-of-sequence thrust (G), with associated hanging wall anticlines. The anticlines are in general upright and tight, locally with overturned forelimbs, and characterized by thickening of the hinge zone and thinning of the forelimb. Lateral variations caused by oblique ramps, fault segment linkage, and lateral changes in the fold geometry and the fold plunge make the thrust system a complex deformation zone.

The fracture system has been divided into three populations, namely; i) Perpendicular fractures including conjugate shear fractures and extensional fractures, ii) conjugate hybrid shear fractures, and iii) thrust fractures. Based on the systematic relationships to the fold axis, the perpendicular and hybrid fractures, are interpreted as syn-folding fractures, whereas observations of folded thrust fractures support a pre-folding event. This study thereby suggests a 2 stage kinematic fracture model, where the pre-folding thrust fractures indicate a NW-SE to N-S contraction, and the syn-folding fractures reveal NW-SW to E-W contraction. Fractures that do not fit into this model are assumed to be a result of lateral local variations or reactivation of existing fractures. When comparing the fracture intensity to the fold domains, the highest intensity is situated in the hinge zone. This implies a fold mechanism with fixed hinge folding, most commonly ascribed to fault-propagation folding or transported fault-propagation folding.

Assuming good permeability for large throughgoing fractures and good porosity when there is a high intensity of short bed-terminating fractures, the study suggests a model with good fluid pathways in the forelimb near the major thrusts, and well developed short fractures in the major fold hinges, indicating the location of a possible reservoir.

Acknowledgement

I would like to thank everybody that has helped me to make this thesis coming to an end. First of all, I would direct major thanks, to my two supervisors Alvar Braathen and Steffen G. Bergh. Thank you for giving me all the fantastic possibilities to join exciting fieldwork, field courses abroad and conferences. I would to point out especially great feedback on the manus and a good attitude for correcting my bad English.

Further there are many that should be thanked. Dr. Simon Buckley is thanked for teaching me everything about Lidar scan and data processing, Professor Fridtjof P. Riis is for all the good ideas on the 3D model and possibilities in Petrel and Professor Atle Mørk for providing his knowledge about the Triassic shales. Others to be thanked are Nicky and Brit from Bellingham, USA, for correcting an early version of my first chapters, Rita Sande Rød and Eli-Anne Ersdal, for correcting later versions of my thesis and for the greatest psychological support. Nancy Schmidt is thanked for a great collaboration in field and super friendship, Pierre Mauries for good field and office company and Øyvind Jakobsen for great step-in, when the field assistant let me down. Otherwise, all students from the university of Tromsø and UNIS, students from the field course in USA, and everybody else helping out making my life easier. A last thanks goes to Fabrice Caline for answering all my weird questions, joining slack-line balancing, being very supportive and bringing in some fresh air and smiles into my life.

Thank you everyone!

Tine Larsen

Table of contents

CHAPTER 1 GENERAL INTRODUCTION AND GOAL OF WORK.....	1
1.1 PREFACE	1
1.2 INTRODUCTION.....	2
1.3 GEOGRAPHIC LOCATION AND LOCAL TOPOGRAPHY.....	3
1.4 GEOLOGICAL FRAMEWORK	4
1.4.1 <i>Regional geological setting</i>	5
1.5 PREVIOUS WORK	8
1.5.2 <i>Tertiary deformation and Spitsbergen fold-and-thrust belt</i>	8
1.5.3 <i>Mediumfjellet fold-and-thrust stack</i>	11
1.6 METHODS, ANALOGUE AND DIGITAL DATASETS, AND APPLIED SOFTWARE.....	13
1.6.1 <i>Fracture sampling</i>	13
1.6.2 <i>Fracture analysis</i>	13
1.6.3 <i>Lidar scan and 3D modelling</i>	14
1.7. STRUCTURAL NOMENCLATURE.....	16
1.7.1. <i>Introduction</i>	16
CHAPTER 2 THE NATURE OF FRACTURE DEVELOPMENT AND IN LIGHT OF FOLD-AND-THRUST BELTS	17
2.1 INTRODUCTION.....	17
2.2 FOLD AND THRUST GEOMETRY	17
2.2.1 <i>Thrust geometry</i>	17
2.2.2 <i>Thrust related folds</i>	18
2.2.3 <i>Thrust systems</i>	20
2.3 FRACTURE DEVELOPMENT.....	21
2.3.1 <i>Basic fracture types</i>	21
2.3.3 <i>Symmetrical fold and fracture relationship</i>	21
2.3.4 <i>Paleostress reconstruction</i>	25
2.3.5 <i>Fracture intensity</i>	25
2.3.6 <i>Additional fracture types</i>	26
CHAPTER 3 LITHOLOGY DESCRIPTION.....	27
3.1. INTRODUCTION.....	27
3.2 GIPSDALEN GROUP	28
3.2.1 <i>Gipshuken Formation</i>	29
3.3 TEMPELFJORDEN GROUP.....	29
3.3.1 <i>Kapp Starostin Formation</i>	30
3.4 SASSENDALEN GROUP.....	33
3.4.1 <i>Vardebukta-, Tvillingodden- and Bravaisberget Formation</i>	34
3.5 INTRUSIVES	34
3.6 THE STRATIGRAPHIC IMPORTANCE OF DEFORMATION	34
3.6.1 <i>Macro-scale structures</i>	34
3.6.2 <i>Fracturing</i>	35
3.7 SUMMARY AND INTERPRETATION.....	35
CHAPTER 4 STRUCTURAL DESCRIPTIONS.....	37
4.1. INTRODUCTION.....	37
4.2 DESCRIPTION OF FOLD-THRUST STRUCTURES IN DOMAINS AND SUBAREAS	39
4.2.1 <i>M1 fold-and-thrust domain</i>	39
4.2.2 <i>M2 fold-and-thrust domain</i>	39

4.2.3 M3 fold-and-thrust domain.....	45
4.2.4 Gavltinden fold-and-thrust domain	50
4.2.3 Summary of fold-and-thrust domains	53
4.3 DESCRIPTION OF FRACTURES IN DOMAINS AND SUBAREAS	59
4.3.1 Subarea M2-b.....	60
4.3.2 Subarea M2-c	63
4.3.3 Subarea M3-a.....	66
4.3.4 Subarea M3-b.....	66
4.3.5 Subarea M3-c	68
4.3.6 Subarea G-a.....	69
4.4 FRACTURE INTENSITY	70
4.4.1 Tentative interpretation	70
4.5 SUMMARY	76
CHAPTER 5 STRUCTURAL ANALYSIS AND DISCUSSION.....	81
5.1 INTRODUCTION.....	81
5.2 FOLD AND THRUST GEOMETRY	81
5.3 KINEMATICS AND CHRONOLOGY OF FRACTURES	84
5.3.1 Pre-folding fracturing (stage 1).....	85
5.3.2. Syn-folding fracturing (stage 2).....	88
5.3.3 Out-of-sequence fracturing (stage 3?).....	93
5.3.4 Non-systematic fractures	93
5.4 FOLD GROWTH LINKED TO FRACTURING.....	94
5.5 FOLD-AND-THRUST BELTS AND FRACTURE RESERVOIRS.....	97
CHAPTER 6 CONCLUSION AND FUTURE WORK	101
6.1. CONCLUSION.....	101
6.2. FUTURE WORK.....	102
REFERENCES.....	103
APPENDIX I	113
APPENDIX II.....	116

Chapter 1

General introduction and goal of work

1.1 Preface

Structural research has been numerous on Svalbard and the Spitsbergen fold-and thrust belt has been one of the areas where the studies have been concentrating on. However, the knowledge of this area is still limited. This study will contribute to this subject by looking into the fracture development. The thesis is built up by first introducing the study area and previous work in chapter 1. Only a limited overview from the geological periods and evolution are presented, because the focus should rather be on relevant stratigraphy and events for the thesis. Chapter 2 unravels relevant theory subjects to make the base and background for the following descriptions. Chapter 3 describes the stratigraphy of Mediumfjellet, made from own observations, whereas chapter 4 will give a detailed description of the area. First a general description the fold and thrust geometry, before getting more into the fracture distribution. The discussion in chapter 5 brings up current problems regarding the fracturing in a fold-and-thrust belt and comparison to other works. As a final, chapter 6 round the thesis of by presenting the conclusion. I would like to recommend important literature for the interested reader. Dalmann (1999) gives a good introduction to the stratigraphy in Svalbard, whereas Harland et al. (1997) present an overview of Svalbard's geology. Bergh et al. (1999) summarizes the Spitsbergen fold-and thrust belt, and Bergh and Andresen (1990) present earlier studies at the Mediumfjellet.

1.2 Introduction

The Spitsbergen archipelago reveals a nearly consistent section of rocks ranging from Precambrian to Tertiary age (Dalmann, 1999). During dextral movements of the Greenland margin, caused by the opening of the Arctic and Atlantic Ocean in Eocene, the western Spitsbergen underwent a transpressional event resulting in a thick- and thin-skinned Spitsbergen fold-and-thrust-belt (Bergh and Andresen, 1990; Bergh et al., 1997b). The study area is centrally located in the fold-and-thrust belt, to the Mediumfjellet mountain range (figure 1.1). It is a thrust stack situated in the thin-skinned part of the fold-and-thrust belt, comprising fault-bend-fold and fault propagation fold structures in Permo-Triassic strata (Bergh and Andresen, 1990; Bergh et al., 1997b).

Macroscopic folds are common structures in fold-and-thrust belts. Both from scientific and resource point of view, there is an incentive to develop an understanding of the relationship between folding, faulting and fracture distribution. Outcrop analogues can be used as a guide to understand the subsurface, which is explored through seismics and core drilling. Fractures are important permeable paths for fluid flow and the porosity of low-porosity protolith rock is highly depended on them. They can be studied easily in outcrops used as analogue models to understand their occurrence for gas and hydrocarbons, hydrothermal water and groundwater flow. The fracture development is dependent on the state of stress at any point of time, and the orientation of the structures. Similar the spacing and frequency is controlled by the properties of the deforming rock and bed thickness.

The study at Mediumfjellet has been carried out to describe and interpret the fracture geometry in the folded and thrust strata. Datasets are based on field measurements, airborne lidar scanning and aerial photographs. The aim was to evaluate the different fracture patterns along strike in the present thrust sheets, do comparison of the fractures between the different thrusts, and fracture intensity related to fold domains. The ultimate goal has been to develop 3D spatial fracture model. The Thesis is part of a larger project; "Mediumfjellet thrust stack in the Tertiary fold and thrust belt of Spitsbergen – developing an analogue petroleum model". The work has been undertaken as part of a collaborative project between the University of Tromsø and the University Centre in Svalbard which is lead by prof. Alvar Braathen (UNIS) and prof. Steffen G. Bergh (UiT).

1.3 Geographic location and local topography

Svalbard is the largest island of the Svalbard archipelago (figure 1.1), and is situated in the north-western, uplifted part of the Barents Shelf at 78°33'N, 14°6'Ø. The study area of this thesis is located on the north-western side of the Isfjorden within the Oscar II land about 50km from Longyearbyen (figure 1.1). Mediumfjellet is a mountain ridge, bounded by two major glaciers; Sveabreen in the NE and Wahlenbergbreen in the SW. The Yoldia bay of Isfjorden, bound the mountain to the SE. The total areal of the study area is about 5,5km², where the ridge is about 3km wide and 10km long. The landscape is alpine, with steep slopes and high peaks where the highest peak is about 855 m above sea level. The climate in Svalbard is dry and cold with no or little vegetation, provide excellent outcrop possibilities. However, the work in this study area requires glacier walks and climbs in steep mountainsides. And the accessibility may provide challenges with special equipment and logistics. The study area may be reached by helicopter or by boat.

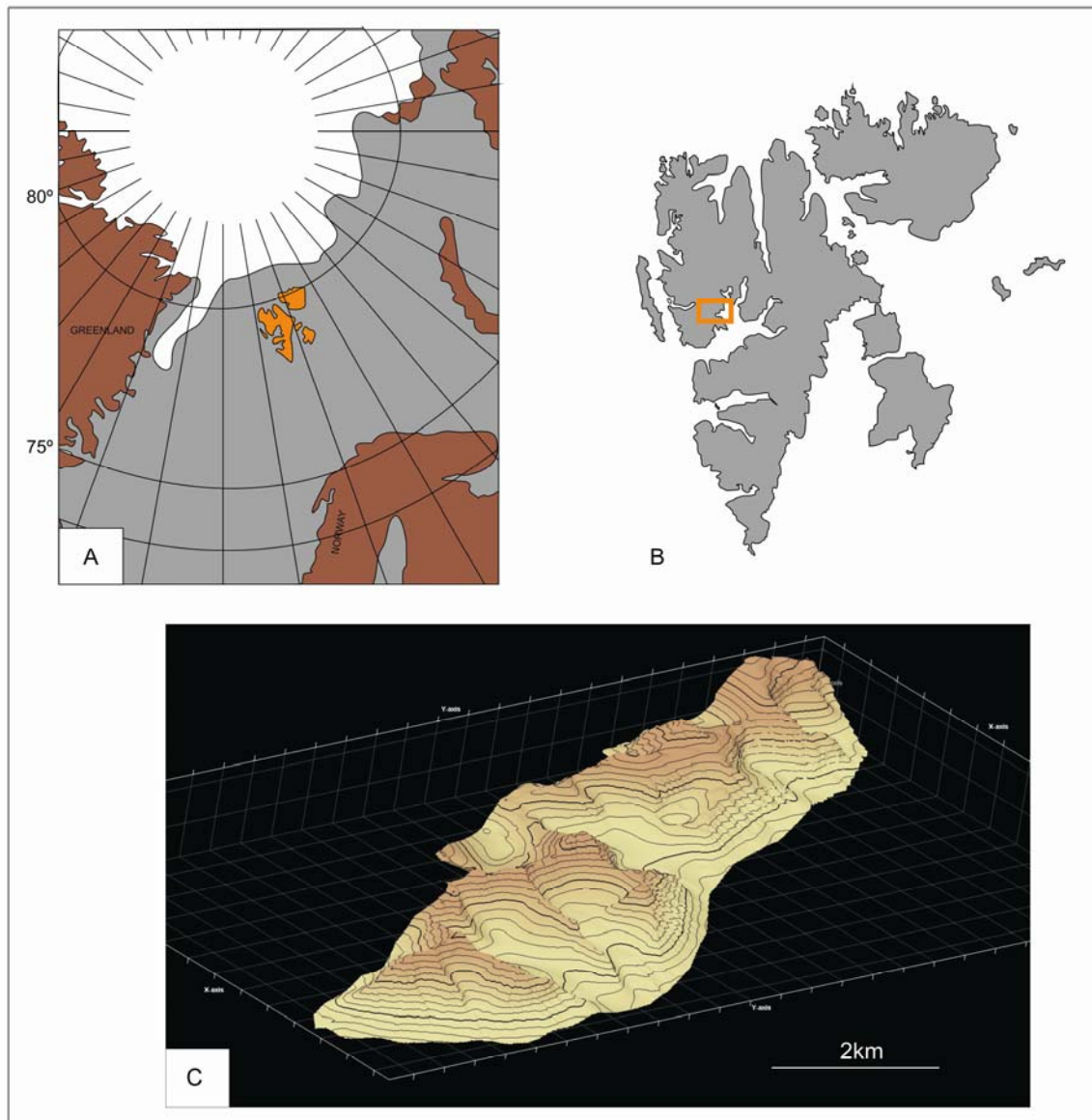


Figure 1.1: Geographical location and local topography. A) Geographical map placing the location of Svalbard. B) Svalbard map giving the location of the study area. C) DEM of Mediumfjellet showing the local topography. The lowest point in the model is at the sea level, whereas the highest point is 850meters above sea level. Note that the Y-axis marks the N-S line with the right side towards north.

1.4 Geological framework

Svalbard is situated at the north-western corner of the Barents shelf and is the elevated, but only a small part of the Barents shelf above sea level. The Barents shelf is a passive continental shelf, going from Norway and northwards to NW of Kongsfjorden. West of Svalbard, the shelf stops abruptly and changes into seafloor and active seafloor spreading (Dalmann, 1999). Rocks found at Svalbard may work as analogues to the stratigraphy on the Barents shelf, but can also be resulting from the local tectonics. Although the following

sections will concern the regional geological setting briefly, this study mainly focus the Tertiary deformation.

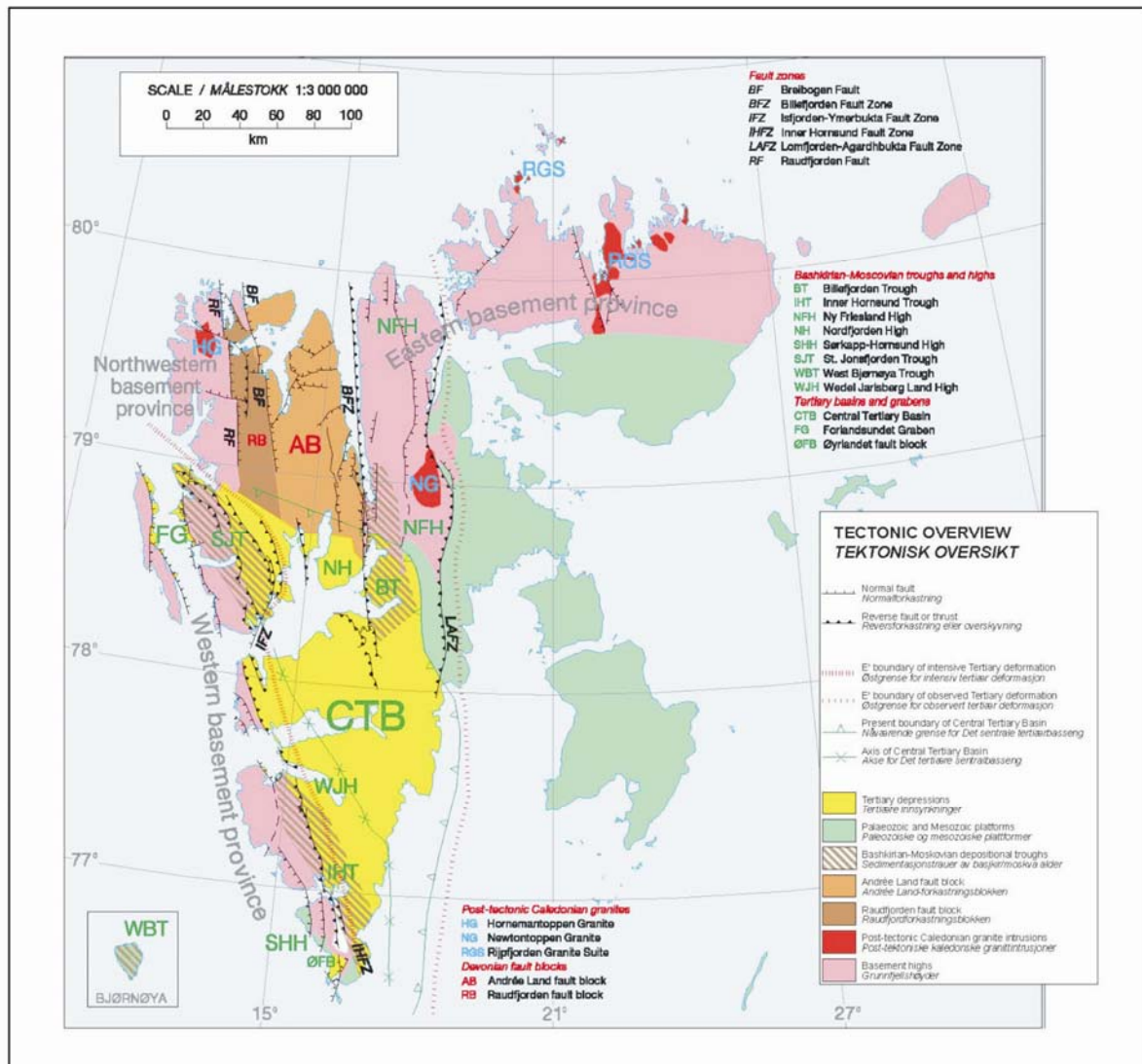


Figure 1.2: Tectonic map showing the structural zones of Svalbard. Note the Western basement province indicating the area for Tertiary deformation in Western Svalbard. (From Norwegian Polarinstitute)

1.4.1 Regional geological setting

Although the present study is concerned with the Tertiary deformation, a brief setting of the stratigraphy and the structural outline will be given (figure 1.2; figure 1.3). This is relevant because the structural elements and stratigraphy through time may have controlled the structural style of the study area during the deformation events.

Within the Svalbard Archipelago, there are several major NNW-SSE striking tectonic lineaments or fault zones (figure 1.2), that are assumed to have initially formed during the

Caledonian orogeny and later been re-activated during the Devonian/ Carboniferous and Tertiary tectonic events (Steel and Worsley, 1984). These fault zones probably had a major impact on the structural and sedimentological development of the region. For example in the Carboniferous they suffered extensional reactivation, while during the Early Cenozoic they experienced both compressional, extensional and strike-slip reactivation (McCann and Dalmann, 1995).

Cambro-Silurian basement rocks (or Hekla Hoek) are found in three separate provinces, the SW province, the NW province and the NE parts of the island. These rocks are low- to middle grade metamorphic and the metamorphism grade can be related to several orogenic events including the Baikalian (600-650 Ma), Grenvillian (950-100 Ma) and Caledonian (475-420 Ma) orogenies (Harland, 1997).

The Devonian rocks in Svalbard, were formed during an extensional phase, likely related to collapse of the Caledonian orogenic belt, producing several graben systems along the fault zones. The Devonian succession is extremely thick and has been measured to be as much as 8 km. These basins consist of red terrestrial alluvial conglomerate and fluvial delta sandstone deposits changing upwards to grey lacustrine shales and marine mudstones, reflecting a change from semi-arid to humid climate (Steel and Worsley, 1984; Worsley 1986; Harland, 1997). During the Svalbardian event (late- Devon), deformed the sediments by folding and thrusting, resulting in uplift and erosion (Worsley, 1986; Nøttvedt, 1993; Harland, 1997).

During the Carboniferous the region experienced first, a local compressional phase (Birkenmajer, 1981) followed by a late mid-Carboniferous rift basin development along the N-S trending lineaments (Steel and Worsley, 1984). Carboniferous basin infill sedimentary rocks are characterized by continental alluvial fan and floodplain sediments transforming into shallow marine evaporites, dolomite and limestones.

Permian to Cretaceous times was characterized by a stable marine platform conditions, outlined in the stratigraphy as several regressive and transgressive sequences of limestone, spiculite, shale and sandstone. These units were deposited on a shallow marine to deep marine platform. (Steel and Worsley, 1984) (See chapter 2 for detailed information about Permian and Triassic rocks). The top Cretaceous marks a major regressive event and is evidenced by a disconformity above slightly tilted substratum. This uplift of the Arctic Barents platform was Late- Cretaceous caused by initial opening of the Arctic Ocean (Gjelberg and Steel, 1995). The northern part of the Barents Sea has been uplifted about 3000 m (Harland, 1997).

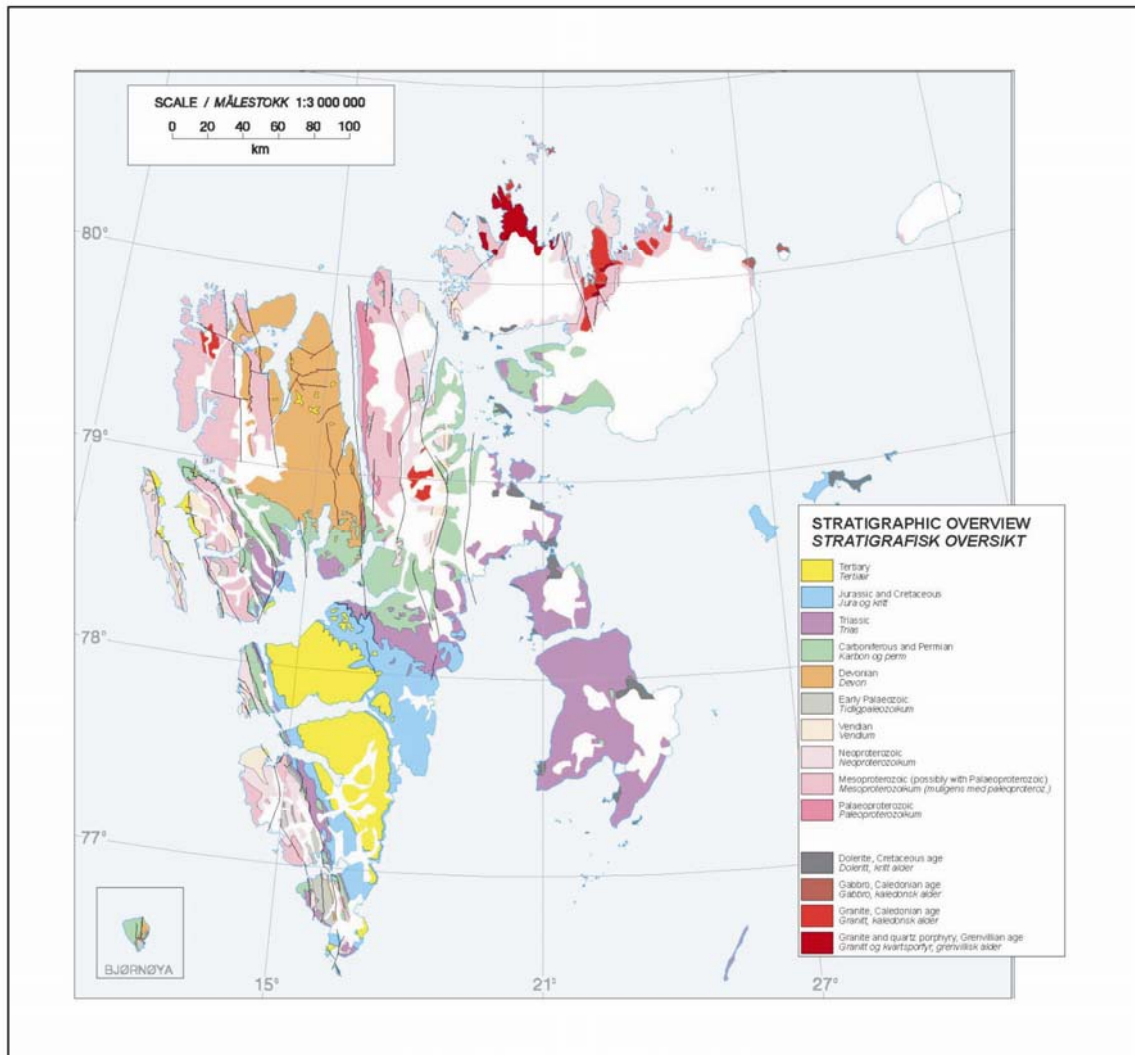


Figure 1.3: Stratigraphic map of Svalbard and Bjørnøya (from Norwegian Polarinstitute).

The opening of the North Atlantic and Arctic Ocean continued during the Tertiary as a result of dextral transform movements between Svalbard and Greenland. This created a complex pattern of structures including the Tertiary fold-and-thrust belt in regional zones across western and Central Spitsbergen, which includes zones of transpression and transtension (Harland 1969; Steel et al., 1985; Maher Jr. et al., 1997, Lowell 1972, Talwani and Eldholm, 1977). Sediments were shed into foreland basin as a result of the transpression-driven crustal thickening, leaving an 1800m thick (inferred 3500m thick) horizontal oriented package of clastic sediments.

1.5 Previous work

1.5.2 Tertiary deformation and Spitsbergen fold-and-thrust belt

The Tertiary fold-and-thrust belt, extend from NW of Kongsfjorden to the south of Sørkapp, however local compression can be traced to north of Bjørnøya (Faleide et al., 2008). As previously mentioned, the Tertiary deformation is assumed to have formed by an intra-continental dextral transformed movement between Greenland and Svalbard. The Eurasian plate and the North American plate started to drift apart and caused by a triple junction about a separate Greenland continent. This caused large shearing on both sides of Greenland (Talwani and Eldholm, 1977) and the opening of the Atlantic and Arctic Oceans (Harland, 1969). The shearing contributed a deformation area from Ellesmere Island, the north tip of Greenland and the western side of Spitsbergen. Accordingly, the time and matter of this event has been largely controversial (see Maher et al., 1991). Harland (1969) was the first to describe the Spitsbergen fold and thrust belt and suggested an early Tertiary deformation, however, authors has argued that the deformation took place during the late Cretaceous time (e.g. Lyberis and Manby, 1993). Harland (1969) described both elements of compression and extension and suggested a dextral transpression and transtension between Greenland and Svalbard, followed by later works (e.g. Lowell, 1972; Harland and Horsefield, 1974; Birkenmajer, 1975; Talwani and Eldholm, 1977; Myhre and Eldholm, 1982; Maher et al., 1995). Subsequently, later work has suggested numerous of models with several stages of deformation (e.g. Andresen et al., 1994; Bergh et al., 1997; Braathen and Bergh, 1995; Maher Jr et al., 1997, Braathen et al., 1997, Welborn and Maher, 1992, Maher and Welborn, 1992). Four distinct deformation zones can be distinguished (figure 1.4); a Hinterland zone of basement involved thrusting, a Western zone of thick-skinned folds and thrusts revealed in a major East-facing monocline, a Central zone of thin skinned folds and thrusts and an eastern foreland zone of horizontal strata, slightly deformed above decollements (Bergh et al., 1997; Braathen, 1999b). Recent work, suggests a five stage kinematic evolution of the fold-and-thrust belt province (figure 1.5) (Bergh et al., 1997; Maher Jr. et al., 1997; Braathen et al., 1997; Braathen et al., 1999b). An early transpressive event was characterized by a northwards compression which strongly folded the area of Brøggerhalvøya (stage 1) (Bergh et al. 2000). This became a zone of weakness for later fold-and-thrust belt evolution. The following major fold-and-thrust contractional event in Svalbard is recognized by WSW-ESE directed shortening (stage 2 and 3). This event was characterized by in-sequence thrusts formed in several decollement horizons towards the foreland,

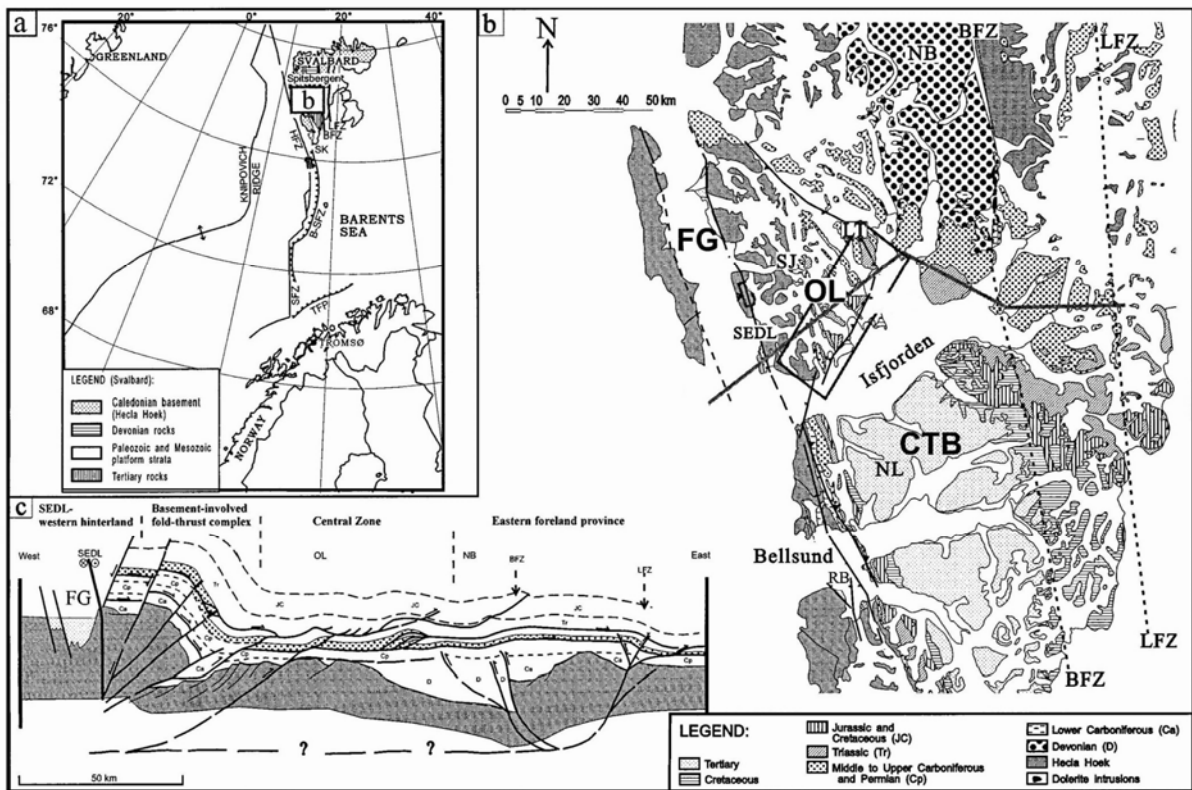


Figure 1.4: a) Regional location map of Svalbard and the Barents Sea. b) Stratigraphic map of Western, central Spitsbergen. c) Schematic cross-section through the western deformation province illustrating the four deformation zones (modified from Braathen et al., 1999). HFZ-Hornsund fault zone; BFZ - Billefjorden fault zone; CTB - Central Tertiary basin; LFZ - Lomfjorden fault zone; FG - Forlandsundet graben; RB - Renardodden basin; LT - Lappdalen thrust front; NB - Nordfjorden block; NL - Nordenskiöld land; OL - Oscar II land; SEDL - Svartfjella-Eidembukta-Daudmannsodden lineament; SJ - St. Jonsfjorden; SK - Sørkapp; B-SFZ - Bjørnøya-Sørkapp fault zone; SFZ - Senja fracture zone; TFP - Tromsø Finnmark platform.

consistent with imbrications and flat-ramp-flat migrating fault structures (Braathen et al., 1999b). This in-sequence contraction was followed by an event of out-of-sequence thrusts (stage 4), probably caused by a reactivation of, deeper seated thrust in the west. The last event (stage 5) was characterized by local extension and formation of normal faults, occurring in the uplifted western part, probably due to collapse or/and an overall transtensive setting in the west in Oligocene (Braathen and Bergh, 1995; Bergh et al., 1997; Maher Jr. et al., 1997). Based on the timing and distribution of the structures, a critical fold-and-thrust wedge taper model was suggested (Braathen et al., 1999a).

Oscar II land is located in the Western (thick skinned) and Central zone (thin skinned) (figure 1.4). Good exposures of the Permian- Mesozoic section, makes the area a key site of contractional Tertiary tectonic styles in Svalbard (Bergh et al., 1997). Bergh and Andresen (1990) subdivided Oscar II land into three deformation zones: 1) a western thick skinned fold-thrust complex dominated by basement involved steep thrusts that are partly rotated in a

major fold complex, 2) a central zone of thin skinned fold-and-thrust structures above a decollement in the Gipshuken Formation (chapter 3), and 3) an eastern zone characterized by a frontal duplex system with a floor thrust in Permian evaporates and a

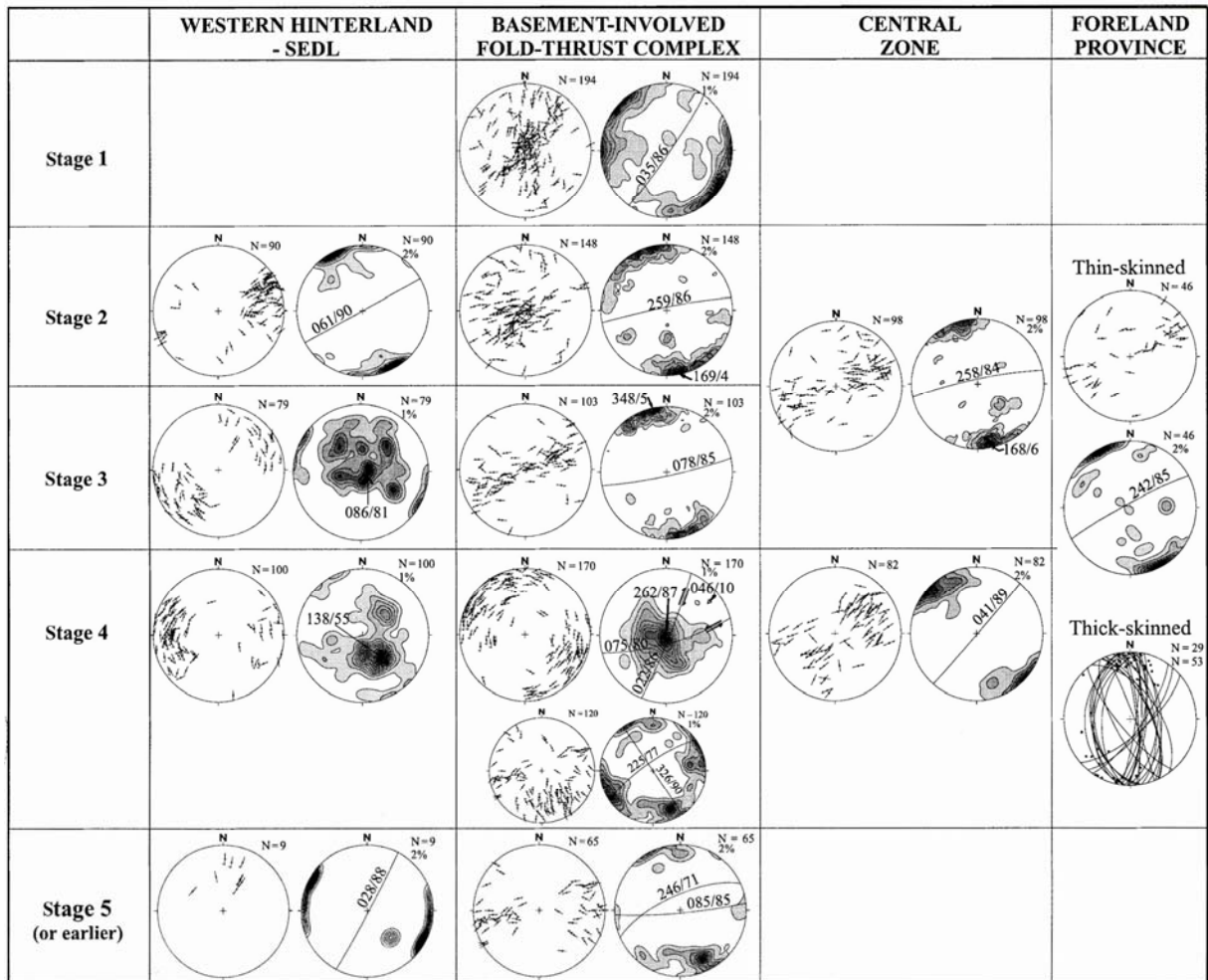


Figure 1.5: A summary diagram showing the five kinematic stages of deformation in the four deformation provinces in Spitsbergen fold and thrust belt. Note that only stage 2 and 3+4 are represented in the Central zone (Modified from Braathen et al., 1999).

roof thrust in Mesozoic shales. The so-called thrust front of the eastern zone is expected to be controlled by properties of the lithology and/or pre-existing faults, for example extensional faults, bounding Carboniferous basins below (Welbon and Maher, 1992). The stratigraphic step-up of the thrusts from a lower to higher decollement defines the boundary between the Central and Eastern structural zones. The kinematics is rather complex, including two transport directions (ENE and NNE), and thought to involve in-sequence and out-of-sequence thrust propagation (Braathen et al., 1999b; Wennberg et al., 1994). The folding and thrusting

of Oscar II land reveals a major thrust front with wider deformation zone than further south and north. The transition from low to high displacement is marked by the Isfjorden-Ymerbukta fault zone. Braathen et al. (1999) and Karlsen (2000), showed that the Isfjorden-Ymerbukta fault-zone is characterized by a complex strainpartitioning or decoupling of strain regarding a NE-SW shortening due to an oblique ramp, where the stress direction are rotated clockwise to E-W, near the fault zone (figure 1.6).

1.5.2 Mediumfjellet fold-and-thrust stack

Mediumfjellet is situated in the structural eastern zone (figure 1.6) of Oscar II land and is part of the Lappdalen-Mediumfjellet thrust front. Mediumfjellet reveals four major thrusts; M1, M2, M3 and G (figure 1.6) (Bergh and Andresen, 1990). The thrust M1 is recognized where steeply dipping Triassic strata in the forelimb of a hanging wall is thrust over flat lying Triassic strata below. This thrust is interpreted to be a hanging wall and footwall flat, which splay out from a second thrust, M2. The M2-thrust is located within the Permian gypsum (chapter 2) and terminates with a tip line in the center of the anticline as a. The third thrust M3, is the structural uppermost thrust at Mediumfjellet, is confined to the Permian Gipshuken Formation before it cuts steeply up-section through the Permian Kapp Starostin Formation in the footwall, before flattening out in the Triassic shales. Small thrust imbricates merge up from the thrust into the Kapp Starostin Formation. Strata in the hanging wall are folded in a huge fault-propagation anticline.

All these three major thrusts seem to define a flat-ramp fault propagating thrust system. The two major anticlines in the southern face of Mediumfjellet has previously been interpreted to be a fault propagation fold, which is changing into a major box/chevron-type, fault bend fold, further north. In particular, chevron and box-type folds characterize the central parts of the Mediumfjellet thrust stack. The displacement on thrust M3 is calculated from geometric re-constructions to be 700m at the southern side of Mediumfjellet, reducing to 200m some 3km further north. The fourth thrust, the Gravlinden thrust, G, is an out-of sequence thrust which is found 3km northwards along strike from Yoldia bay, but is covered by ice north of Gavltinden. The displacement on Gravlinden thrust is approximate 1km. It is interpreted to be developed later than M1, M2 and M3 as a new or reactivated; westerly seated thrust and not related to the others. G cuts with low angle through the underlying,

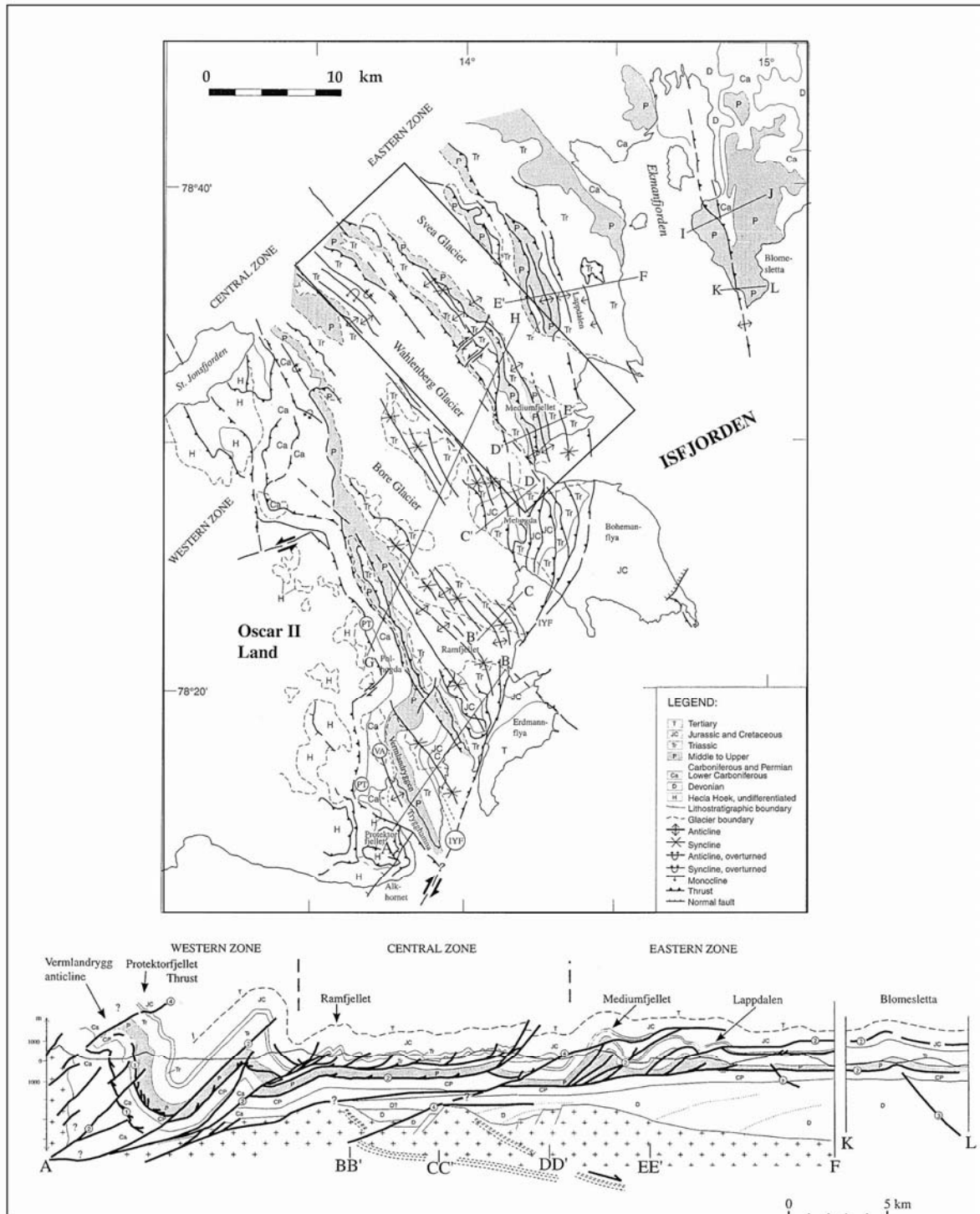


Figure 1.6: A structural map over Oscar II land, showing the location of Mediumfjellet, with Bohemansfløya to the south and Lappdalen to the north (Modified from Bergh et al., 1997). The cross-section underneath is marked as several lines at the map. Note that the location of Mediumfjellet is marked on the cross-section.

earlier formed fold-and-thrust systems, and locally cuts stratigraphically down section (Bergh and Andresen, 1990).

The Mediumfjellet-Lappdalen thrust front is proposed to have evolved in a two stage kinematic manner (figure 1.5) (Bergh and Andresen, 1990): i) Formation of a fold-and-thrust system, developing in an eastward, piggyback sequence with a characteristic ramp-flat geometry of thrusts producing fault propagation folds and fold bend folds (stage 2 or 3). ii) In a later stage of contraction, out-of-sequence reverse faults formed, overriding earlier folds and thrusts, by truncation of earlier structures, resulting in a hinterland dipping duplex (stage 4).

1.6 Methods, analogue and digital datasets, and applied software

1.6.1 Fracture sampling

Totally 1600 fracture orientations (right hand rule) were sampled in several stratigraphic layers of the Kapp Starostin Formation. The datasets covers several localities, both along and across strike, the latter also in different structural domains (e.g. forelimb, hinge etc.). The sites also cover domains of the three of thrusts; M1, M2 and G. Structural-element data collected records fracture orientation, spacing, fracture characteristics (e.g. hairline fracture, through going fracture, fracture fill, rugged or smooth fractures) and mode of deformation (opening or shearing). All data are measured and observed along bed linear scan-lines (1- 30 m) across bedding strike. Such observations were combined with recordings of bed thickness and bed orientation for each meter. Only beds with well developed fractures were chosen for measurement (see chapter 3).

1.6.2 Fracture analysis

Fractures were categorized into host beds, localities, structural domains, thrust domains, and high-angle versus low-angle orientation. The orientations were plotted as contoured poles to plain in stereo plots. Polar stereonet are used, with the lower hemisphere Schmidt net projection in a prototype stereo plot program developed at the Geology department of University of Tromsø. Fracture sets were determined recognizing common fracture orientations or attributes, in accordance with the main peaks in concentration of the contoured stereo plots. The fracture were then divided into population based on their occurrence; perpendicular-, conjugate- and thrust fractures. Additional, the non-systematic fractures are termed unknown fractures.

Low-angle-to-bedding fractures (thrusts) were picked out and restored. The back rotations were made by removing regional fold axis plunge and thereafter unfolding the bedding to horizontal. For the folds with plunge less than 10 degrees, plunge removal would not make much difference. In these cases, the fold plunges are therefore not taken into

account. The steep-angle-to-bedding conjugate fracture sets (later described as hybrid fractures), where observed and specially noted from field, and could therefore easily be recognized in the stereonet.

Fractures on the bedding surface were also interpreted from photos taken in field and Lidar scans. Photo-based interpretations were conducted where outcrops allowed it. It was also possible to measure orientations for big through going fracture sets in the Lidar scan. In combination, remote sensing (Lidar) of moderate resolution could be compared to the higher resolution dataset on measured fractures in the area

Fracture intensity where displayed in a diagram using the computer program Matlab. Number of fractures per meter scan-line where plot versus the bed thickness in order to find a linear trend. Also local example, where same bed and bed thickness was followed over the fold domains.

1.6.3 Lidar scan and 3D modelling

Laser scanning is a measuring apparatus sending out infrared light that measure the returning light bouncing back. This allows calculating the distance to the reflective surface. In this

Mediumfjellet	
Laser scan equipment	
Riegel LMS Q240i-60 airborne laser scanner	
Hasselblad with 35 mm lens H1 22hp camera	
iMar iIMU-FSAS inertial measurement unit	
Dual frequency GPS	
Dataset	
Measurement rate	10 kHz
Pointspacing	1.5m
Accuracy	0.1-0.15m
Number of datapoints used	c. 8/m
Number of triangles in top level	c. 16/m
Number of levels	9
Number of images	500
Size of area	7 km x 3km x 800m
Field of view (vertical)	90°

Table 1.1: Information table about the Lidar scan data sets from Mediumfjellet. Note the high accuracy.

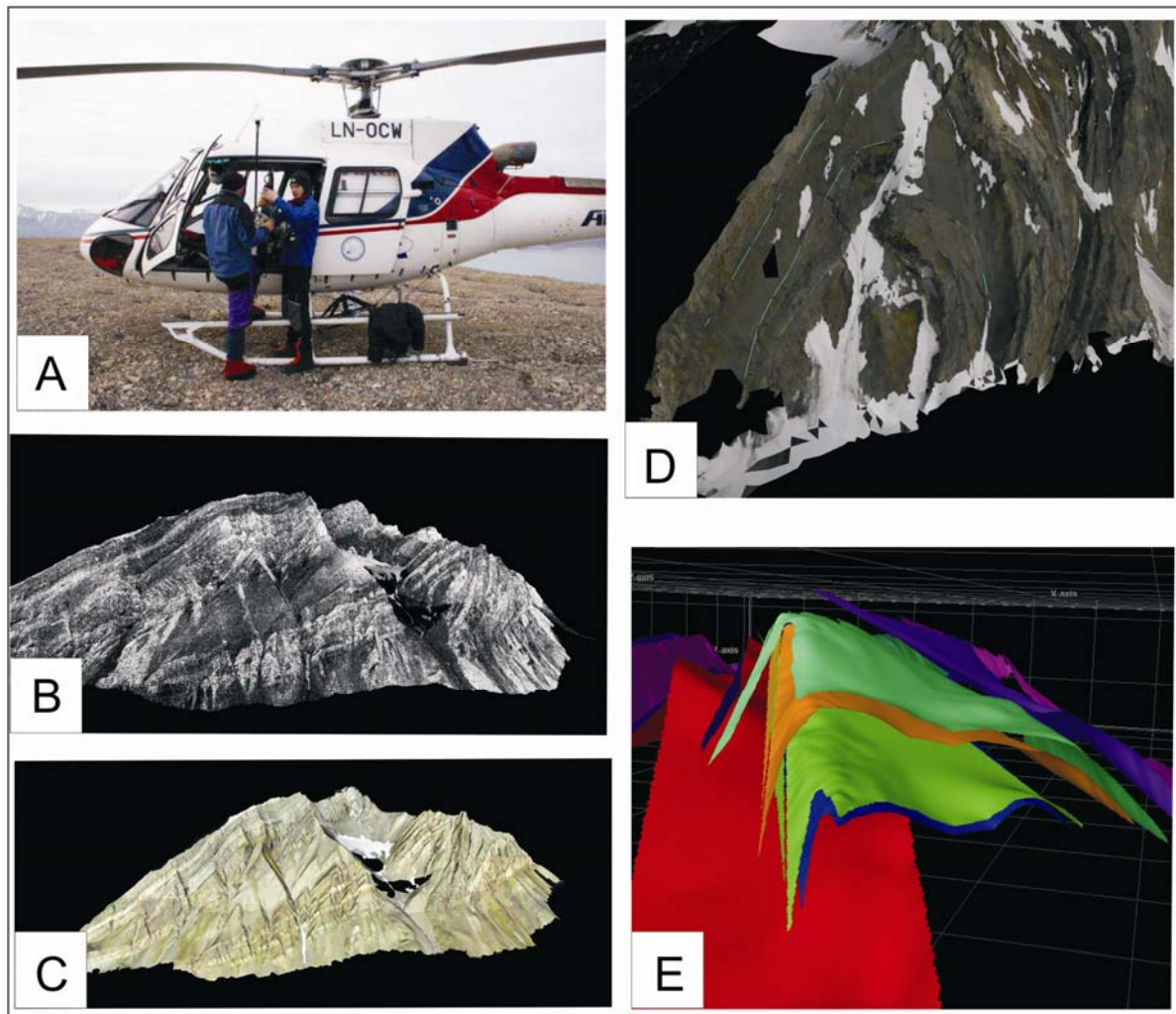


Figure 1.7: Figures illustrating the methods. A) Helicopter based oblique Lidar scan (Photo: Simon Buckley). B) Pointcloud. C) Photo textured DEM model.. D) Bed boundary interpretation in Riscan and Lime. E) Creating surfaces in Petrel.

study there we used a helicopter based Lidar-scanner. This scanner was used in parallel with a high resolution digital camera, inertial measurement unit and a Global position system. The Heliscan system (figure 1.7) (Skaloud et al., 2006), was mounted in a helicopter of type AS350B, which was used to carrying out the research in over eight hours flying time.

The scan-related images were taken parallel with the Lidar scan, overlapping with approximately 70%. During processing, they were draped on top of the laser-scanned DEM model. Riscan Pro was used for processing and partly geological interpretations, whereas the software LIME (Buckley et al., 2008) was used for interpretation, thereby outline coordinated data points along the top and bottom boundaries in three characteristic beds within the Kapp Starostin Formation and between the main formation boundaries (figure 1.7). The interpreted lines were again exported and imported into Petrel, where surfaces were applied between the

same bed boundaries. This resulted in a 3D model allowing us to study the fold-and-thrust geometry and the lateral variations along the actual beds. (figure 1.7). Petrel also allowed taking out cross-sections along strike. Three cross-sections were chosen and later put into ColorDraw for improvements. All the figures in this thesis are all made by the author, drawn in ColorDraw by hand.

1.7. Structural nomenclature

1.7.1. Introduction

This chapter will give a very short (in table format) introduction in to the terminology used to describe the structures in Mediumfjellet thrust stack. Relevant background theory will be described more detailed in chapter 2.

	Terms	Author
Fold description	<i>Interlimb angle</i>	Fleuty (1964)
	<i>Vergence</i>	Compton (1985)
	<i>Fold description</i>	Fossen and Gabrielsen (2005)
Thrust faults	<i>Thrust fault, blind thrust, flat, footwall flat, ramp, frontal ramp, hanging wall flat, lateral ramp, oblique ramp, sole thrust, splay, thrust vergence and tipline</i>	McClay (1992)
Fault related folding	<i>Detachment fold, fault propagation fold and fault-bend fold</i>	Jamison (1987)
	<i>Fault propagation fold</i>	Suppe (1985)
	<i>Fault-bend fold</i>	Suppe (1983)
	<i>Transported fault propagation fold</i>	McClay (1992)
Thrust systems	<i>Duplex, thrust system, imbricate thrust system, imbricate fan, in sequence thrusting, out-of-sequence thrusting and piggy-back thrust sequence</i>	McClay (1992)
	<i>Overstep thrust system</i>	Butler (1982)
Fold Mechanisms	<i>Migrating hinge; fixed limb Fixed hinge; rotating limb</i>	Storti and Talvini (2001)
Fracture geometry	<i>Geometry of fracture sets (a,b,c axis)</i>	Turner and Weiss (1963); Hancock

		(1985)
	<i>Throughgoing fractures,</i>	Gross and Eyal (2007)
Fracture mechanics	<i>Dilational fractures, shear fractures and hybrid fractures</i>	Hancock (1985)

Chapter 2

The nature of fracture development in light of fold-and-thrust belts

2.1 Introduction

This chapter is concerned with the background theory and previous work of the theory. The purpose of this chapter is to give a review of relevant literature in order to describe the sedimentological and structural elements (see chapter 3 and 4) and the discussion and structural analysis (chapter 5).

This chapter is structured the in a similar way as the discussion. Firstly, it will start to give an introduction to fold and thrust systems explaining the different thrust geometries and their related thrust systems and folds. Secondly, the chapter will explain the fracture mechanics at its relation to fold events. Eventually, the chapter will end with addition fracturing.

2.2 Fold and thrust geometry

2.2.1 Thrust geometry

Thin skinned fold-and-thrust systems are characterized by ramp-flat geometry, where the basal thrust run bedding parallel along a weak detachment horizon (flat), before cutting steeply up-section (ramp) and again may level out parallel to bedding in a higher weak horizon. The ramps can be frontal, oblique or lateral (figure 2.1) and are the basis for the geometry of thrust related folds (chapter 2.2.2). The oblique ramp has a characteristic rotation of the thrust sheet (Aptoria et al., 1992). Wilkerson et al. (2001) pointed out five evidences of an oblique ramp; i) Folds plunge steeply at the termination, ii) the cut-off line in the hanging wall trend at high angle to the fault, iii) the stratigraphic contact trend is at high angle to the fault iv) Stratigraphic separation diagram exhibit sudden changes near the terminations and v) the faults show change of orientation.

A fold and thrust system consist of several faults along strike and across strike (Ray, 2006). He showed that the thrust morphology is recognized by a flutelike pattern, with ached channels are separated by small ridges (figure 2.1). He pointed out that where the small ridges

or oblique ramps are located where the lateral thrusts link. These thrust patterns where accommodated by a curved thrust front, which also are supported by Marshak et al. (1992).

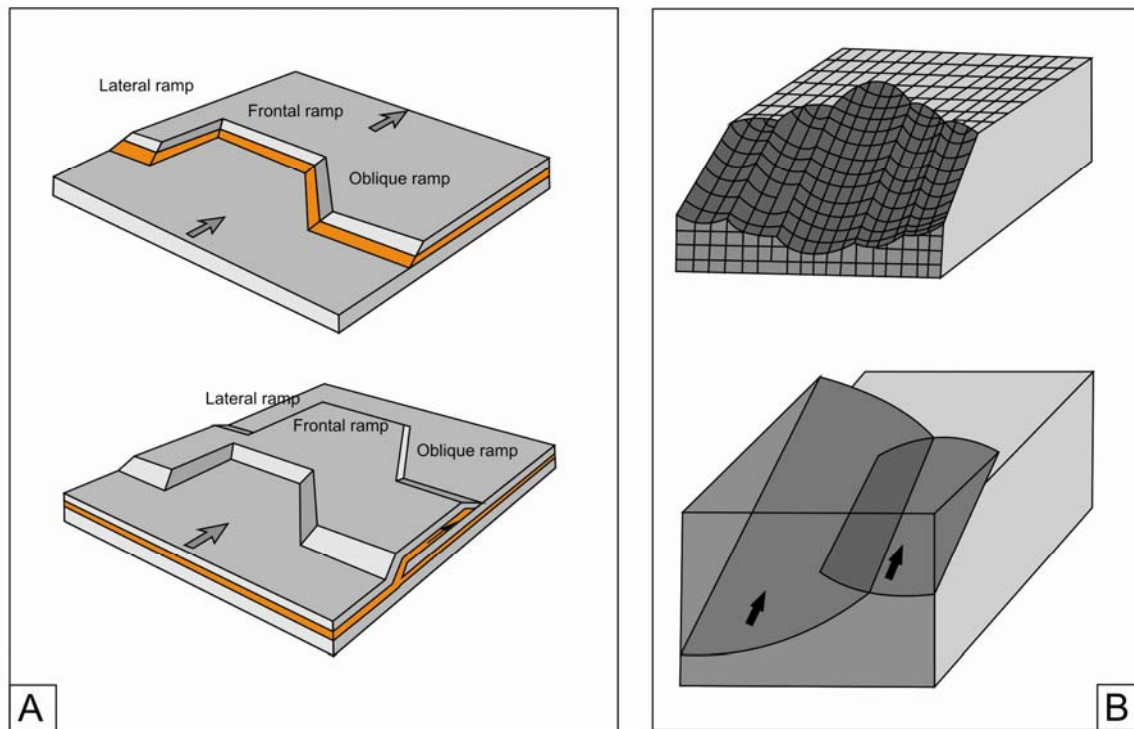


Figure 2.1 Thrust geometry. A: represents the a thrust sheet pushed over a lateral-, frontal- and oblique ramp (modified from McClay, 1992). B: (modified from Ray, 2006).

2.2.2 Thrust related folds

Three fault-fold interaction structures are typically associated with forced folding in thin skinned fold-and-thrust belts: Fault-bend fold, fault propagation fold and detachment folds (Jamison, 1987).

A detachment fold (figure 2.2) is a buckle fold of the hanging wall layers when a fault propagates along the bedding plane. This detachment horizon marks the lower termination of the fold and commonly consists of a weak and ductile layer. The weak strata usually deform and thicken into the hinge of the fold, while the folded, stronger layers above the horizon commonly remain their thickness (Shaw et al., 2005).

A fault propagation fold (figure 2.2) initiate as a detachment fault and forms in the end of the thrust. A fault propagation fold is usually associated with fixed hinge and rotating limb folding. Shearing usually occur, which result in thinned forelimb and thickened hinge zone. When the thrust tip propagates up a ramp into undeformed strata, the fold becomes a fault propagation fold. The slip is decreasing to zero at the tip and the displacement is transferred

into a fold. Cut of syncline commonly occur in the footwall (Suppe and Medwedeff, 1984). The fold geometry is highly depending on the fault angle. At high fault angles, the fold becomes open and upright where the fold-limbs become identical deformed and folded once and the hinge zone is undeformed. Forelimb is steeping and hinge zone is progressively becoming narrower as the fault propagates, the forelimb will then be more deformed than the backlimb. At low fault angles the fold becomes tight, overturned and thinned. The hinge will be bending twice or ever three times as the fault propagates and is expected to be highly deformed. The forelimb is anticipated to be more deformed than the backlimb and is commonly rotated and overturned (Salvini and Storti, 2001).

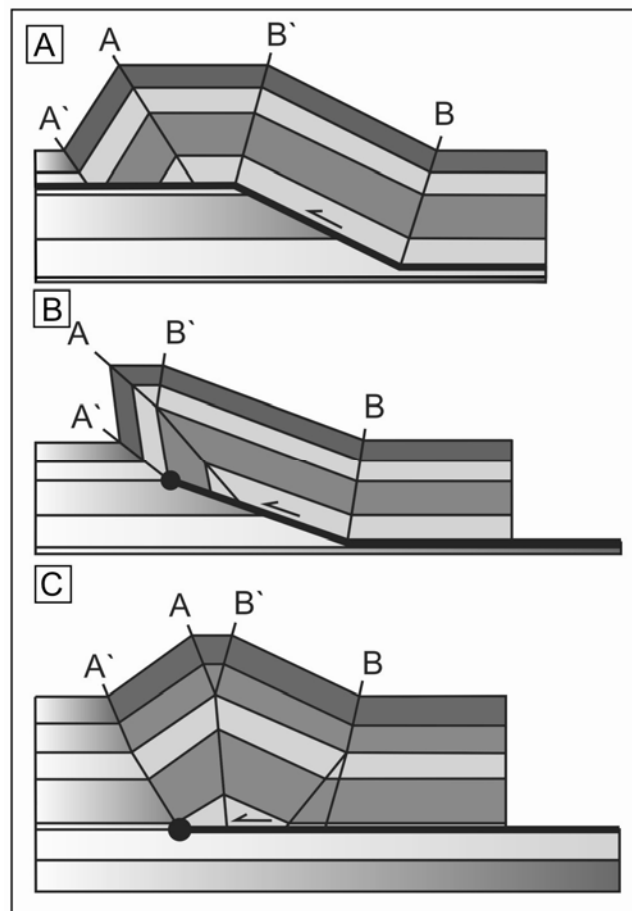


Figure 2.2: The three most common fault related folds associated with fold and thrust belt. A) Fault-bend fold, B) fault-propagation fold, and C) Detachment fold.

A fault-bend fold (figure 2.2) is a forced fold associated with hinge migration, fixed limbs and flexure-slip folding (Suppe, 1983). The fold develops when a thrust is ramping up from one decollement surface to another, and is characterized by two anticline and syncline pairs, one is migrating and one pinned in proportion to the footwall (Suppe 1983). Forelimb and Backlimb will develop at the initiation stage, both folded once. The width of these zones

will grow as the fold is moving up the ramp. When the backlimb reaches the top flat, a deformation zone of double folding will start to develop. The hinterland of the hinge will then be the area with the most expected deformation (Salvini & Storti, 2001). A fault-bend fold has large similarities to a transported fold-propagation fold, and may have developed as an end-member of a double-edged transported fold-propagation fold (Tavani & Storti, 2006). A transported fault-propagation fold is a mixture of a fault-bend fold and a transported fault-propagation fold (hybrid fold)

2.1.3 Thrust systems

A fold-and-thrust belt consists of several thrust systems. A thrust system is a zone of geometrically, kinematically and mechanically linked with closely related thrusts (McClay, 1992). The following section will therefore deal with only the relevant topics for Mediumfjellet (see McClay (1992) for more information).

The thrust system of the study area has earlier been interpreted to consist of two thrust-sequences (see previous work, chapter 1); in-sequence and out-of-sequence. In-sequence thrusting is a thrust sequence which has formed in a order in one direction, whereas out-of-sequence thrusting are not formed in this order, and commonly truncates earlier thrust systems (McClay, 1992). Accordingly, in-sequence thrust sequences may be forward breaking (piggyback sequence), propagating in front of the thrust sequence or back breaking, propagating in the back of a thrust sequence. An imbricate fan is a forward breaking sequence, which consists of an array with stacked thrust sheets developed as fault-propagation folds or fault-bend folds (see chapter 2.2.2), where previous formed thrust sheets have been lifted and rotated towards the hinterland and carried by lower and younger thrusts (Boyer and Elliott, 1982). When lifting the earlier formed thrust, it will bend the backlimb and tighten the syncline, compared to a single fault-propagation fold, this will cause more deformation to the backlimb (Boyer and Elliott, 1982).

2.3 Fracture development

2.3.1 Basic fracture types

Fractures are referred to as a general term for sub fracture types such as joint, fault, fault zone, deformation band, compaction band and stylolite. Three fundamental fracture modes explain the basic fracture mechanics (figure 2.3) (Kulander et al., 1979). Mode I are extensional fractures or joints. Joints develop perpendicular to the axis of least tectonic stress. They may extend from centimeters to hundreds of meters in scale confined to one bed or throughgoing

fractures in several mechanical interfaces. Stylolites and compaction bands are anti mode I fractures or stress corrosion anti cracks and forms perpendicular to the axis of most tectonic stress. Shear fractures also termed faults are formed by shearing, parallel to the fracture (mode II) or with rotation (mode III). Shear fractures are the result of strong internal shear in a rock body or reactivated joints under compressional stress conditions. Shear fractures has the same length as joints and develop, depending on the rock, with relatively constant low angle to the direction of highest tectonic stress (25-40°). They often develop in pairs as conjugate sets, commonly with an approximate angle of 60° between them. The three fracture modes may also appear alone or in any combination. Hybrid shear fractures are a mixed mode where shear fractures may develop caused by extension (figure 2.3).

2.3.3 Symmetrical fold and fracture relationship

Several researchers have established conceptual models where they linked symmetrical fracture geometry in a fold, to be closely related to the folding event in a homogenous state of stress (e.g. Price, 1966; Stearns, 1968; Hancock, 1985). Based on the laboratory experiment (see above) they could say something about the expected fractures when inferring a certain state of stress (e.g. Jaeger and Cook, 1979). Shear fracturing, dilatational fracturing and hybrid fracturing where all interpreted to be present in folded sedimentary strata (figure 2.4; Hancock, 1985). Price (1966), presented four fracture orientations which are the most common in a fold where extensional fractures occurs parallel and perpendicular to the fold axis and conjugate shear fractures are present with the acute bisecting angle perpendicular to the fold axis. However Stearns (1968) proposed a model of 11 typical fracture orientations (figure 2.3) which where represented by five different fracture sets, whereas each set included one extensional fracture and two conjugate shear fractures. He assumed that the sedimentary strata were folded in an elastic way. A neutral surface divided by compression (under) and extension (above), whereas the axis of least principal stress changes across the surface. This means for example that conjugate sets may change the direction of the bisecting acute angle whether it occurs above or beneath the neutral surface. Similar studies where done by Price and Crosgrove (1990), where they distinguished between an orthogonal fracture set with extensional fractures parallel and perpendicular to the fold axis, and a shear fractures with the acute bisecting angle both perpendicular and parallel to the fold axis aswell as parallel to the bedding (figure 2.4) . Hancock (1985) explained fractures which did not fit into the suggested model, to be formed prior or after the folding, which where supported by Price and Crosgrove (1990). Most of these classification diagrams where only regarding cylindrical folds, anyhow

some studies have also been taken more complex fold geometry into account. Some authors

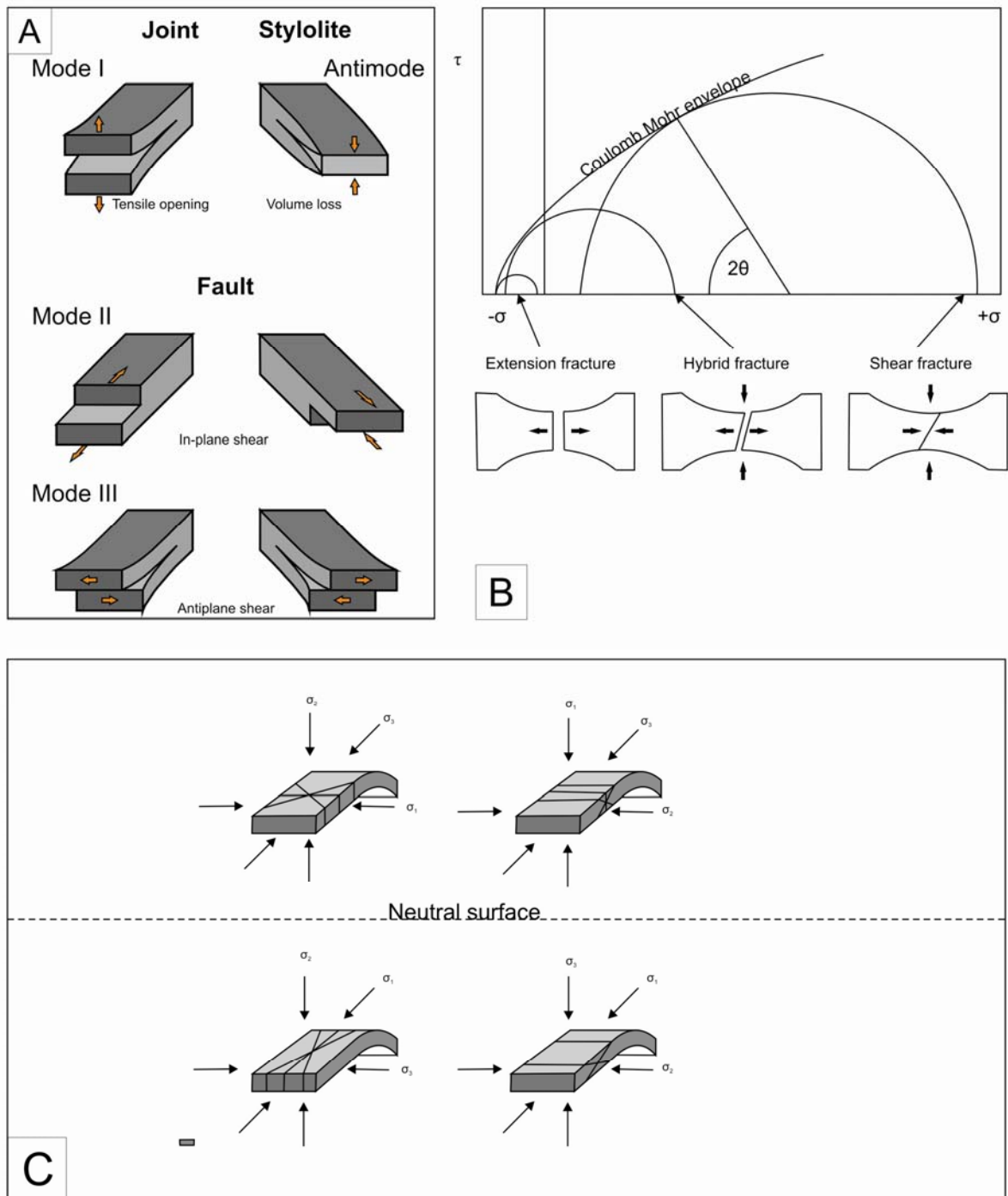


Figure 2.3 Figures showing the fundamental of fracturing. A) Fracture modes (modified from Lacazette, 2001). B) Mohr columb circles for extensional, hybrid and shear fractures (modified from Ramsey and Chester, 2004). C) Stearns (1968) eleven fracture orientations classified in five fracture sets, where the two upper models represent fracturing above a neutral surface and the two lower, beneath the neutral surface (modified from Bergbauer and Pollard, 2004).

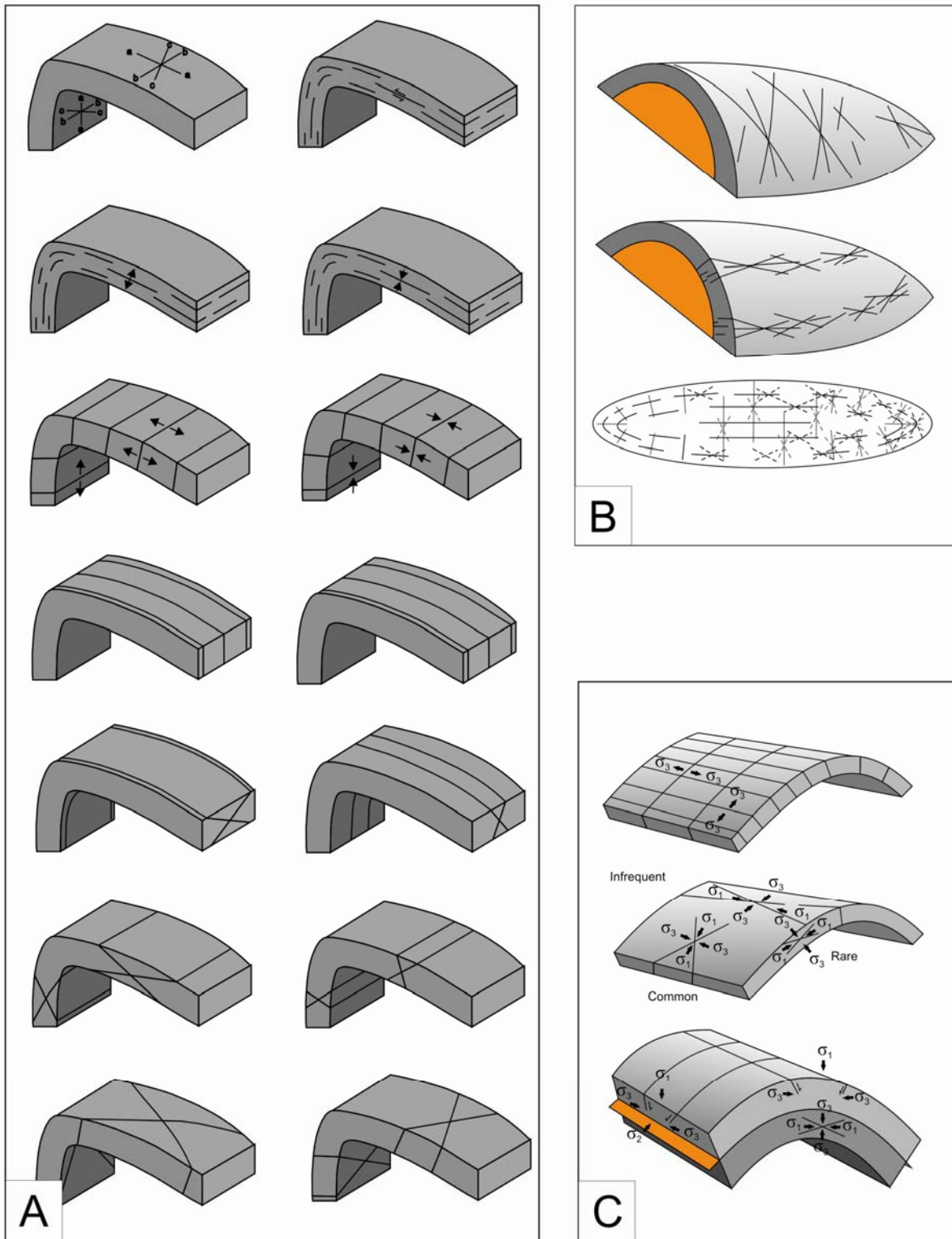


Figure 2.4 Fold related fracture classification schemes. A: represents the (modified from Hancock, 1985). B: (modified from Price and Crossgrove, 1990) C: (Stearns and Friedmann, 1972; modified from Cooper et al., 2006)

explained that when the direction of the fold axis or greatest curve changes, the fractures will be rotated thereafter (Stearns, 1968; Stearns and Friedman, 1972; figure 2.4). Also studies on

fold related fracturing do not consider the temporary fold evolution, how the initial folding differs from the main fold event on the fracturing. Bellhansen et al. (2006) looked at this problem and developed a 4D relationship between the fracturing and folding in the Sheep Mountain Anticline in Wyoming. He used the fracturing to determine the different stages of the fold event. Similar studies have later been established (e.g. Ahmadhadi, 2007; Mynatt and Pollard, 2008).

The fractures in this study, will be explained after Hancock's (1985) classification (Figure 2.4), which describes a model based on sedimentary layering and fold hinge geometry.

2.3.4 Paleostress reconstruction

Fractures can be used to reconstruct the stress regime from the time the fracture developed (Engelder and Geiser, 1980). Three different stress axes define the state of stress (σ_1 , σ_2 and σ_3). σ_1 defines the axis of maximum compressional stress, whereas σ_3 defines the axis of least stress (figure 2.3). Extensional fractures and shear fractures are both thought to be end members of brittle fracture types. However, Ramsey and Chester (2004) showed that there occur hybrid fractures, which develop as a transition from compression to extension (figure 2.3). Conjugate sets consist of two fractures with a crossing relationship. They consist of a blunt and an acute angle, where the acute bisecting angle is parallel with the largest principal stress direction and the blunt angle is parallel to the least principal stress. Shear fractures commonly consist of slip data. These slickenside data will show the direction of transport. Similarly, extensional fractures can also be used as a stress indicator. Extensional fractures will develop parallel with the greatest principal stress and perpendicular to the least principal stress (Stearns, 1968). Hybrid fractures are caused by extension where the acute angle develops perpendicular to the greatest principal stress, similar to extension fractures. Although, the method can be used in the same way, as for the shear fractures.

2.3.5 Fracture intensity

Fracture intensity is the number of fractures occurring per meters along the measured scan-line. Fracture spacing is the distance between each fracture. Spacing and connectivity is largely depending on 1) rock properties such as composition, grain size and porosity, (e.g. Stearns & Friedman 1972) 2) bed thickness (e.g. Huang and Angelier 1989) and 3) structural position (Hancock, 1985). Within the stratigraphic column there occur many mechanical interfaces. Fine grained and thick beds will have greater spacing and lower fracture frequency,

but will have clear paths for fluid flow. Coarse grained and thin beds will have small spacing and high frequency, which terminates against overlying beds and reduce the fluid flow (Cook et al., 2006). Studies have shown that the ratio of fracture spacing to bed thickness is about 1 (Price, 1966, Gross 1993). Horizons that behave ductile and deform internally will work as fracture counteract.

2.3.6 Additional fracture types

Natural hydro fractures develop when the pore pressure is exceeding the internal strength of the rock in the direction of least tectonic stress (mode I) (Engelder and Lacazette, 1990). The pore pressure will also weaken the rock in a compressive setting (mode II and III). When filling the pore space with water, the pressure on the grains will become larger. Pore pressure can build up in several ways; 1) Water expand more easily than the minerals around, when heated. 2) Compaction and weight from overlying sediments. 3) Impermeable layers can block the water to escape.

Silica fractures develop when biogenic silica compaction react thermo chemically from opal A to opal CT. This and happens at temperatures from 2-55°C. Also CaCO₃ increases the nucleation rate. The phase change reduces the volume and porosity at kilometer scale. These can ether lead to incidences of high subsidence, but also areas of intense fracturing (Davies, 2005).

Chapter 3

Lithology description

3.1. Introduction

This chapter gives a detailed description of the Mediumfjellet stratigraphy. Four main stratigraphic units are present in Mediumfjellet; (i) the Gipsdalen Group, ii) the Tempelfjorden Group, iii) the Sassendalen Group and iv) intrusions (figure 4.1). The following section will be structured after these four groups; however the main focus will be on the Tempelfjorden Group and Kapp Starostin Formation. Each group with the formations will be introduced before the lithology is described.

The descriptions are made after own observations and has been the foundation for the choice of characteristic beds which can be used laterally as structural marker horizons. A detailed description of the Kapp Starostin Formation is significant because the rock-properties highly influence the fracture development (see chapter 2 for more details).

The upper part of Gipshuken Formation is described shortly and represents the lowermost unit of the logged section. The Kapp Starostin formation represents the upper part and the rest of the logged section. The Kapp Starostin lithology description is based on 22 separate units (see appendix I for detailed unit descriptions). Eventually, the Vardebukta-, Tvillingodden- and Bravaisberget Formations are described shortly from field observations. Their occurrence of strongly tectonized and slopeforming properties made it hard to make a detailed lithology log description.

3.2 Gipsdalen group

The Gipsdalen Group is deposited between Serpukhovian to Artinskian age, overlaying the Billefjorden Group. To sum up the stratigraphy, the group consists of clastic graben sediments, marine shelf carbonates and evaporites in a total thickness up to 1800m (Dalmann, 1999). The group is divided into at least three subgroups, each of them representing local areas or graben systems; e.g. the Dicksonland Subgroup Treskelen Subgroup and Cambellryggen Subgroup. These subgroups are regional overlaid by Wordiekammen Formation and Gipshuken Formation. Gipshuken Formation is the only formation which is represented at Mediumfjellet and exhibit the lowermost part of the logged section (figure 3.1).

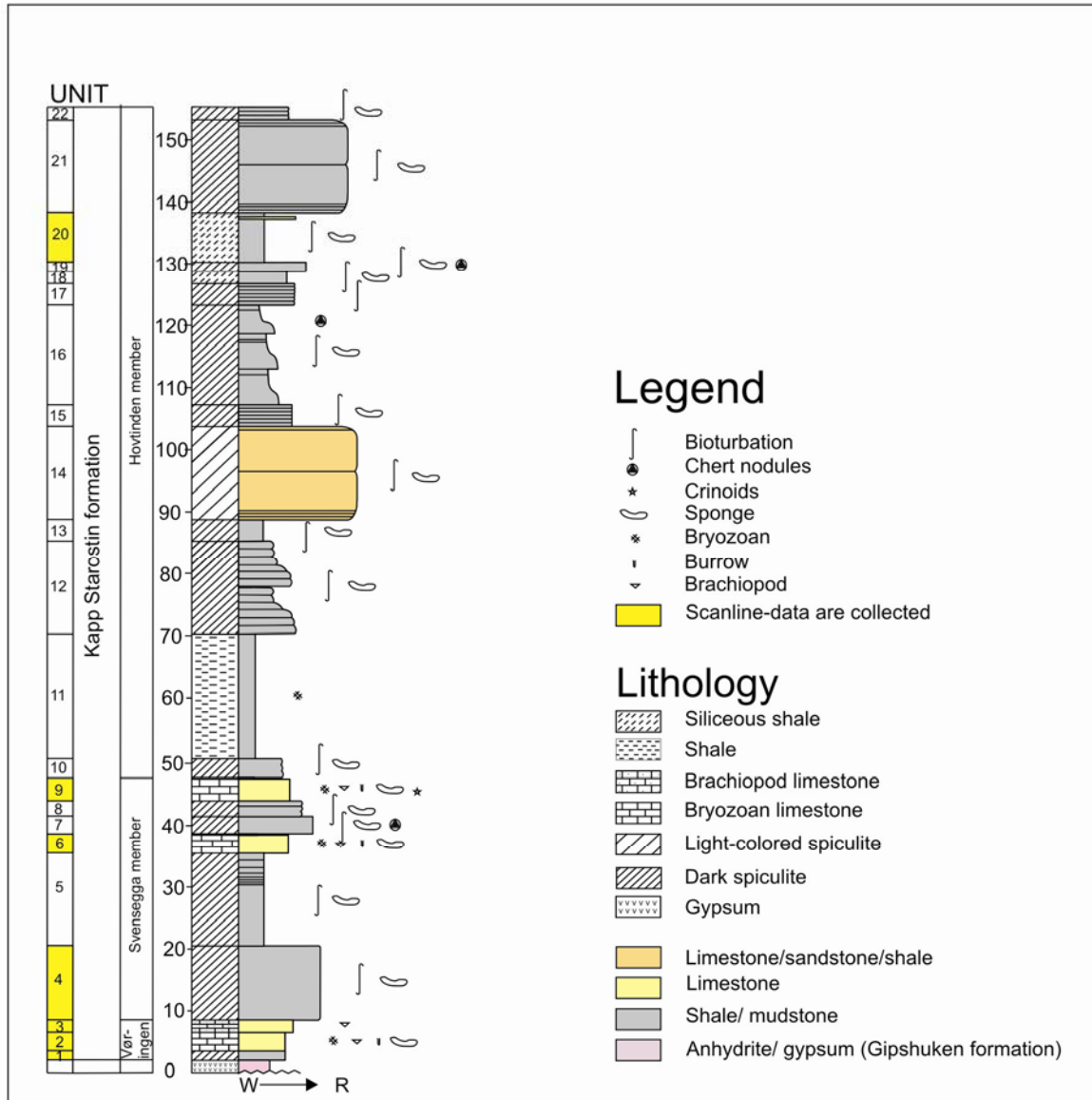


Figure 3.1: Stratigraphic log of Gipshuken Formation and Kapp Starostin Formation. The log also displays the fracture studied strata, marked with yellow. Note that the log is not scaled after grain sizes, but after mechanical properties. W: weak, R: rigid.

3.2.1 Gipshuken Formation

The Gipshuken Formation was first described by Nathorst (1910) and Cutbill and Challinor (1965). The type section is located in Dickson land and measured to be approximately 280m thick (Dalmann, 1999).

The Gipshuken Formation is subdivided into Vengeberget, Zeipelodden, Kloten, Skandsdalen, Tempelet and Sørfonna members. However, the outcrops at Mediumfjellet are very limited and make it impossible to subdivide into separate members. The Gipshuken Formation is found in several localities at Mediumfjellet and is associated with major thrust faults.

The formation was described from slopeforming sections, which were strongly tectonized, mainly at locality M2-5 (figure 3.2). The logged section was described just below the Kapp Starostin Formation and refers to figure 3.1.

Lithology description

The Gipshuken Formation at Mediumfjellet consists mainly of white and grey gypsum and anhydrite. The rock has white and grey colored layers, probably alternation of gypsum/anhydrite and carbonate rich layers of thin dolomite beds. The total thickness can not be measured because the lower boundary is not exposed in the outcrops. This description is comparable to similar observations made in Spitsbergen (e.g. Lauritzen, 1981).

3.3 Tempelfjorden group

The Tempelfjorden Group overlies the Gipsdalen Group and is thought to be deposited during a mid- to late Permian age. The group consists in general of silicified shales, cherts, sandstones and limestones. The change from gypsum in the Gipshuken Formation to silicified limestones is thought to be a shift from warm to cooler conditions (Dalmann, 1999). The Tempelfjorden Group is subdivided into several laterally correlative formations; Tokrossøya Formation in Sørkapp, Misery Formation at Bjønøya and Kapp Starostin Formation in Spitsbergen. Similar documentations have also been done at the Barents Sea (Ehrenberg, 2001). In the present study, the Kapp Starostin Formation represents the main part of the logged section, which also has been the main target of the fracture analysis.

3.3.1 Kapp Starostin Formation

The Kapp Starostin Formation was first described by Cutbill and Challinor (1965) and has later been described by numerous of authors (e.g. Gee et al., 1953; Siedlecka, 1970; Ezaki, 1994; Ehrenberg et al., 2001; Grundvåg, 2008). The type section is located at Festningen and is 380 m thick (Dalmann, 1999). Kapp Starostin has also been measured to be up to 460 m at St. Jonsfjorden (Dalmann 1999), 330m at Vindodden (Grundvåg, 2008) and totally pinches out southwards east of Sørkapp-Hornsund high (Dalmann, 1999). The thickness of the Kapp Starostin Formation at Mediumfjellet is measured to be only about 155 meters (figure 3.1).

The Kapp Starostin Formation in the Isfjorden area is further subdivided into three members; Vøringen Member, Svenskegga Member and Hovtinden member. Vøringen member is characterized by fossiliferous limestones, Svenskegga Member consists mainly of spiculites and some limestone beds and Hovtinden Member consist of silicified shales,

siltstones, sandstones and limestones. The observations made in field, show similarities to the type section, subsequently a boundary between the members was tried to be established.

The succession was in Mediumfjellet described from cliff forming sections at locality M3-2 (figure 3.2). Our log was described from bottom to top in several outcrop sections by correlating the beds laterally. The contact to Gipshuken and Vardebukta Formation was not exposed at this locality, but has been investigated at locality M3-4 (Gipshuken Formation) and M3-3 (Vardebukta Formation). The following lithology description is based on the unit descriptions in appendix 1 and refers to figure 3.1. Six different lithologies were found, the following description will accordingly refer to the units representing each lithology.

Lithology description

The lowermost part of the Kapp Starostin Formation is represented by Vøringen Member. The uppermost unit of the member is characterized by a grey colored, cliff-forming brachiopod limestone with widely variable grain sizes. The grain sizes range from grainstone to wackestone, and contains abundant whole macrofossils; brachiopods, bryozoans and echinoderms, whereas the matrix is sandy (Unit 3; figure 3.1; figure 3.2). The brachiopod limestone is a lateral marker horizon for the bed boundary between the Gipshuken Formation and Kapp Starostin Formation and can be compared to similar descriptions made by other authors (e.g. Malkowski and Hoffman, 1979; Ehrenberg et al., 2001)

Bryozoan limestones are common in the lower part of the Kapp Starostin Formation (units 1, 2, 6, 9 and partly 20; figure 3.1; figure 3.2). They are light yellow to grey colored where the individual beds show an upwards coarsening and thickening. They have a high content of brachiopods, echinoderms, crinoids, sponge spicules, bryozoans and burrows, whereas the two latter are dominant. According to grain size and clast content, the rock can be classified as packstone and wackestone, with silicified chert or shale as matrix. Ehrenberg (2001) described similar rocks in her classification of facies and facies association.

The light-colored spiculite is found in the middle of the Kapp Starostin Formation (unit 14; figure 3.1; figure 3.2). The unit consists of thick beds of grey mudstone with a yellowish weathering color. The beds are coarsening upwards into sandy layers modified with heavy

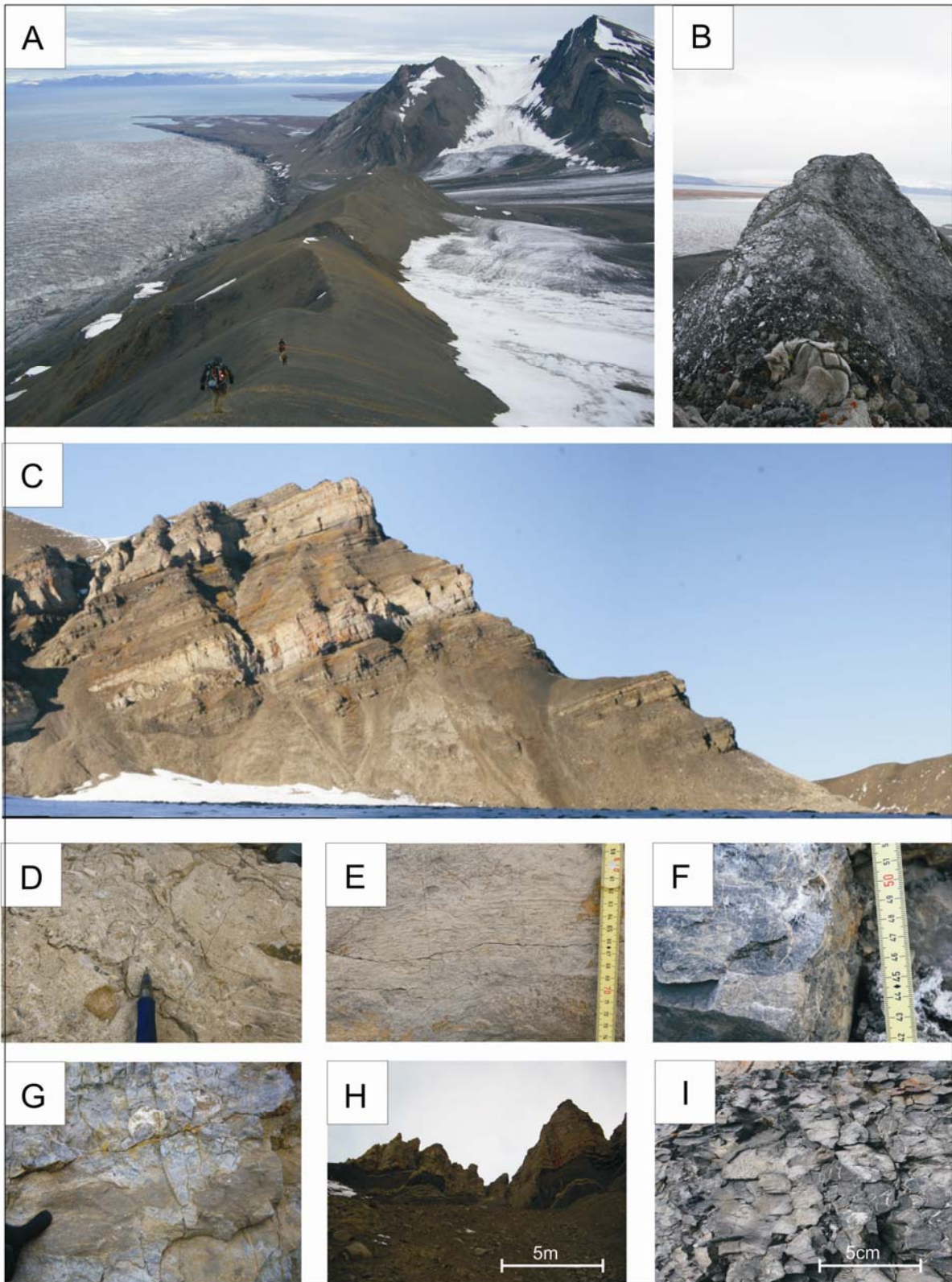


Figure 3.2: Photos from the litho stratigraphic section described at Mediumfjellet. A: Slopeforming Triassic shales; B: Gipshuken Formation; C: An overview photo of the logged section, D: Brachiopod limestone of the Vøringen member; E: Bryozoan limestone; F: Dark spiculite with calcite filled hairline fractures; G: Light colored spiculite with sand slingers; H: Uppermost part of the logged section; I: Silicified shale.

bioturbation and vary from sand lenses to green and gray irregular shales. Common fossils are brachiopods and sponge spicules. These lithological characteristics are similar to observations made elsewhere of the Kapp Starostin Formation. Examples of this are, in Spitsbergen (Grundvåg, 2008) and on the Finnmark platform (Ehrenberg, 2001).

Dark spiculite makes up significant parts of the Kapp Starostin Formation (units 4, 5, 7, 8, 10, 12, 13, 15, 16, 17, 19, 21 and 22; figure 3.1). The main characteristics are dark grey colored, silica rich and silty beds. The beds are thin, nodular and highly bioturbated with lots of spicules. Ehrenberg (2001) has described similar beds offshore on the Finnmark platform.

The siliceous shales are found in the upper part of the Kapp Starostin Formation (unit 18 and 20; figure 3.1; figure 3.2) and consist of dark colored, thin beds and fine grained mudstone. The beds are undulating and highly bioturbated revealing some bioclasts and silica spicules. Brachiopod limestone beds are found within the units at several localities, but they seem to pinch out laterally. Similar beds have been found on the Finnmark platform by (Ehrenberg 2001).

Thin bedded paper or plate like, slopeforming, dark shale is found in the lower Hovtinden Member of the Kapp Starostin Formation (unit 11; figure 3.1). The succession is about 20 m thick, and has a high content of bryozoan fossils. Thin, similar beds can be found within the bryozoan limestone beds (unit 6 and 9; figure 3.1). Similar beds have been described by Ehrenberg (2001) and Grundvåg (2008).

3.4 Sassendalen Group

The Sassendalen Group is deposited in early to middle Triassic and was first described by Buchan et al. (1965) in the central Spitsbergen. The Group overlies the Tempelfjorden Group and consists mainly of marine shale, to silt and sandstone (figure 3.2). The succession is interpreted to consist of several transgressive-regressive sequences with a concordant and possibly erosive boundary to the underlying Kapp Starostin Formation (Mørk et al. 1989; Mørk and Borøy, 1984). This contact is recognized globally by its massive extinction of marine species, as discussed in (Dalman, 1999).

The Group is subdivided into three formations comprised by the Vardebukta, Tvillingodden and Bravaisberget Formation. The formations can be correlated extensively lateral to the Barents Sea, Sverdrupsbasin, the Norwegian shelf, and are a potential source rocks for hydrocarbons (Mørk, 1984). The Triassic shales are slopeforming rocks and are commonly associated with the major thrust at Mediumfjellet. The shales are commonly strongly tectonized and often cut by dolerite intrusions. As the formations have not been the

target for the study, it has only been described briefly from locality M3-3 and is not part of the logged section.

3.4.1 Vardebukta-, Tvillingodden- and Bravaisberget Formation

Lithology description

The lowermost Formation of the Triassic succession in Mediumfjellet, is the Vardebukta Formation, and marks the boundary from cliff forming silica-rich rocks to Slopeforming shales. The outcrop consists of an upwards coarsening succession from shale intercalated with thin yellowish sandstones to grey fine grained sandstone. Then the succession is again fining upwards to shale interbedded with thin yellow sandstone beds.

The boundary to the Tvillingodden Formation can not be precisely determined from the outcrop, but is thought to be where the shale becomes darker. The succession consists of dark organic rich shale and seems to conformable overlying the Vardebukta Formation. Thin yellowish sandstone beds occur in the slope scree, but can not be seen in the outcrop.

The Bravaisberget Formation is most likely not exposed at Mediumfjellet as there are no outcrops of sandstone overlying the Tvillingodden Formation.

3.5 Intrusives

In the Mediumfjellet mountain range, diabase sills and a number of dikes has intruded into and affected individual stratigraphic horizons. Weak layers such as gypsum in the Gipshuken formation and shales (Triassic shales) are often hosting diabase sills, while diabase dikes crosscut and split stiffer units, such as the Kapp Starostin Formation.

The diabase consists of mainly plagioclase and pyroxenes and has a phaneritic hypidiomorphic granular texture. The intrusions have been ascribed to a large igneous province and associated rifting in the arctic basin (Harland, 1997). Although poorly constrained, the intrusives are of age about 140 Ma, near the Jurassic-Cretaceous boundary.

3.6 The stratigraphic importance of deformation

3.6.1 Macro-scale structures

The macro-scale structures seem to be highly influenced by the lithology. The major thrusts cut along the weak beds, such as the gypsum/ anhydrite in the Gipshuken Formation and the Triassic shales. The Mediumfjellet-Lappdalen thrust front has earlier been interpreted to be a result of step-up (flat-ramp geometry) thrusting between two weak detachment horizons, cutting steep through the Kapp Starostin Formation (see chapter 1, for previous work).

3.6.2 *Fracturing*

To study the fractures it is firstly important to get familiar with the stratigraphy, secondly it is important to recognize the same bed laterally, third and last, it is important that the fractures are well developed and easy to distinguish.

In the studied Kapp Starostin Formation, there were found six separate units which consist of well developed fracture sets (figure 3.1). These are units 1, 2, 3, 6, 9 and 21 (appendix 1) where units 1, 2, 6, 9 and partly 20, belongs to the bryozoan limestone and unit 3 to the brachiopod limestone. These rocks stand out as more massive and rigid than the other units. Since the light colored spiculite, the dark spiculite and the siliceous shale consist of very thin and undulating beds, these beds have developed an extremely chaotic and varied fracture pattern. Hairline fractures are common, often filled with calcite (figure 3.1) and are not easy to follow. However, a few fractures in unit 5 were yet collected for comparison with the other beds.

The Triassic shales are commonly strongly deformed because of associated thrusts. However several observations have been made on well developed fractures in the sandstone beds. Those fractures have not been the focus of this study and may be an alternative for residual work. The Gipshuken formation is similarly strongly tectonized but is more ductile, and internal plastic deformation have occurred with poor developed fracture systems.

The diabase intrusions stand out as a rigid and cliff forming rocks and are seen to have acted very rigid with respect to the deformation, and host very high frequencies of fractures, often coated with slickensides may be used as indication for kinematic transport directions.

3.7 Summary and interpretation

The stratigraphy of the Kapp Starostin Formation at Mediumfjellet is described with six different lithologies: 1) siliceous shale, 2) dark paper shale, 3) brachiopod limestone, 4) bryozoan limestone, 5) light-colored spiculite and 6) dark spiculite.

The stratigraphic lithologies have a major influence on both large macro-scale and micro-scale structures. The macro-scale structures are dependent on the weakness of the layers and are represented by the Gipshuken Formation and the Triassic shales, developing flat-ramp geometries. Similarly, the micro structures are largely influenced by the rock mechanics. The brachiopod- and bryozoan limestones have seemingly clear, planar and often throughgoing fractures developed. These beds are represent by unit 1, 2, 3, 6, 9 and 20 (figure

3.1; appendix 1) and are excellent for studying laterally. The dark spiculite consist of more irregular fractures and unit 5 is also studied for comparison the limestones.

Chapter 4

Structural descriptions

4.1. Introduction

This chapter starts with introducing and describing the macro-scopic structural elements in the study area. Thereafter the fracture system of Mediumfjellet will be described (see appendix 2 for all data collected), which is the main focus of this thesis. In the end of the fracture intensities are described, before finishing with a summary. The combination of presented datasets forms the basis for the discussion in chapter 5.

The structural description of the Mediumfjellet thrust stack is divided into four major thrust systems; M1, M2, M3 and G (figure 4.1). These main provinces have previously been described by Bergh and Andresen (1990) and Bergh et al., 1997. The thrusts were interpreted to be an imbricate thrust stack of in-sequence thrusting (M1, M2 and M3), where the oldest thrust is thought to be the M3-thrust and the youngest the M1-thrust. The Gavltinden thrust (G) is considered an earlier thrust system that is truncated by an out-of-sequence thrust (Bergh and Andresen, 1990).

The chapter will first describe the four thrust-domains. The Gavltinden thrust domain is here described as one separate subarea. The M2- and M3- thrust systems are each split into three subareas (a, b and c), where subarea a is placed farthest north (figure 4.1). The three subareas of the M2- and M3- thrust system at the Mediumfjellet ridge naturally splits into three main subareas divided by glaciated areas. The modern glacial erosion naturally provides excellent outcrop possibilities for along-strike variations, and hence correlations between the subareas can easily be established. The chapter will then describe the structural elements in each subarea, including and important localities. Localities were chosen based on their position in the thrust-systems. Where the outcrop allowed, fractures and bed orientation datasets were collected at the same stratigraphic beds along-strike and in all the structural domains (M2, M3 and G).

The fracture descriptions are systematized in the same way as the description of the fold-and-thrust system. The fractures are described for each subarea and fold domains (backlimb, hinge and forelimb). The fracture sets are split into three main populations and

described separately: 1) Perpendicular fractures that cut through the strata normal to the bedding, 2) Conjugate fractures are here in a population that cuts through the strata with a

<i>Sub-domain</i>	<i>Subarea</i>	<i>Locality</i>	<i>Scan-line number</i>	<i>Scan-line trend</i>	<i>Bedorientation data</i>
M2					
	M2-a	M2-1	None		Yes
	M2-b	M2-2	4b-1-07	130°-310°	Yes
			4b-2-07	130°-310°	Yes
			4b-3-07	175°-355°	Yes
			4b-4-07	120°-300°	Yes
		M2-3	4c-4-08	130°-310°	Yes
			4c-5-08	130°-310°	Yes
			4c-6-08	117°-297°	Yes
			4c-7-08	025°-205°	Yes
			4c-7b-08	177°-357°	Yes
			4c-8-08	025°-205°	Yes
		M2-4	4R-07	110°-290°	Yes
		M2-5	4d-1-07	085°-265°	Yes
			4d-2-07	095°-275°	Yes
			4d-3-07	015°-195°	Yes
			4d-4-07	015°-195°	Yes
			4d-5-07	090°-270°	Yes
	M2-c	M2-6	None		Yes
		M2-7	None		Yes
M3					
	M3-a	M3-1	3i-1-07	030°-210°	Yes
		M3-2	3g-1-07	025°-205°	Yes
			3g-2-07	125°-305°	Yes
			3g-3-07	170°-350°	Yes
	M3-b	M3-3	3b-1-07	150°-330°	Yes
			3b-2-07	168°-348°	Yes
		M3-4	3c-1-07	030°-210°	Yes
			3c-2-07	030°-210°	Yes
			3c-3-07	130°-310°	Yes
			3c-4-07	030°-210°	Yes
			3c-5-07	030°-210°	Yes
			3c-6-07	030°-210°	Yes
		M3-5	3h-07	160°-340°	Yes
		M3-6	None		Yes
	M3-c	M3-7	M3-7_9-08	040°-220°	Yes
		M3-8	3e-1-07	160°-340°	Yes
			3e-2-07	160°-340°	Yes
			3e-1-08	155°-335°	Yes
			3e-2-08	155°-335°	Yes
		M3-9	None		Yes
G					
	GT-a	GT-1	None		Yes
		GT-2	2e-1-07	015°-195°	Yes
			2e-2-07	015°-195°	Yes
			2e-3-07	040°-220°	Yes
			2e-10-08	020°-200°	Yes
		GT-3	None		Yes

Table 4.1 Table with an overview over the thrust domains and subareas with their measured scan-lines for each locality. Each scan-line has an identification number which have been referred to in the text. Note that the scan-line trend gives the direction of the fracture measurement, which is usually also a fracture-set direction.

high angle, and that has the bisecting angle revealing an axis perpendicular to the bedding. 3) A fracture population of low-angle-to-bedding faults (also named as thrust). In order to discriminate between fracture sets formed prior to folding and those formed synchronous with folding, the fracture sets are restored with bedding back to subhorizontal. Table 4.1 provides an overview of the three sub-domains and their subareas including localities, scan-lines, scan-line trends and bed measurements.

4.2 Description of fold-thrust structures in domains and subareas

The structural descriptions are based on field work carried out summer 2007 and 2008, photo-textured Lidar scan (e.g. figure 4.9) and 3D modelling from the lidar scans (figure 4.8).

4.2.1 M1 fold-and-thrust domain

The M1-thrust is the eastern-most thrust of Mediumfjellet and is located in the flat area between Mediumfjellet and Muslingodden (figure 4.1). The thrust fault is poorly exposed, and the evidence for a thrust is based on the assumed hanging wall cut-off of the forelimb at the M2 anticline, where steeply dipping Kapp Starostin Formation strata of the forelimb are placed next to subhorizontal strata of Triassic shales. The M1- thrust has earlier been interpreted (see chapter 1) as a nearly horizontal thrust or detachment from the eastern end of Mediumfjellet and eastward (Bergh and Andresen, 1990). Wennberg (1990) suggests a connection from Mediumfjellet on the southern side of Sveabreen and the God'deryggen fault at the north-eastern side of Mediumfjellet and Sveabreen.

4.2.2 M2 fold-and-thrust domain

The M2-thrust crops out in subareas M2-a, M2-b and partly in M2-c (figure 4.1). The thrust ends in a tip line in a macro-scopic anticline displayed in subarea M2-c. This anticline is the hanging wall structure of the M1-thrust, and as such the M2-thrust is interpreted to connect to the M1-thrust underneath Mediumfjellet (see chapter 1; Bergh & Andresen, 1990).

Subarea M2-a is located east of Gavltinden (figure 4.1; see also figure 4.11), at the boundary to the Sveabreen and north of the Mediumbreen. In this subarea, the backlimb of the major M2 anticline is exposed and has been studied. Strata belonging to the Kapp Starostin Formation and overlying Triassic shales are involved in the folding. An irregularly occurring diabase dyke crosscuts the Triassic shales. The M2 backlimb geometry of the M2 anticline is

seen as a steeply dipping (ca. 70° WSW), yet fairly straight fold flank, with decreasing dip towards the fold hinge (e.g. 130/25). This indicates the location of the anticlinal closure in the area (figure 4.2). Bedding orientation data reveals best fit great-circle and with an associated π -point,

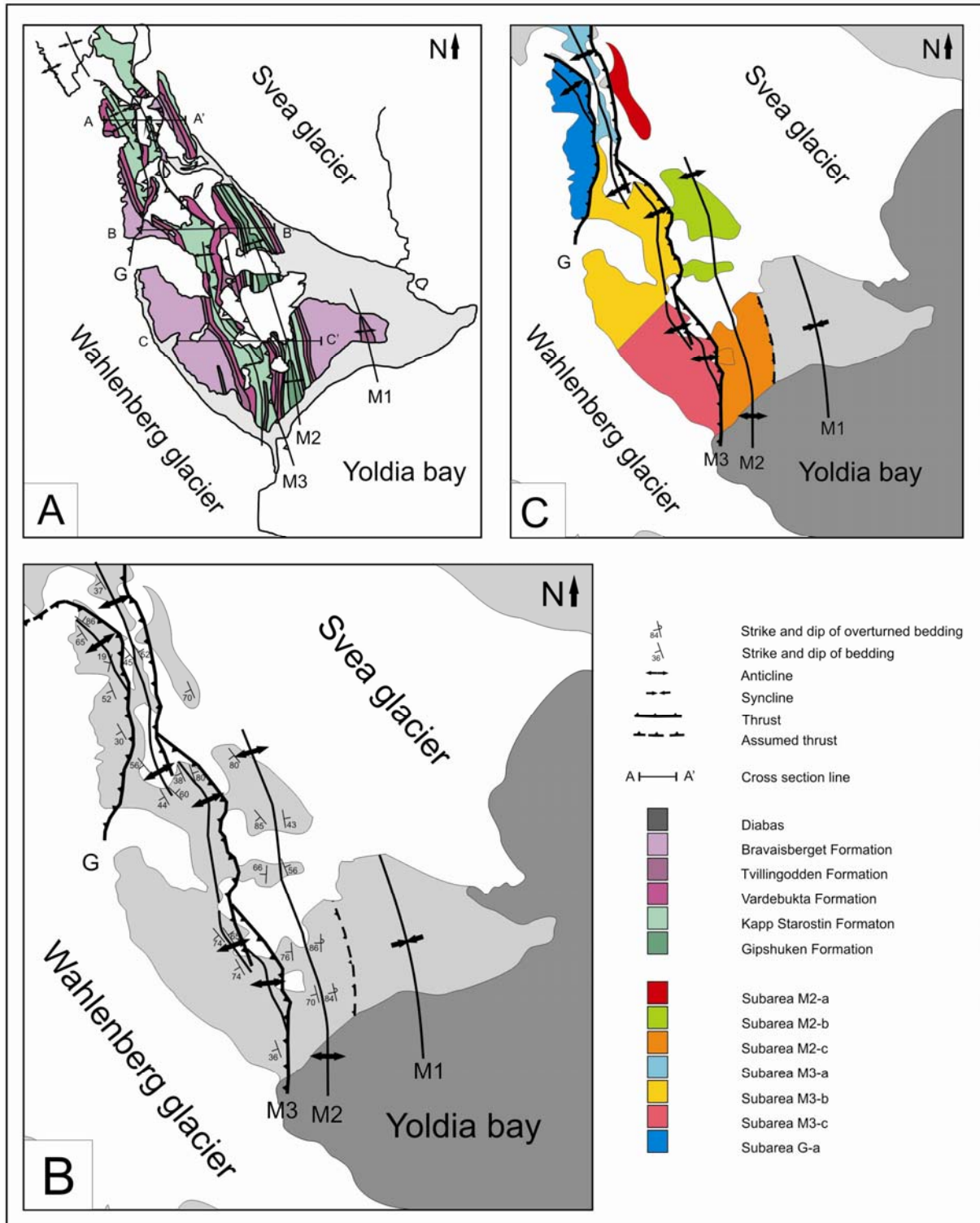


Figure 4.1: Three different maps of Mediumfjellet. A: Bedrock map including structural elements. The mint green color of Kapp Starostin Formation indicates the areas for scan-line measurements (modified from

Norwegian polar institute). B: Structural map including the bed orientations measured in field. C: Outline of the study area, with colors for the different seven subareas of Mediumfjellet including the structural macro-scale elements.

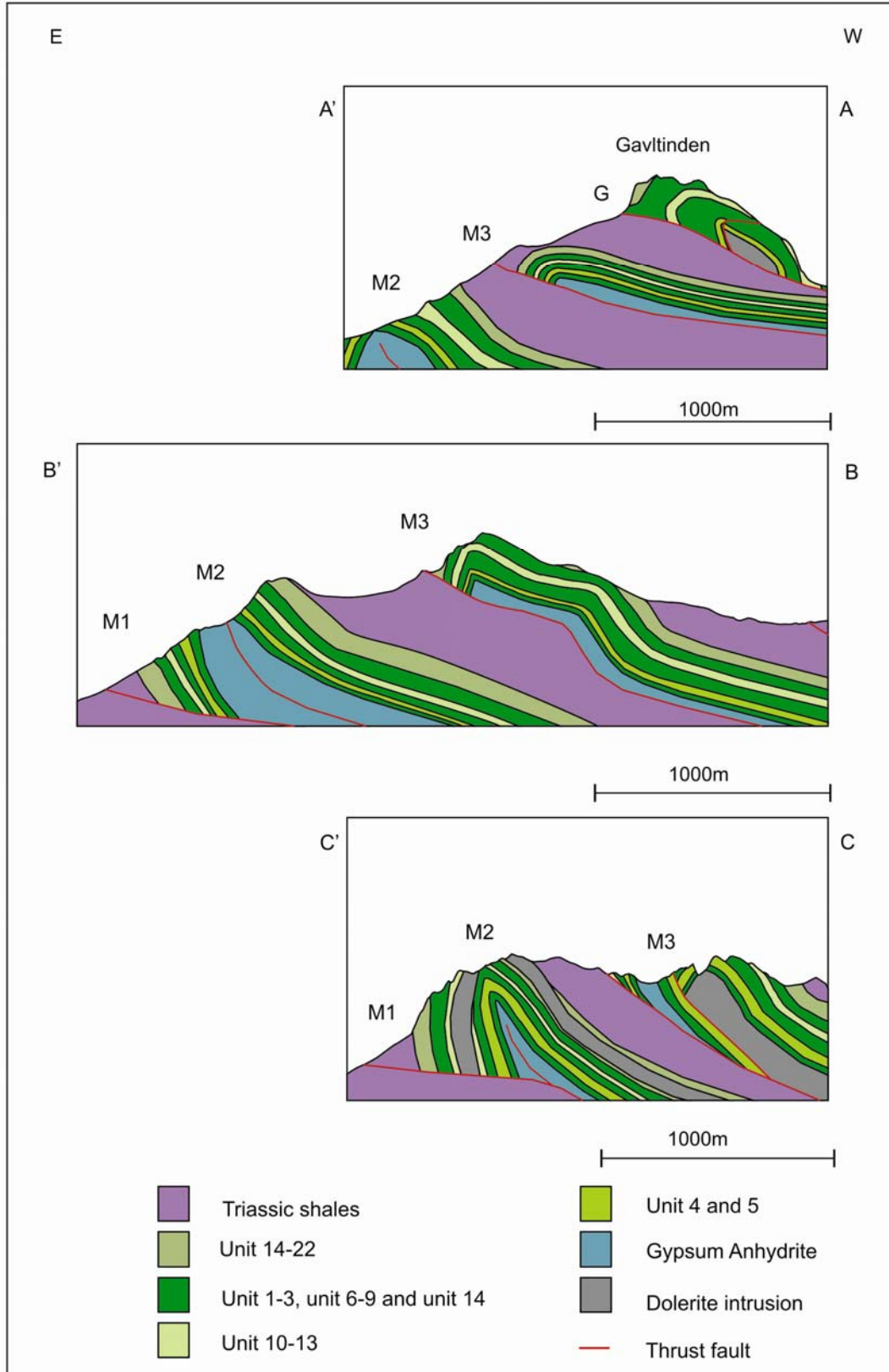


Figure 4.2: Three geological cross-sections made from Lidar scan interpretations. The cross-section lines are seen on the map in figure 4.1. Section A'-A represent subareas M2-a, M3-a and G-a, section B'-B represent subareas M2-b, M3-b and G-a and section C'-C represent M2-c and M3-c. The Lidar scan interpretations are exported into Petrel where surfaces are can connect the lines and cross-sections can be made. Note that the units in the legend refer to figure 3.1 (chapter 3).

showing that the fold plunges gently to the SSE (figure 4.11). Worth mentioning is that a superb example of a small thrust fault cuts through one of the upper beds in the Kapp Starostin Formation near the fold hinge, developing a small fault-propagation fold (figure 4.3).

Subarea M2-b is located south of the Mediumbreen and SW of the Sveabreen (figure 4.1; figure 11). This area is the continued structural position of subarea M2-a (figure 4.1). In which, the M2-thrust and anticline are fully exposed. The anticline is bounded below by the M1-thrust and has the M2-thrust in its core (figure 4.2). The fold core consists of deformed layers of the Gipshuken Formation, which are imbricated, thickened and disharmonically folded. Both limbs of the major M2-anticline is made up of the Kapp Starostin Formation. Triassic shales are found in the western M2-backlimb beneath the M3-thrust (figure 4.2). The M2 -fold is thought to be the continuation of the M2-fold from subarea M2-a. Geometrically, the major M2-anticline is near symmetrical and tight, with an axial plane dipping subvertically to the WSW (figure 4.11). The backlimb is gently curving, steep (e.g. 175/79) and relatively undeformed, while the forelimb is thinner, steep (e.g. 350/70), and more folded and faulted (figure 4.4). The interlimb angle is about 30°, the fold axis strikes SSE-NNW and plunges gently to the SE (Figure 4.11). The M2-thrust cuts through the centre of the fold core at locality M2-3, but the displacement is small, about 20 meters (figure 4.2; figure 4.4).

Subarea M2-c is situated in the south, near Yoldiabukta, and makes up the southernmost part of the Mediumfjellet thrust stack (figure 4.1; figure 4.11). The structural position is similar to that of the fold system of subareas M2-a and M2-b. Subarea M2-c is characterized by a major hanging wall anticline with a blind thrust in the core (figure 4.2). The anticline consists of rocks of the Kapp Starostin Formation, with Gipshuken Formation strata in the core. The Triassic shales crop out on the ridge west of the fold in the backlimb. A diabas dyke looks like a sill, but in the digital elevation model this feature can be seen as a low-angle-to-bedding dyke, that along strike seems to cut the Kapp Starostin Formation with. The asymmetric anticline has a straight and relative gently dipping backlimb and a steep, overturned forelimb. The hinge zone is narrow with an

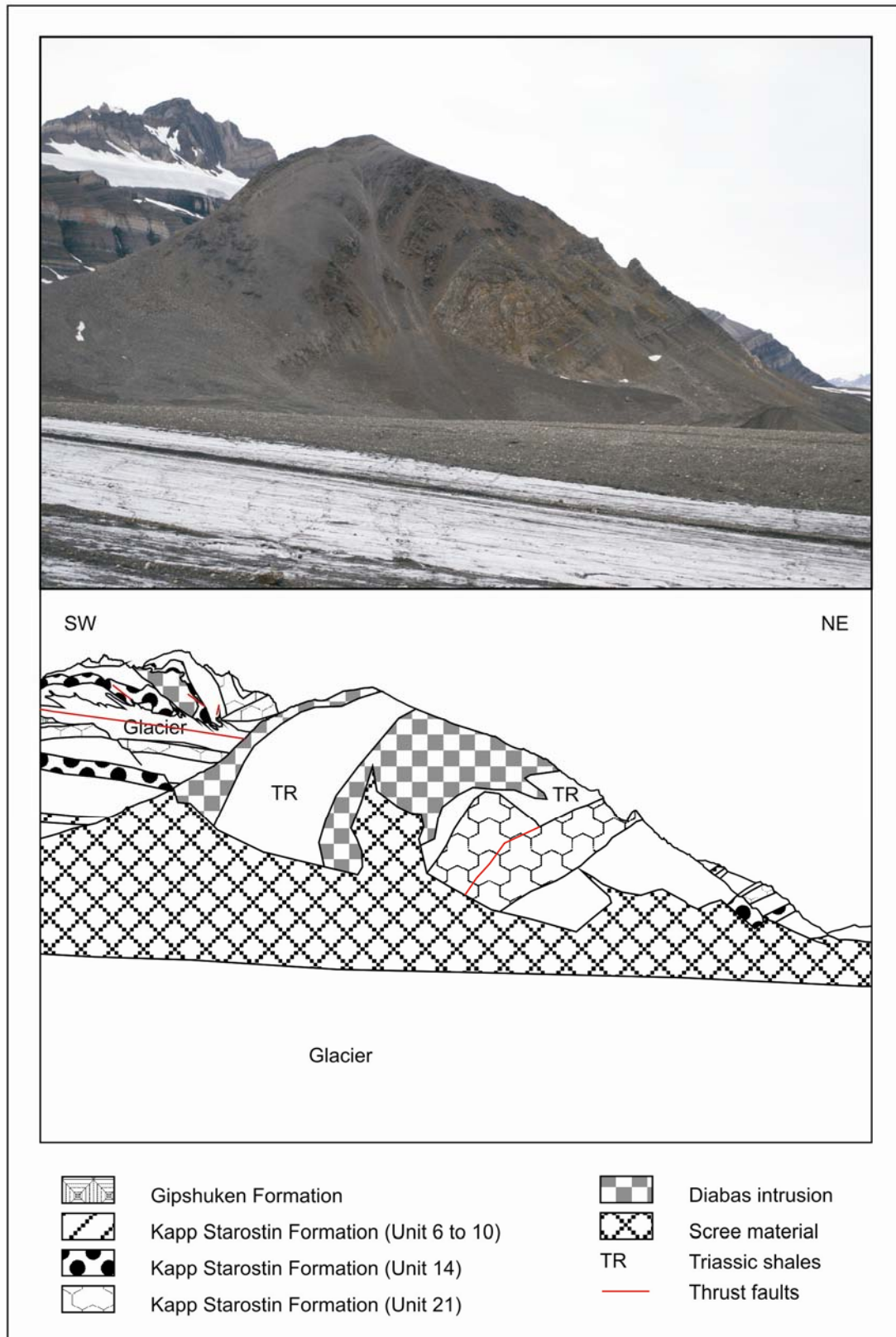


Figure 4.3: Photo interpretation of subarea M2-a. The photo displays the backlimb of an assumed anticlinal. A small fault-propagation fault can be seen in the middle of the photo. Gavltinden and the Gavltinden thrust can be seen in the background. Note that the units refer to figure 3.1 (chapter 3).

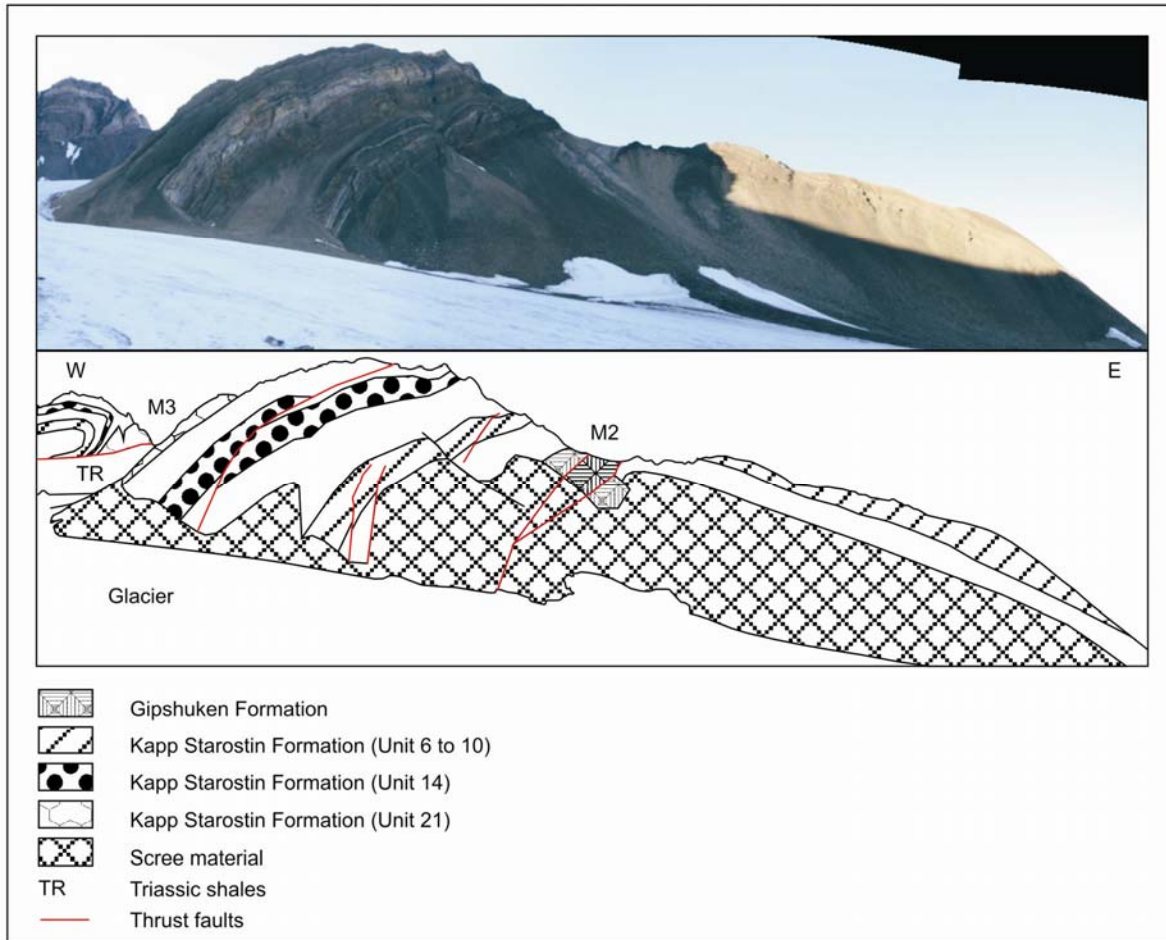


Figure 4.4: Photo interpretation of subarea M2-b. The M2-thrust cuts through the anticline hinge zone. Note the small low-angle-to-bed thrust faults. The overturned anticline from subarea M3-b can be seen in the background with the belonging M3 thrust beneath.

interlimb angle of about 60° . The fold plunges gently to the south and the axial plane strikes N-S and dips steeply towards the west (figure 4.11). In the northern mountainside of the exposed fold, the core is cut by a major fault. This fault crops out as a hanging wall flat and footwall ramp thrust, and is associated with a transported fault-propagation fold in the hanging wall (figure 4.2). The Gipshuken Formation is not exposed in the fold core, but is present in a lower section in the mountain side revealing the backlimb (figure 4.9). However, the Gipshuken Formation is expected to be present also in the core of the fold.

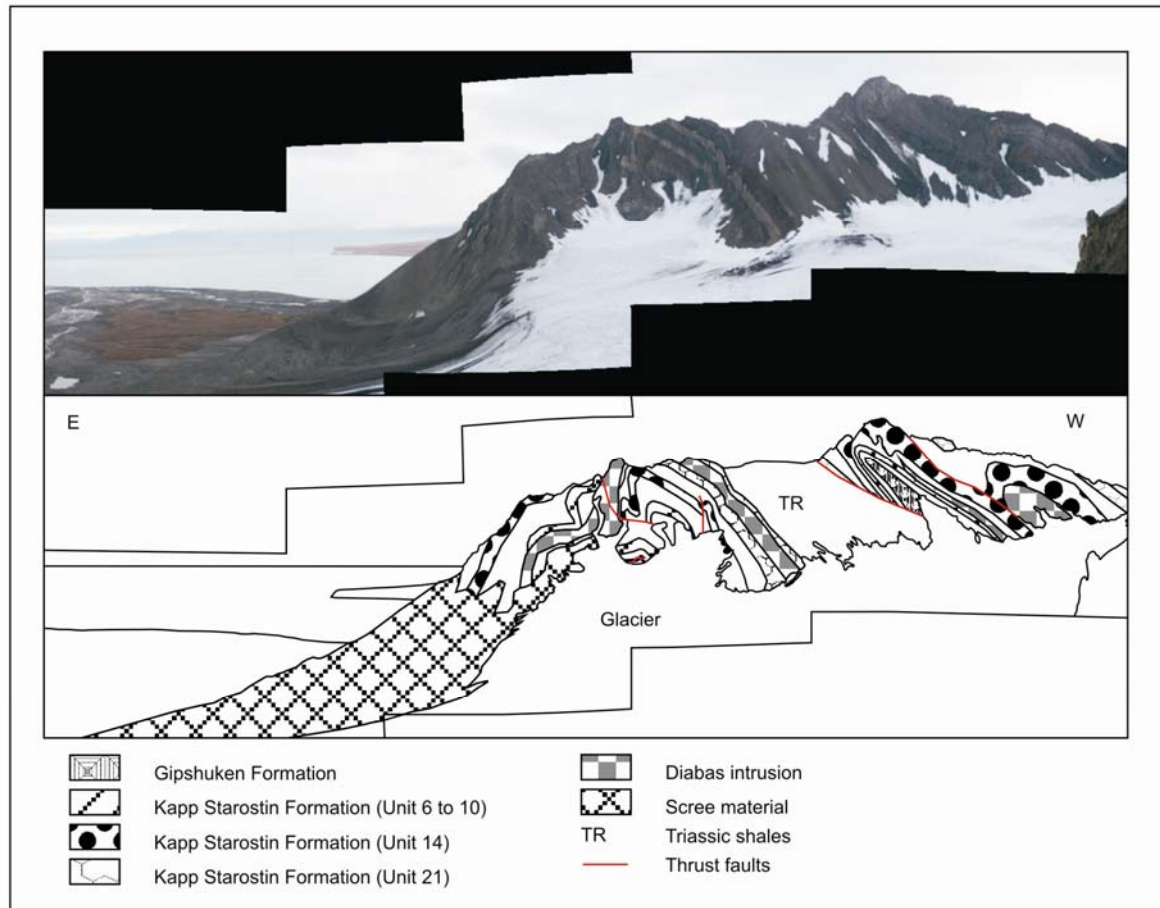


Figure 4.5: Photo interpretation of subarea M2-c and M3-c. Note that the M2-thrust slightly cuts through the anticline. Subarea M3-c to the west displays the two faults with a first order anticline in the front and a second order anticline in the back. The Yoldiabukta and Bohemansfloya can be seen in the background.

4.2.3 M3 fold-and-thrust domain

The M3-thrust is the best displayed thrust of Mediumfjellet and is exposed along strike for at least 10 km from Yoldiabukta past Gavltinden (figure 4.1). The thrust splits into several smaller thrusts but they are here all mentioned as the M3 thrust. The thrusts are earlier interpreted (chapter 1) to splay from a decollement surface in the Gipshuken Formation and cut steeply up section to the Triassic shales, partly replacing the gypsum/anhydrite in the Gipshuken formation on top of the Triassic shales (figure 4.2).

Subarea M3-a is located far to the north in the field area, east of Gavltinden (figure 4.1; figure 4.11). The subarea consists of a major anticline in the hanging wall to the M3-thrust. The fold has only been studied in the backlimb and hinge to near forelimb regions, due to lack of access (figure 4.6). Kapp Starostin Formation strata and Triassic shales are involved in the folding as seen in the outcrops. The bedding is folded into an asymmetric, open to tight, east facing macro-sopic anticline with an overturned eastern limb. The fold can be traced

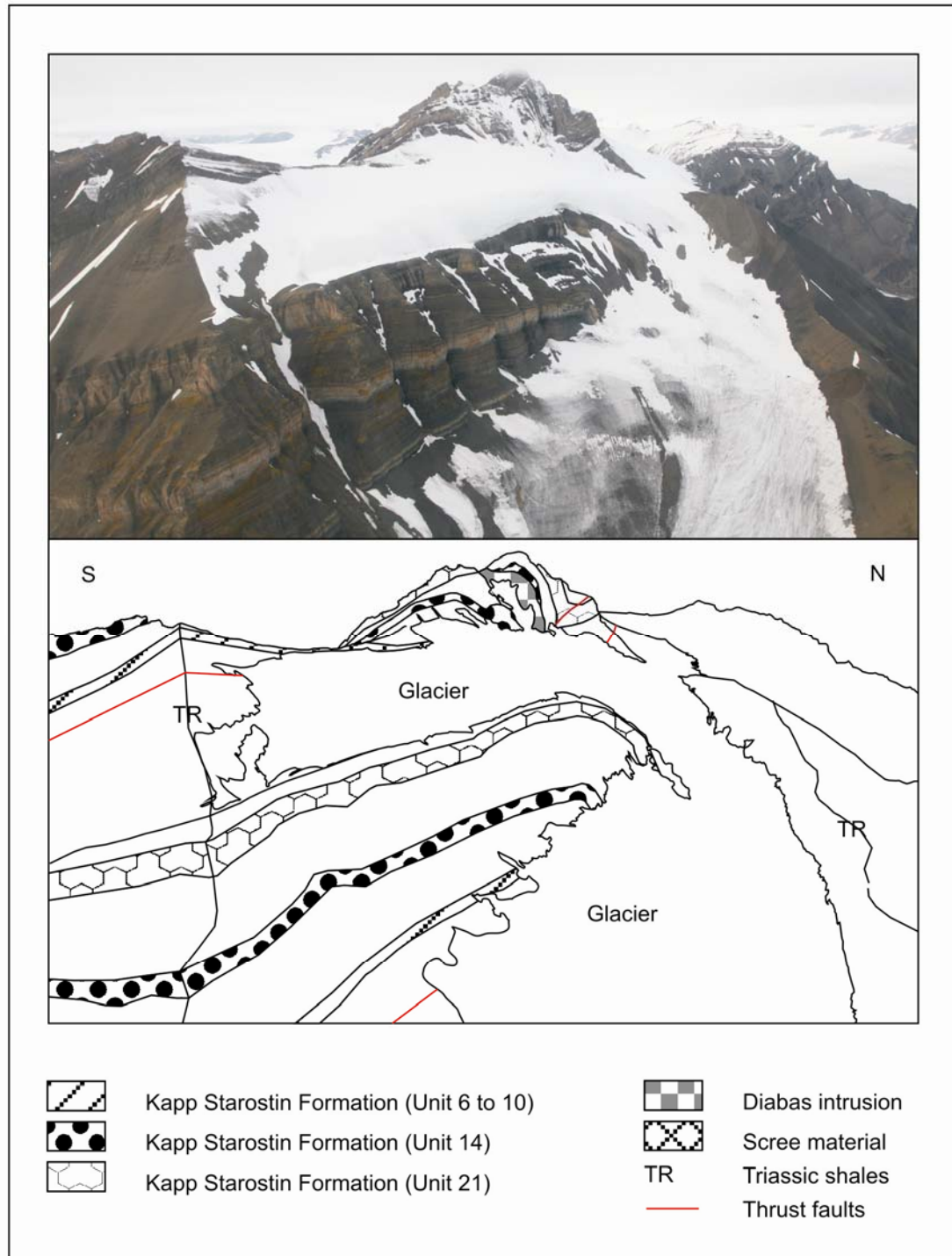


Figure 4.6: Photo interpretation of subarea M3-a. The M3-anticline disappears underneath the glacier. The Gavltinden and Gavltinden thrust can be seen in the background.

along strike to subarea M3-b (figure 4.1). Throughout the area, the axial plane dips moderately towards the SW. The backlimb is long, straight and dips 40° to the SW. The hinge zone is tight with a steep, partly overturned forelimb, dipping 50° to NE (figure 4.11).

Subarea M3-b is situated in the central part of the Mediumfjellet thrust stack, just south of the Mediumbreen (figure 4.1). The area is showing a major hanging wall anticline extending along strike from subarea M3-a. The entire fold is exposed in a cliff south of Mediumbreen and was carefully studied as this subarea. The strata involved in this macro-fold include the section from the Kapp Starostin Formation up through the lower Triassic shales, and with the Gipshuken Formation in the core of the anticline (figure 4.2; figure 4.5). The Triassic shales are found both above the Kapp Starostin Formation in the backlimb, and in the footwall beneath the M3-thrust, and are displayed in the cross section (figure 4.2; figure 4.7). Also this area shows a diabase dyke/sill. Its appearance is similar to the one observed further north, in that the dyke obliquely truncates strata of the Kapp Starostin Formation. The overall structural geometry is characterized by a macro-scopic, asymmetric, and open to tight, overturned anticline, which is plunging about 9° to the NW. Based on the Petrel interpretation (figure 4.8); the fold seems to be situated on a lateral ramp creating a complex fold. The hinge zone is narrow and has an axial plain dipping steeply to the SW (figure 4.11). The backlimb is long and dips overall moderately (ca. 50°) to the SW, but steepens along strike southwards (figure 4.8). The forelimb is very steep to overturned (average of 76° to SW), and the strata are thinned and internally deformed. The latter is seen by local meso-scopic, open, synclines and anticlines that can be genetically related to smaller thrust faults or thrust intersections. For example; at locality M3-5, an open anticline and syncline are present (figure 4.7). At locality M3-3, a fault-propagation fold is caused by small thrusts (figure 4.8). Within the core of the macro-scopic fold, smaller disharmonic fold structures are seen in the Gipshuken Formation, but smaller folds are also found within the Kapp Starostin Formation at the southern side of peak 805m. These folds seem to have Z and M geometries (figure 4.8), depending on their position with respect to the axial plane.

Subarea M3-c is located to the southernmost part of Mediumfjellet (figure 4.1; figure 4.11). Steep mountain sides excellently expose the entire M1-M3 thrust stack and associated fault related folds. The Kapp Starostin Formation is the most prominent rock. The Gipshuken Formation occurs in the core of the anticline and along the main M3 thrust, while a diabase sill occurs in the core of the M3 fold. In the Lidar scans, it is evident that this diabase intrusion crosscuts several stratigraphic layers of the Kapp Starostin Formation to the north but runs layer parallel toward the south (figure 4.9). The subarea is recognized by two macro-scopic M3-folds with associated thrusts. The SW-most anticline is small and exists behind a major first order anticline (figure 4.2; figure 4.5). Both folds are asymmetric and NE verging. From the Lidar data it is clear that the M3 thrust split into two

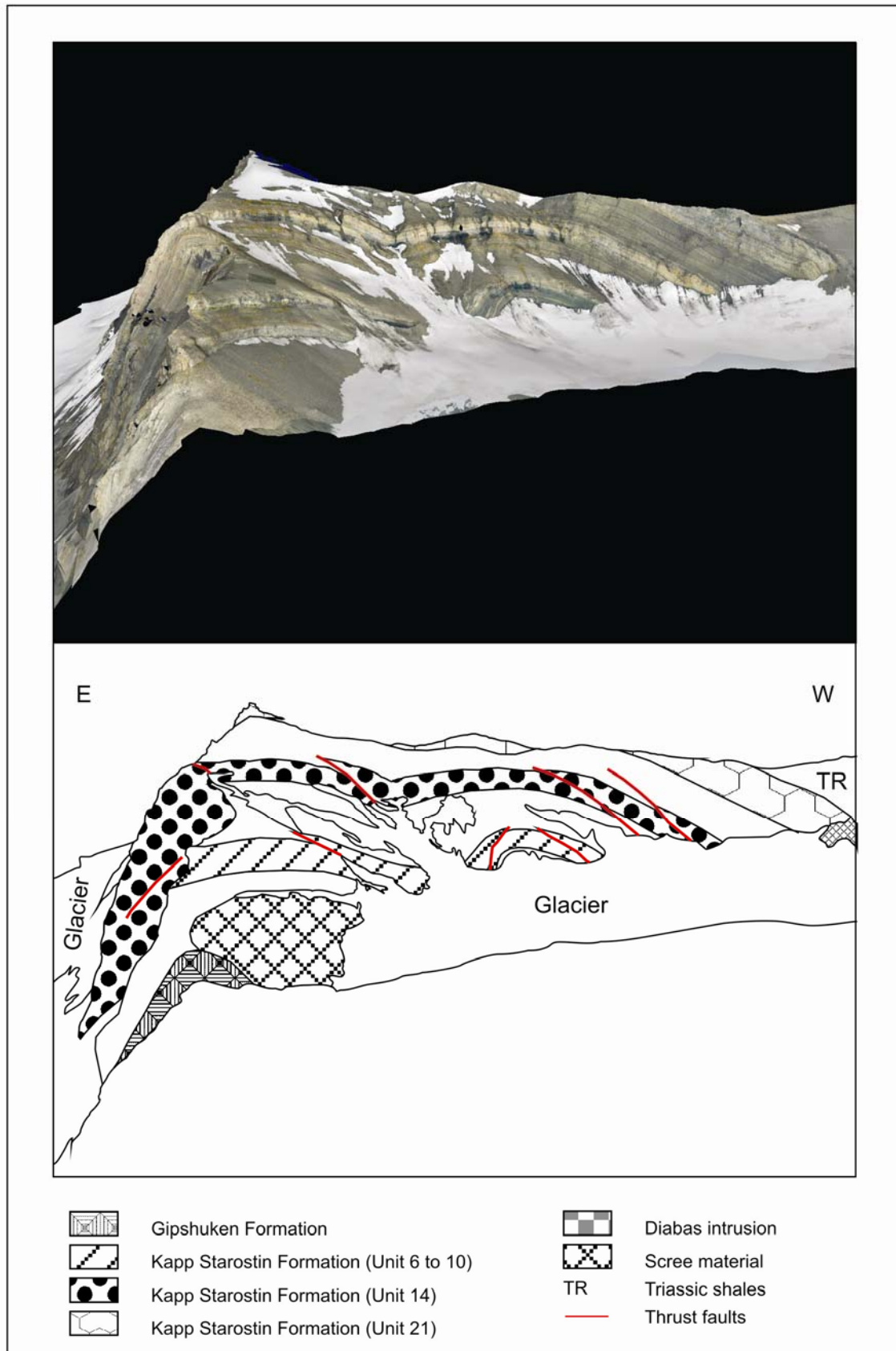


Figure 4.7: Photo textured Lidar interpretation of subarea M3-b seen from the Mediumbreen (see figure 4.1). The macro-scale anticline displays a meso-scale open syncline anticline pair. Note that the low angle to bed thrusts cut the bed with a similar angle and are rotated with the fold.

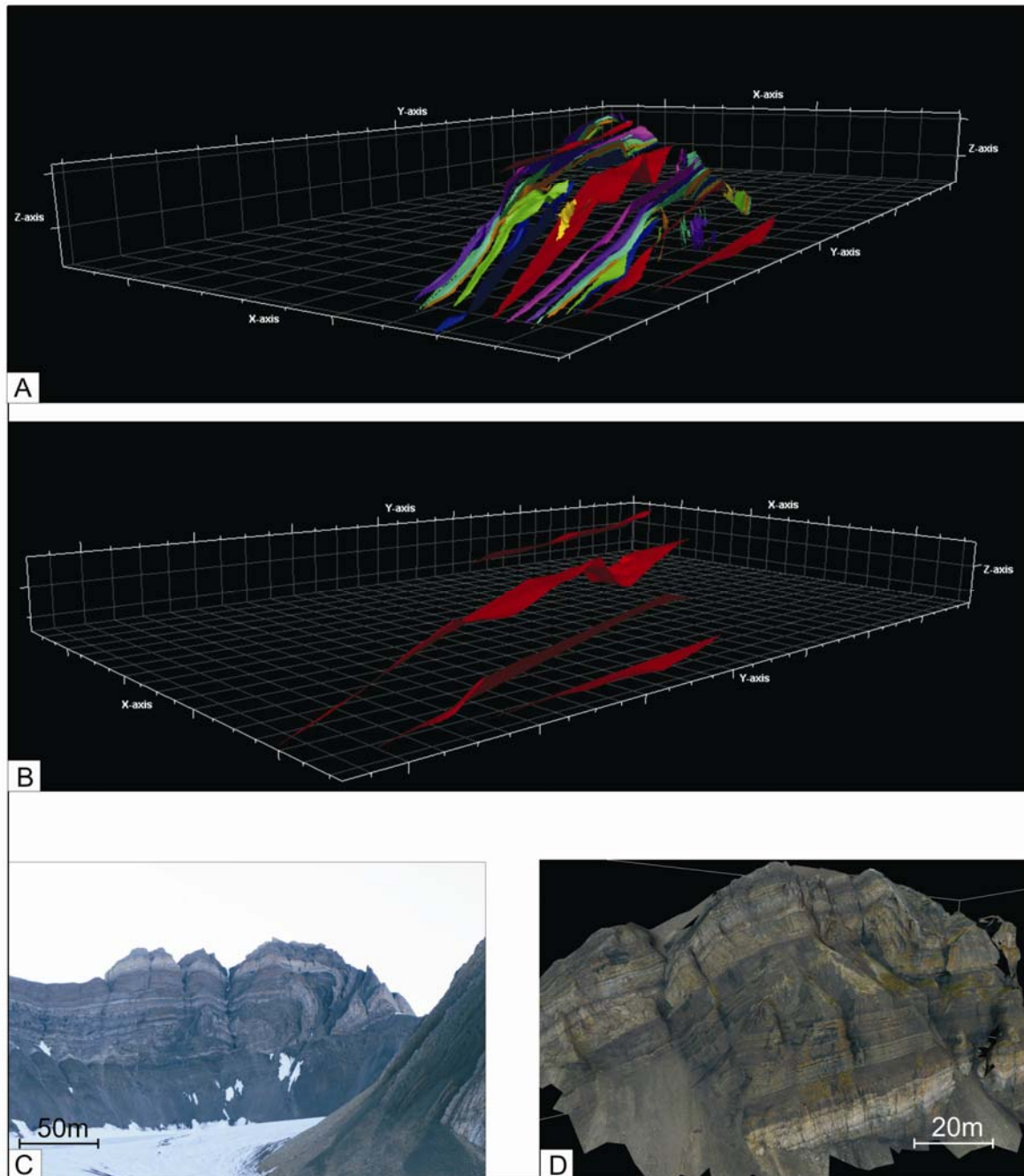


Figure 4.8: A: Gridded surfaces in Petrel, shows the lateral variations. The Y-axis marks the direction of north-south. The thrusts are red, top Gipshuken Formation is yellow, top of unit 3 is blue, bottom of unit 6 is green, top of unit 10 is orange, base of unit 14 is turquoise, top unit 14 is purple and Perm-Trias boundary is pink. The unit numbers refer to figure 3.1 (chapter 3) Note that the thrusts have less displacement southwards. B: Thrust faults displayed alone with no folds. Two lateral oblique thrust ramps can be seen in the M3 thrust. The Y-axis marks N-S direction. C: An overturned anticline in subarea M3-2, with thinned limbs and thickened hinge zone. Note the small folds in the core. D: A fault-propagation fold in the backlimb of the anticline in subarea M3-b.

faults at locality M3-7 and then merges into one fault at the southern end of Mediumfjellet. It thus seems to be a fault linkage of two thrusts (here, both are mentioned as part of the M3-thrust system), which may create a relay ramp with a secondary fold behind the major first-

order fold (figure 4.8). The smaller fold seems to be the continuation of the thrust system from subarea M3-a and M3-b, as the fold at locality M3-7 plunges southwards (figure 4.8), thereby indicating reduced displacement of the thrust southwards. The major fold appears to be of another fault system developed underneath and east of the second order M3-thrust system (figure 4.2). Both folds are asymmetric and NE verging. The major fold has a long and straight, relatively undeformed backlimb that is dipping approximately 50° towards the SSE, and with a more deformed, folded and faulted, tight hinge zone. The forelimb is overturned and dips 80° towards the SSE. The fold hinge plunges slightly towards the NNW, and the axial plane dips steeply towards the SW (figure 4.11). The hinge zone contains small, tight asymmetric syncline-anticline pairs and numerous splay faults in the centre. The minor fold is tight, with a short and overturned forelimb and a steep backlimb that dips 70° to the SW. The fold core hosts a diabase sill, probably the same occurring at the southern face of Mediumfjellet (figure 4.9).

4.2.4 Gavltinden fold-and-thrust domain

The Gavltinden thrust is situated in the western and central part of the Mediumfjellet ridge. The thrust can be traced from about 3 km northwest of Yoldiabukta to Gavltinden (figure 4.1). Prominently, the Gavltinden thrust cuts down the stratigraphic section towards the NNE, as can be seen in the southern outcrops of the subarea G-a. The truncation has a low angle to the bedding, and as Triassic shales are observed under the thrust along its entire length, a full cut-off of the Kapp Starostin Formation is likely (figure 4.2).

The subarea G-a is localized in the Gavltinden mountain area (figure 4.1; figure 4.11) and includes the hanging wall fold of the Gavltinden thrust. Rocks exposed in the area are mainly the Kapp Starostin Formation and Triassic shales, the latter hosting a diabase intrusions. From the outcrops and the Lidar scans it is clear that the diabase dyke/sill is located between the Gipshuken and Kapp Starostin Formation strata and climbs up-section into the Triassic shales (figure 4.10). Some of the nearby units are internally disturbed and bent, probably related forces created by the diabase dyke intrusion. Subarea G-a is dominated by a macro-scopic, tight and asymmetric anticline, which plunges 21° to the NW at locality GT-1. The fold is horizontal at locality GT-2 and plunges subhorizontally to the south-east at locality GT-4 (figure 4.11). The axial plane is subvertical and dips towards the SW. The limbs are straight and nearly vertical; the NE forelimb is slightly steeper than the SW limb. This is shown by the NE limb that dips about 80° to the ENE, whereas the SW backlimb dips 65° to the WSW. The backlimb also displays an open kink-fold at locality GT-2, resulting in making

parts of the backlimb very steep (e.g. dipping 70°) (figure 4.10). The hinge zone of the major anticline is extremely narrow and hosts a diabase sill in the fold core.

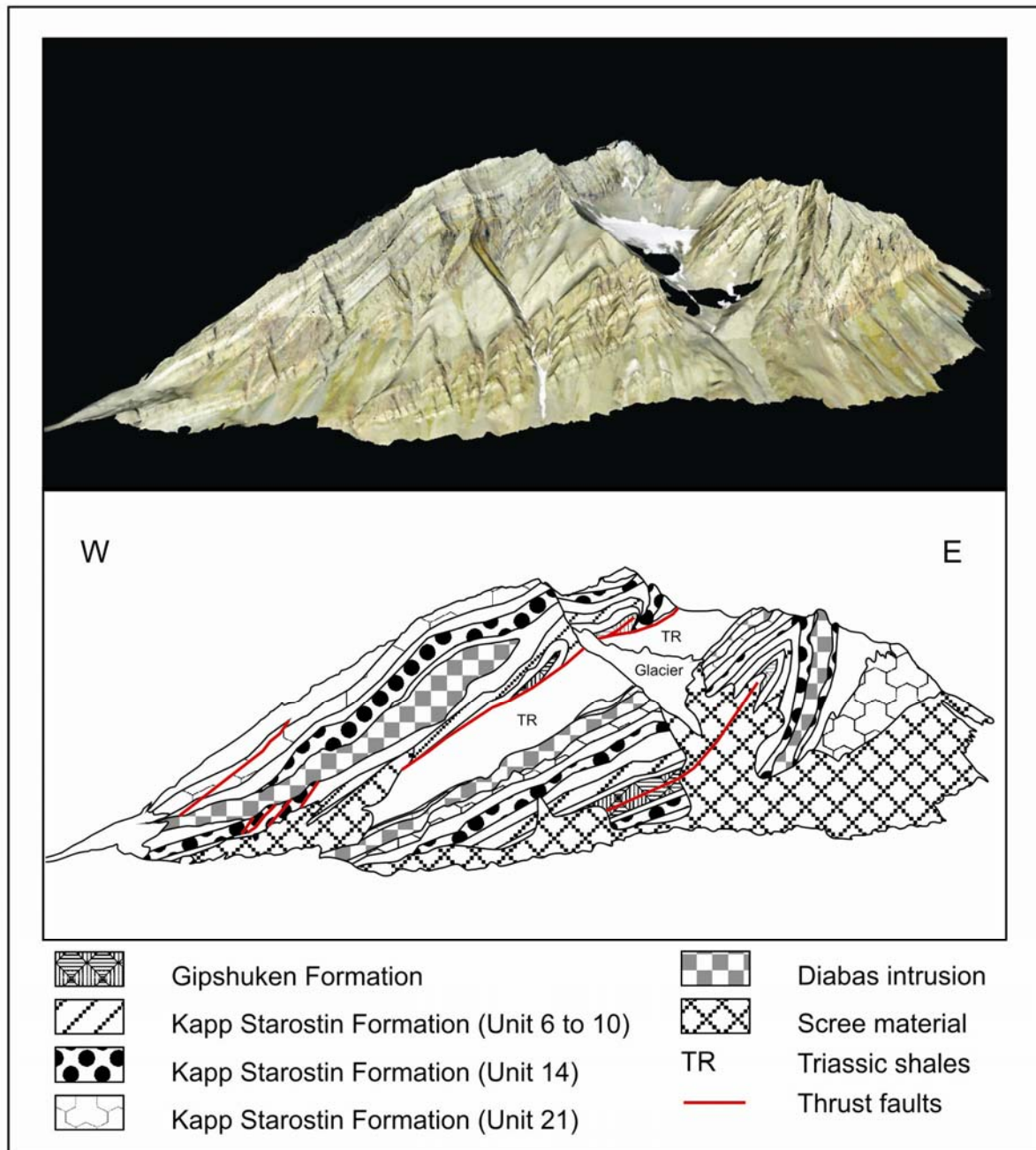


Figure 4.9: Photo textured Lidar interpretation of Mediumfjellet seen from Yoldiabukta (see figure 4.1). Subarea M2-c is to the east and subarea M3-c is to the west. Note that the Gipshuken Formation is placed on top of the Triassic shales. The M3 thrust is also slightly steeper than the M2 thrust.

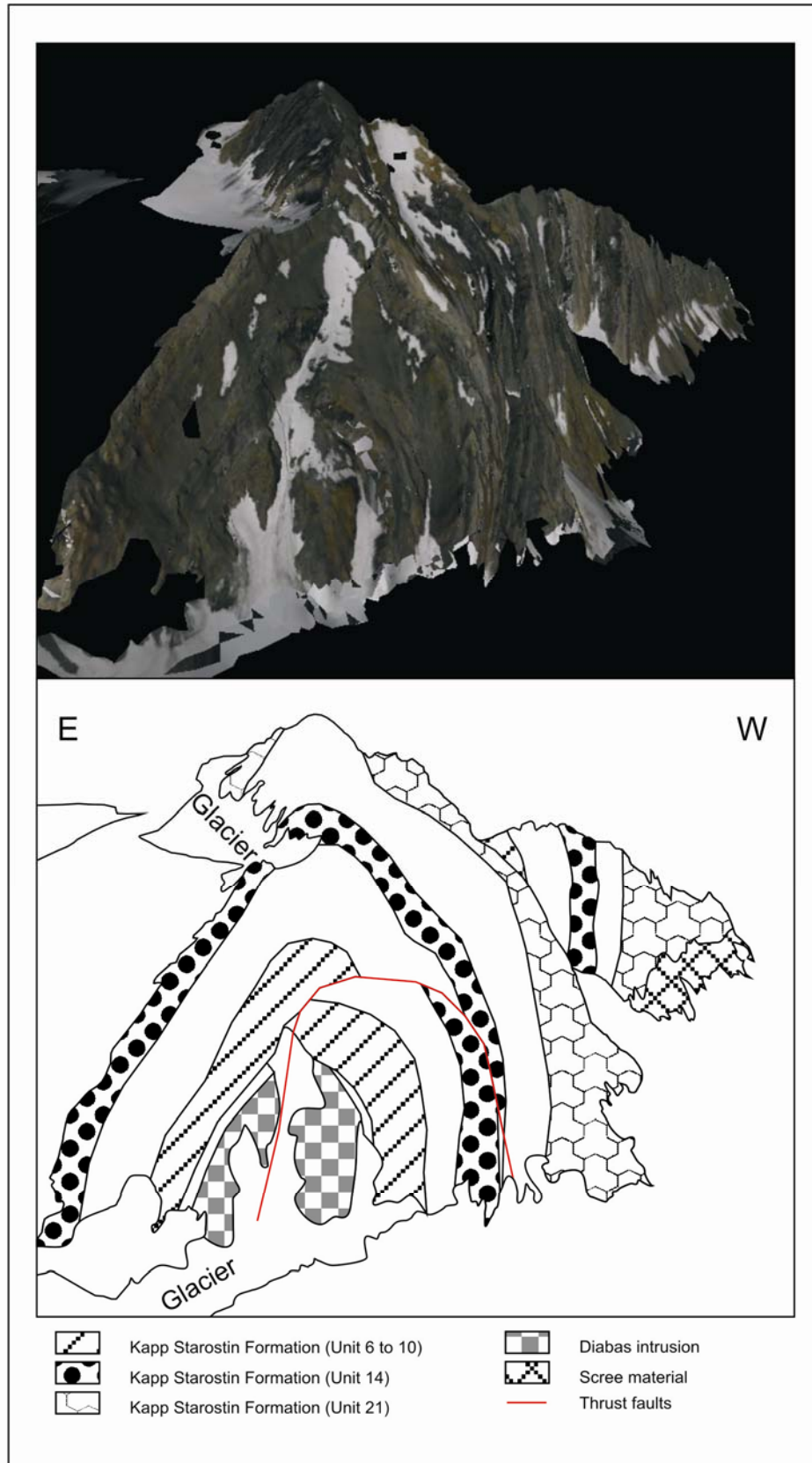


Figure 4.10: Photo textured Lidar interpretation of subarea G-a. The Gavltinden anticline is a very steep and tight fold. The continuation of the backlimb (west) can be seen in the back. Note the low-angle-to-bedding thrust that has been bent with the fold.

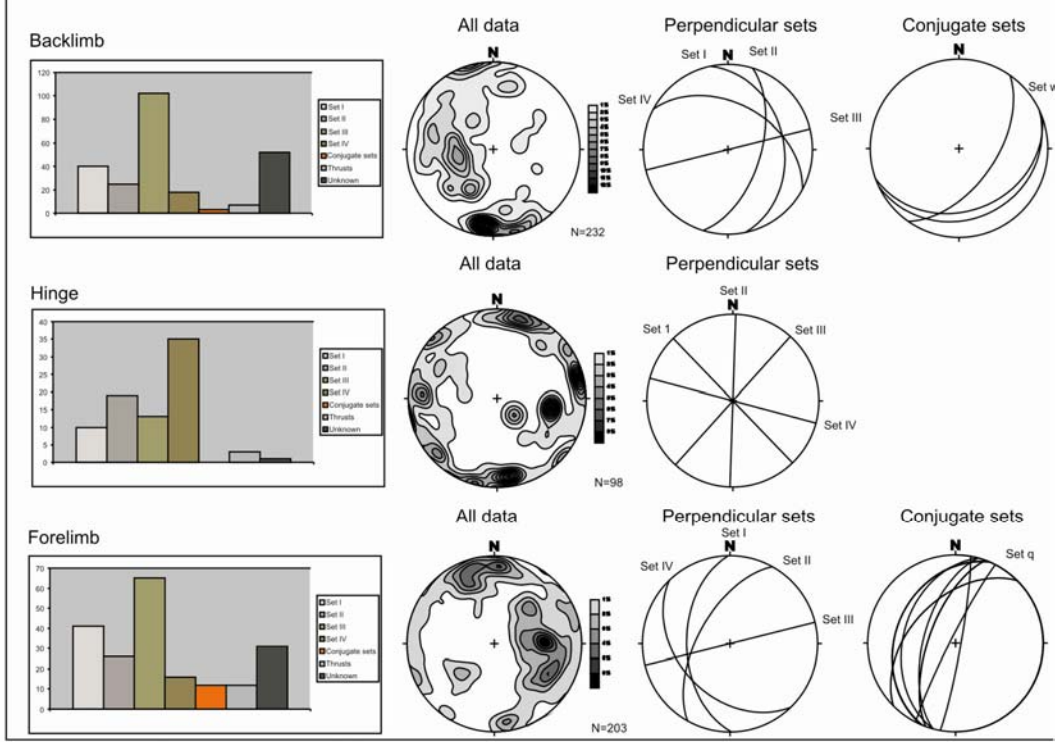
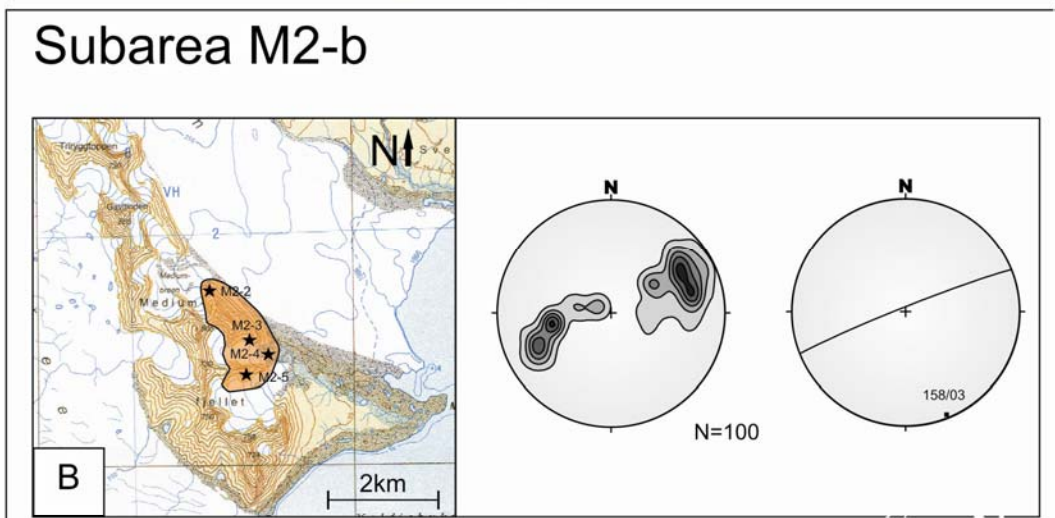
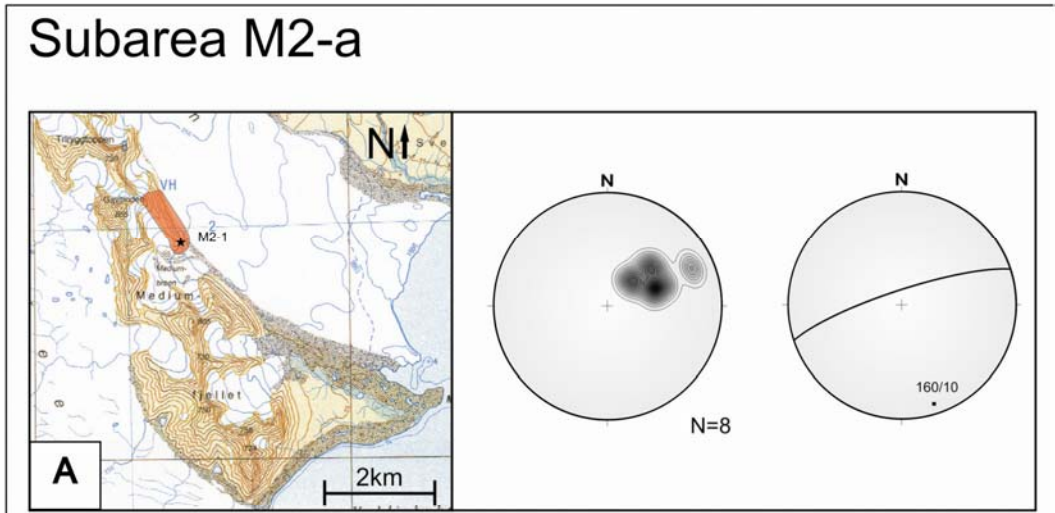
4.2.3 Summary of fold-and-thrust domains

This section summarizes the description of fold-and-thrust geometries written in the previous section, with focus on the local variations. The Mediumfjellet mountain area is split into four thrust domains (M1, M2, M3 and G), with associating hanging wall anticlines (M2, M3, and G). The shape and orientation of the anticlines vary laterally, to some extent. The M2-anticline is not completely exposed to the north, however in the subarea M2-b the fold is relatively tight, and only locally overturned, where the fold axis strikes NNW-SSE. Southwards, the fold axis is rotated clockwise and strikes N-S. The fold is very tight and overturned, indicating less displacement. The anticline seems to be situated on a relative flat footwall thrust (figure 4.2; figure 4.8). The M3-anticlines are well exposed along strike. The fold seems to be small and tight in the north, developing into a major anticline at subarea M3-b, and again developing into two smaller tight and overturned anticlines in the south (figure 4.2). The fold axis is similar to the M2-anticlines, slightly rotated clockwise southwards. The Gavltinden anticline is extremely tight and based on the 3D model the anticline is clearly cut off both in the backlimb and forelimb, which are proves for an out-of-sequence thrust. The Gavltinden anticlinal can not be followed laterally.

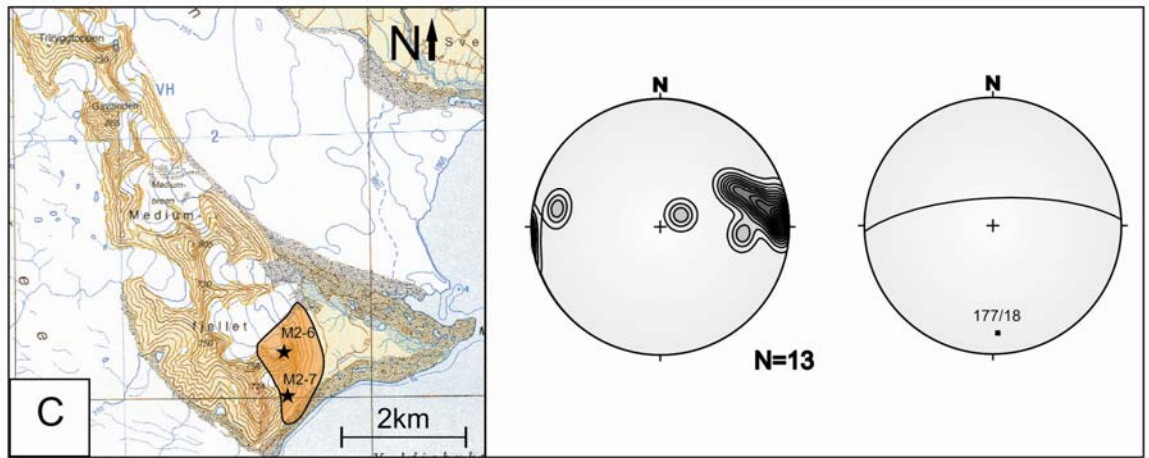
The thrust geometry is summarized by figure 4.8B, which implies great lateral variations. The M1-thrust is poorly exposed and is only assumed to exist. However, the M2-thrust is documented and can be followed laterally. This thrust slightly curves from subarea M2-b to subarea M2-c, with a relatively uniform and steep dip. Dissimilarly, the M3-thrust has greater variations along strike. Based on the 3D modelling, an oblique ramp can be seen at subarea M3-b. The thrust abruptly changes from a flat thrust at subarea M3-a, into a steep ramp at subarea M2-b. Similarly, another smaller oblique ramp is seen southwards in subarea M3-c. The M3-thrust is also in general steeper dipping than the M2-thrust. Gavltinden thrust is a steep dipping thrust, but can not be followed laterally, and thus seems to be uniform along strike. The distance between the M1-, M2-, and M3-thrust decreases southwards, where they seems to gather.

The fold plunge variations are seemingly in proportion with the lateral ramps. The M2-thrust steadily plunges to the SSE, terminating in a steep southwards plunge in subarea M2-c. In subarea M3-b, the fold plunges to the NNW relative to the oblique ramp seen in subarea M3-b. Similarly, are the two anticlines near the southern ramp both plunging against the ramp on either sides. The Gavltinden anticline steeply plunges towards NW, which may indicate a ramp or less displacement of the fold.

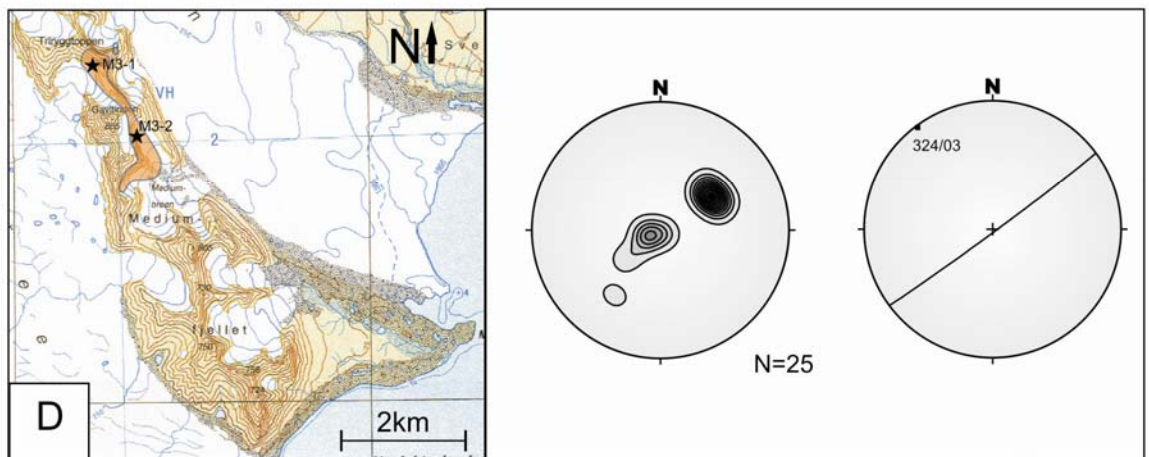
Based on the Lidar scan and the measurements of the fold geometry, two thrust segments with associating relay ramps are thought to exist along the M3-thrust. Based on observations of the two thrusts segments, a small oblique ramp in the Lidar interpretation and folds plunging towards the ramp, may be a clear indication of a thrust linkage in subarea M3-b (figure 4.1). Similarly, a larger oblique thrust ramp and fold plunge may indicate a thrust linkage in subarea M3-b. However, only one thrust has been observed. Though, an open syncline-anticline pair is found in the backlimb of the fold, and thus may indicate a thrust. Yet, the area is buried by the Mediumbreen.



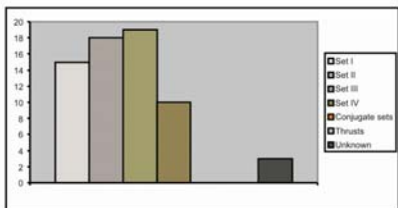
Subarea M2-c



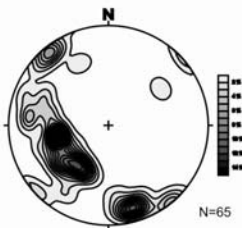
Subarea M3-a



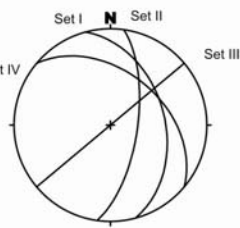
Backlimb



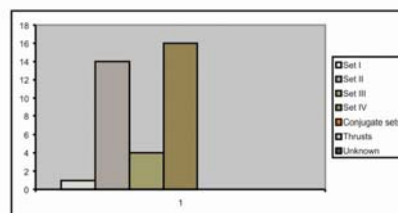
All data



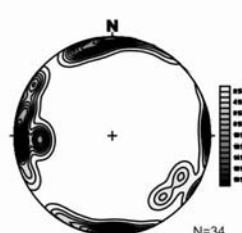
Perpendicular sets



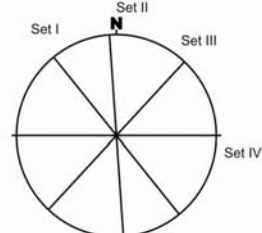
Hinge



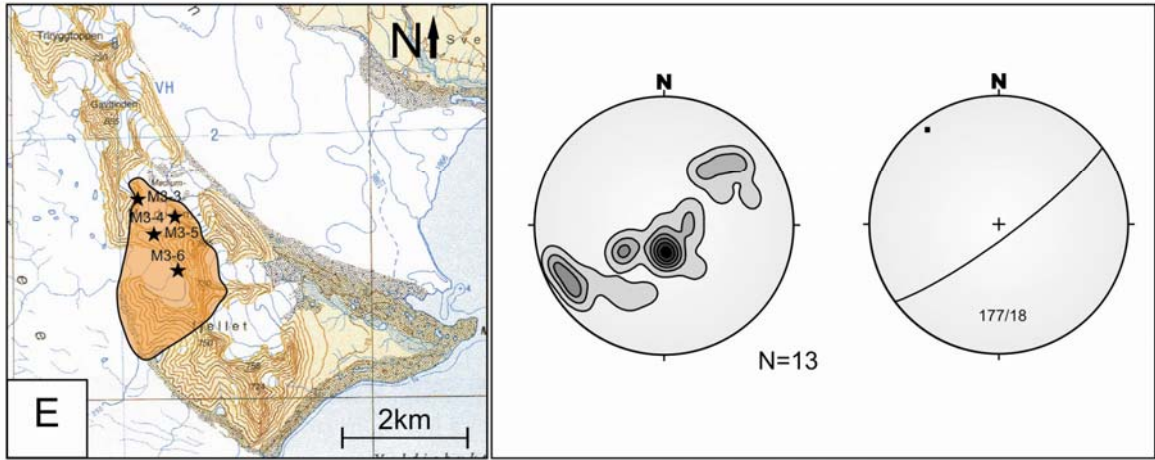
All data



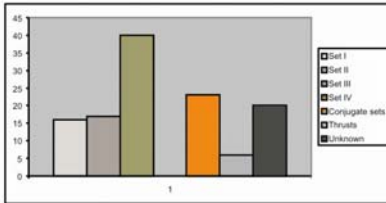
Perpendicular sets



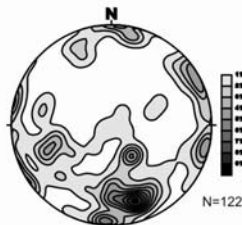
Subarea M3-b



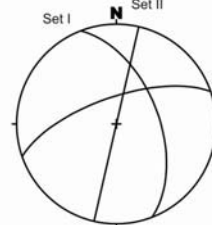
Backlimb



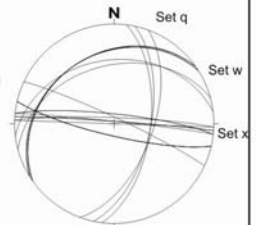
All data



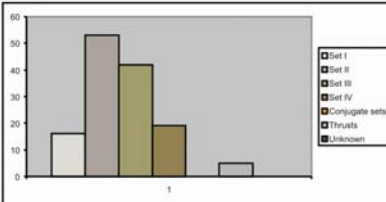
Perpendicular sets



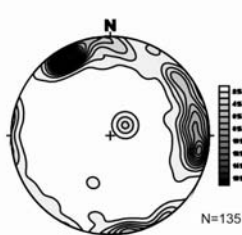
Conjugate sets



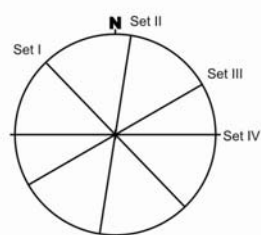
Hinge



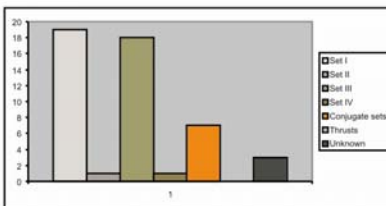
All data



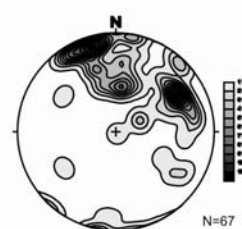
Perpendicular sets



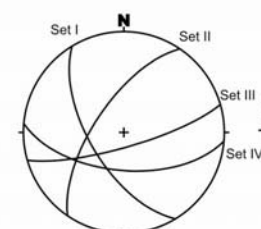
Forelimb



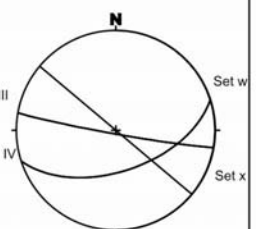
All data



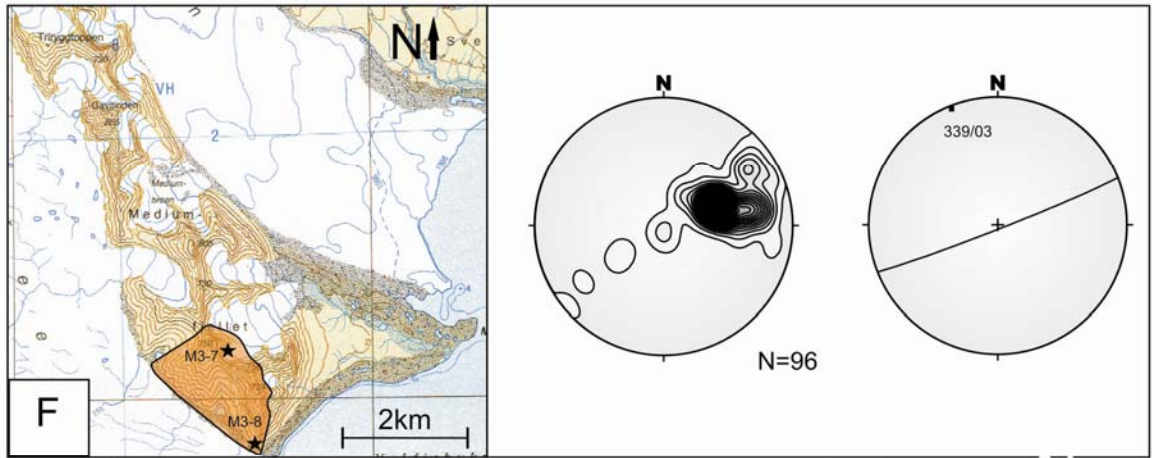
Perpendicular sets



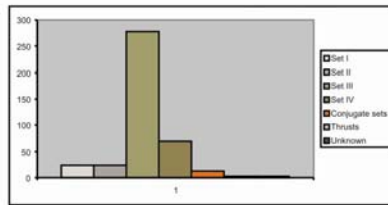
Conjugate sets



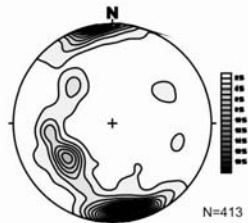
Subarea M3-c



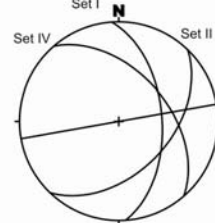
Backlimb



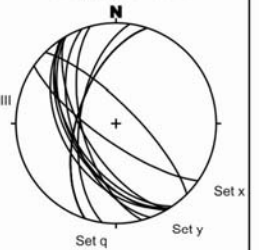
All data



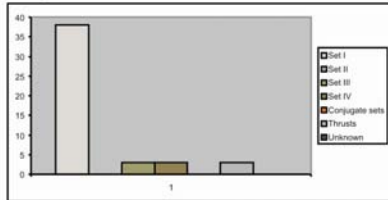
Perpendicular sets



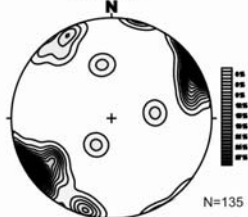
Conjugate sets



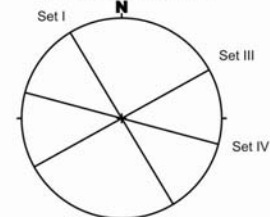
Hinge



All data



Perpendicular sets



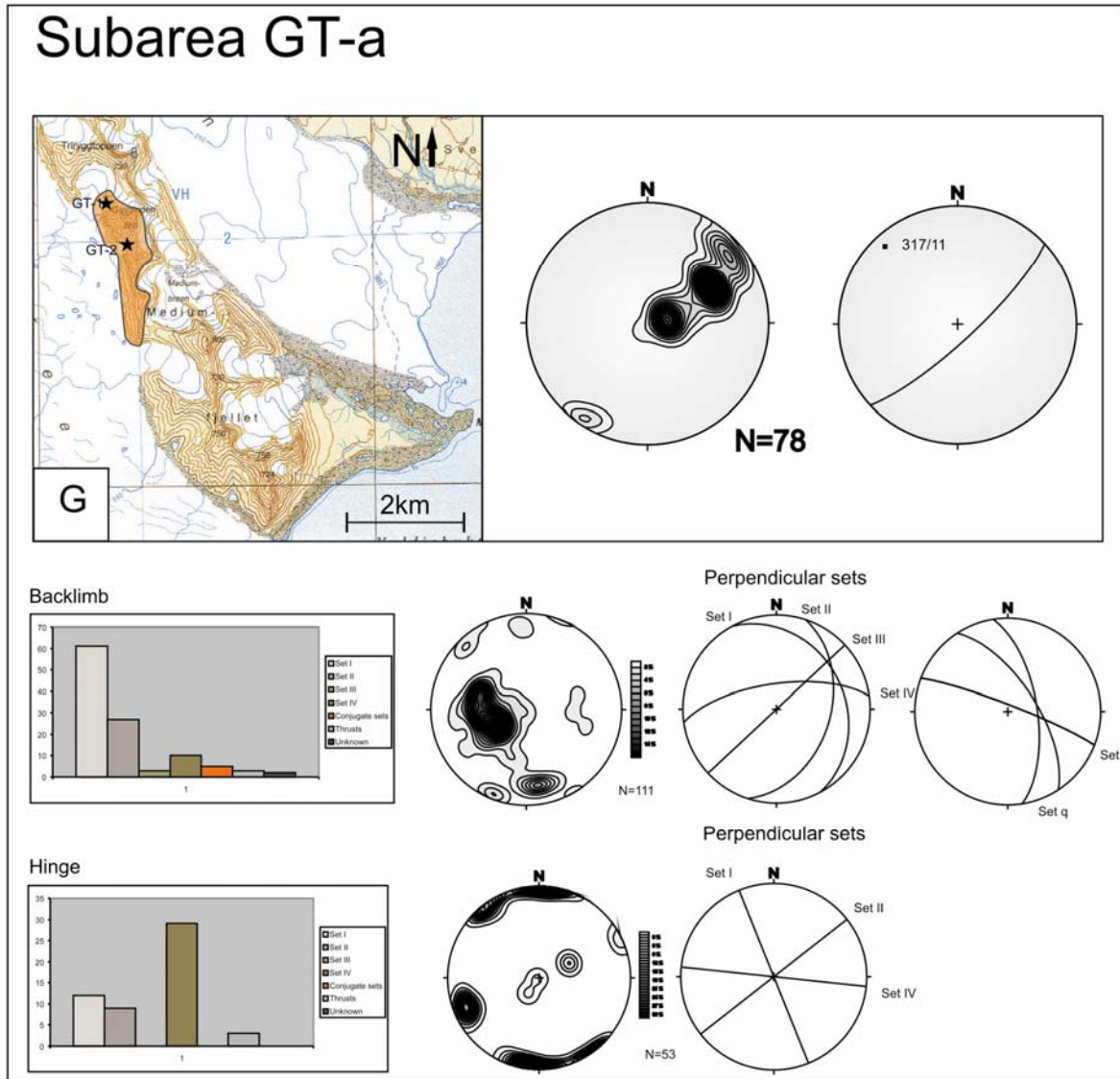


Figure 4.11: Fracture occurrence from each subarea. Each figure displays the map with the current subarea and localities. The contoured poles of the bedding orientation and the best fit great circle with associating π -point are placed next to the map. The fracture data are situated under the map and the bedding, separated by fold domains (backlimb, hinge and forelimb). The diagram to the left show the distribution between the different fracture sets. The contoured poles of all the fracture orientations are displayed in the middle. The perpendicular sets and conjugate sets are shown to the right. A: subarea M2-a. B: subarea M2-b. C: subarea M2-c. D: subarea M3-a. E: subarea M3-b. F: subarea M3-c. G: subarea G-a.

4.3 Description of fractures in domains and subareas

This chapter will explain the distribution of fractures at the Mediumfjellet. The fractures are split into three populations, where each individual fracture population is explained separately. Perpendicular fractures are perpendicular to bedding, conjugate sets are here explained as steep dipping to the strata with crosscutting relationship, and thrusts are fractures appearing low-angle to the bedding (figure 4.12). The thrust fractures consist of fractures occurring within the scan-line or fractures observed elsewhere in the study area.

4.3.1 Subarea M2-b

The fractures measured in subarea M2-b are mainly perpendicular fracture sets. Conjugate fracture sets and low-angle-to-bedding-thrust fractures. Populations of fractures that appear in an unsystematic fashion without a logical explanation are also present (mentioned in figure 4.11 as “unknown fractures” in the fracture distribution diagram).

Perpendicular fractures

Fractures were measured on the backlimb strata of the macro-folded Kapp Starostin Formation units 3, 4, 7, 10 and 21 (figure 3.1; table 4.1), which dips about 30° SW. The recorded fractures comprise four major orientations; each defining a separate fracture set (I-IV) (figure 4.11). All fractures are oriented perpendicular to the bedding surface. Sets I, II and IV are steep and sub-vertical to the bedding orientation, and strikes between NW-SE and NNE-SSW. Set I is parallel to the fold axis which strikes NNW-SSE, while sets II and IV may represent conjugate sets striking NNE-SSW and NW-SE with the acute, bisecting angle nearly parallel to the fold axis. Set III strikes ENE-WSW and is made up of steep to subvertical fractures that are oriented perpendicular to the fold axis. Sets I and III are the most frequently occurring fracture sets (figure 4.11).

Similarly, the hinge zone of the major fold contains four main fracture sets. Set I strikes NNW-SSE and is parallel with the fold axis, set II strikes N-S, set III strikes NE-SW and is perpendicular to the fold axis, and set IV strikes WNW-ESE. All these fracture sets are steep, sub-vertical and oriented perpendicular to sub-horizontal bedding planes of the fold hinge zone. Set II and IV are apparently conjugate sets with the acute angle parallel to the fold axis and occur more often than set I and III (figure 4.11).

The forelimb region of the macro-fold has similar fracture orientations as the backlimb. The overall dips of the investigated beds are about 45° to the ENE. In this portion of the fold, set I strikes NNW-SSE, set II strikes NNE-SSW, set III strikes WSW-ENE and set IV strikes NW-SE. All four sets are perpendicular to the bedding. Set I is near parallel to the

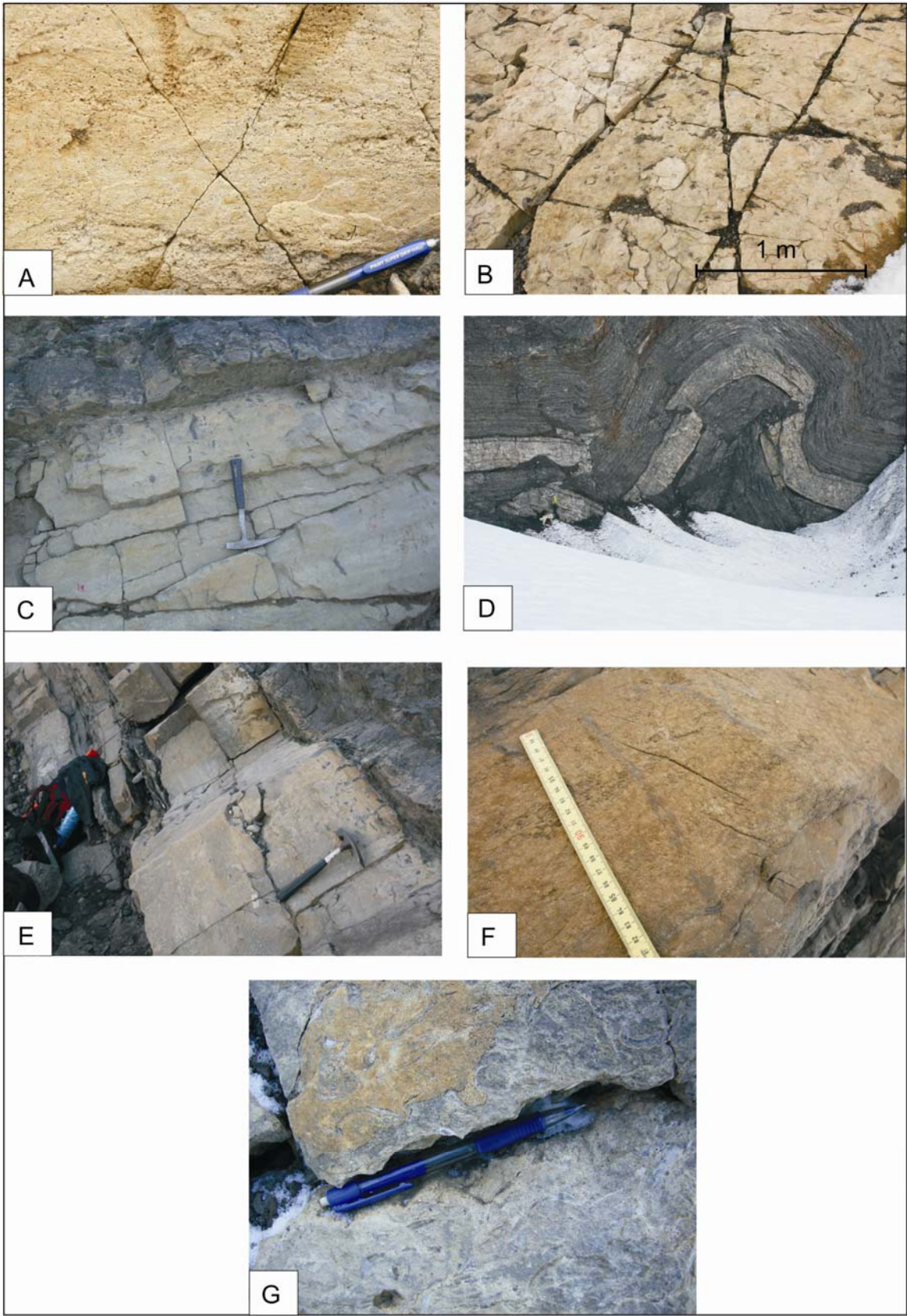


Figure 4.12: Fractures. A: A conjugate fracture set with the acute bisecting angle perpendicular to the bedding. B: Dilatational fractures and shear fractures perpendicular to bedding. C: Low-angle to bedding fracture.

Crosscutting perpendicular fractures. D: Low-angle to bed fractures (thrust) in the fold core in subarea M2-c. E: Smooth and straight fractures. F: En-echelon fractures. G: Roughed fracture surface.

fold axis while set III is almost perpendicular to the fold axis. Set II and IV are apparent conjugate sets with the acute angle parallel to the fold axis. Fracture sets I and II occur most frequently in the forelimb (figure 4.11). Similar fracture set were found in the lidar scan (figure 4.14).

The fractures measured in this subarea are straight and mostly cut through the whole bed. They commonly terminate at the bed boundaries, but some are throughgoing. The fracture surfaces are planar and smooth (common), rugged (less common) or calcite filled (rare).

Conjugate fractures

The apparent conjugate fractures with the acute angle symmetric around the c-axis (perpendicular to the bedding) (figure 2.4A; Hancock, 1984), were also observed in subarea M2-b. The backlimb consist of one set (set **w**) that strikes ENE-WSW. Similarly, the hinge consists of one set (set **q**), which strikes NNE-SSW. Both these fractures have a crosscutting relationship and dip steeply with an average dip of 70° to opposite sides (SE and NW) (figure 4.12). The fractures show no displacement to mm-scale displacement and are normally smooth, but may also be rugged (figure 4.12).

Thrusts

Several low-angle thrusts cut up-section through the Kapp Starostin Formation with displacements between 5 and 20 meters. These thrusts have accompanying fracture sets with similar orientations. Based on their field-site orientation (present orientation) there seems to be several sets with different orientations. In the backlimb, there are three main sets; set A strikes NNE-SSW, set B strikes WNW-ENE and set C strikes NNW-SSE. In the hinge, there is one major fracture set (set A) that strikes NNE-SSW, and in the forelimb there is one set (set C), which strikes NW-SE (figure 4.13). They all dip with an average angle of about 30° to the bedding. Both fore- (east-directed) and back-thrusts (west-directed) are present. The two sets are tentatively conjugate sets with the acute bisecting angle parallel to the bedding. In order to further consider if these sets of fractures developed prior to folding, the thrust orientations have been restored by unfolding the layering back to horizontal. The restored thrusts show three different fracture sets; Set A strikes NNE-SSW, set B strikes E-W and set C strikes NNW-SSE (figure 4.13). Some of the thrust faults cut stratigraphically up-section to the Triassic shales, while others end in small fault-propagation folds, indicating that they are

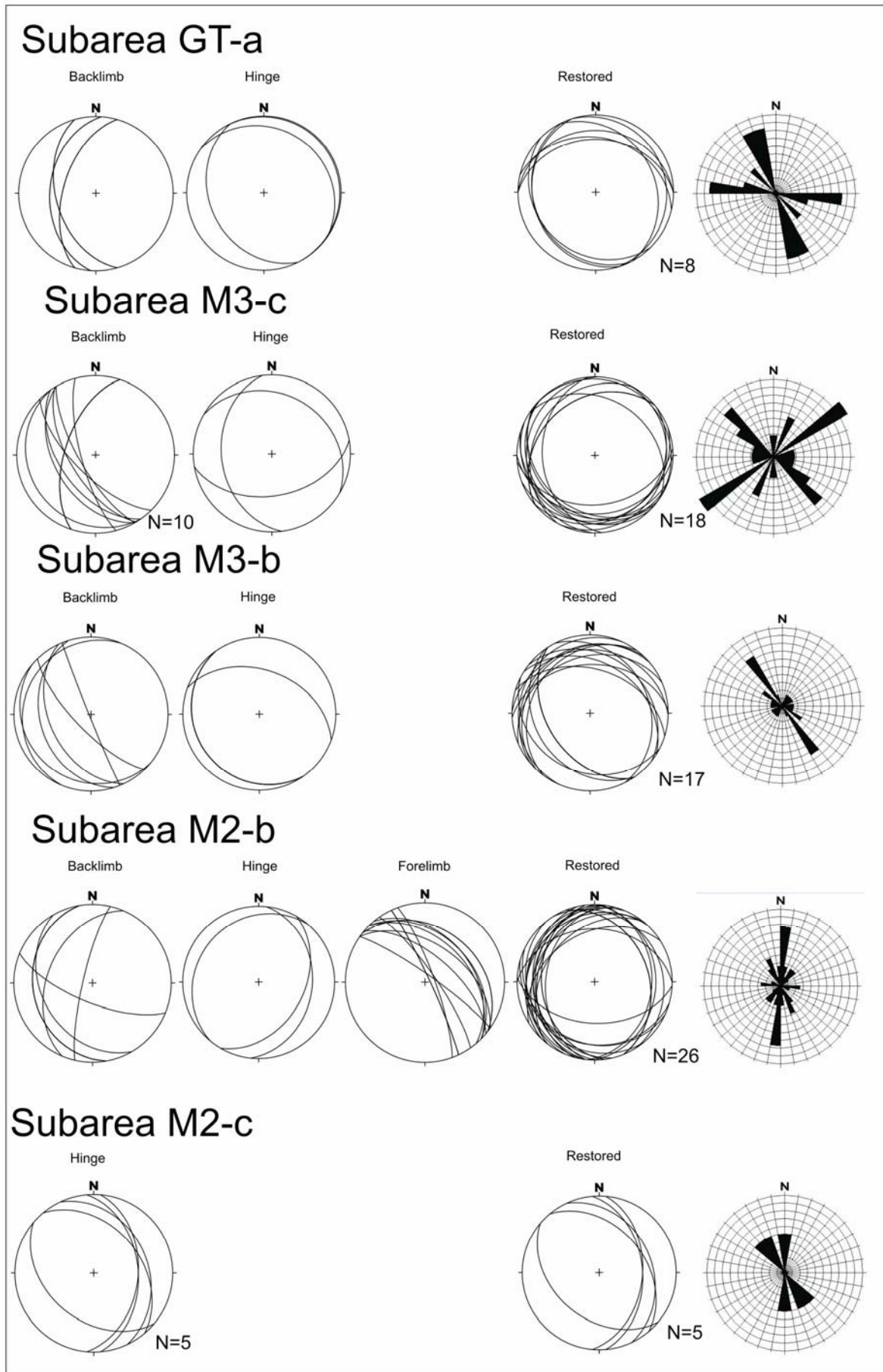


Figure 4.13: Low-angle to bed fractures (thrusts). The three left rows represent thrusts in present position in the backlimb, hinge and forelimb. The two rows to the right represents the thrusts which are restored with the bedding back to horizontal.

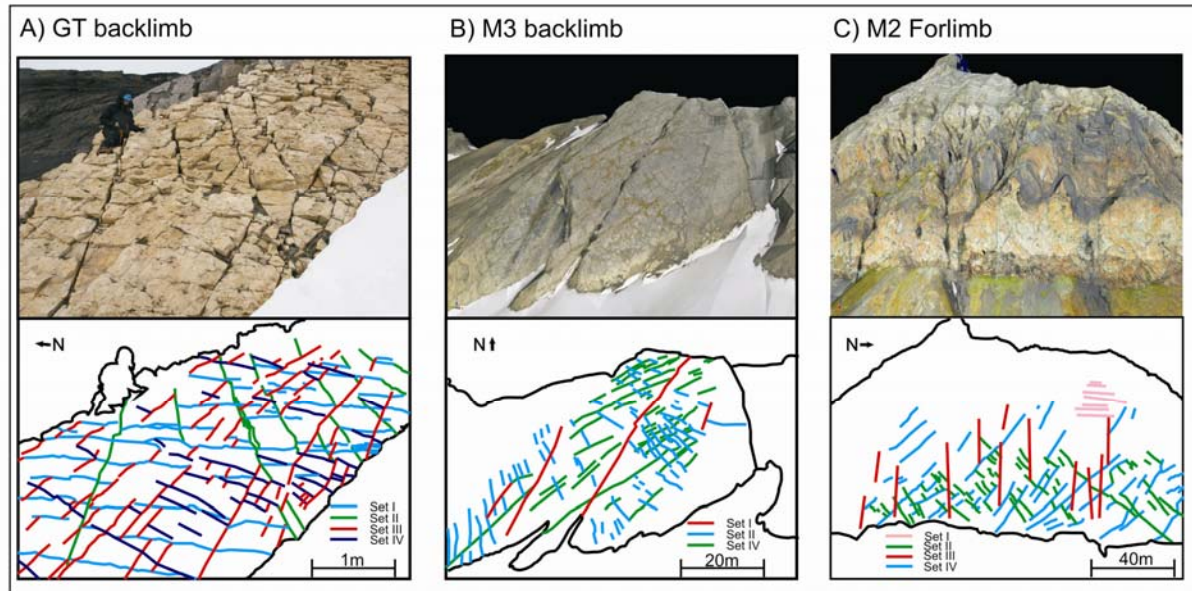


Figure 4.14: Fractures interpreted on bedding surface. A: Fractures interpreted from a photograph taken in field in subarea G-a. B: Fracture sets interpreted of the surface from lidar scans in subarea M3-b. C: Also fractures interpreted from lidar scans in subarea M2-c.

local, as low-angle (to bedding) thrusts. The thrust faults and associated fractures are normally filled with calcite and many display surfaces with slickensides.

4.3.2 Subarea M2-c

Perpendicular fractures

Fractures of subarea M2-c were not measured in the field, due to inaccessible steep cliffs, but were interpreted from the Lidar scan data (figure 4.14). Four sets are visible in the Lidar scans. Set I strikes N-S, set II strikes NE-SW, set III strikes E-W, and set IV strikes NW-SE. Set I is parallel and set III is perpendicular to the fold axis. Sets II and IV seem to be a conjugate pair with the acute angle parallel to the fold axis. The fracture sets are apparently perpendicular to the bedding surface. Set I consist of major throughgoing fractures that locate deep cuts and eroded valleys into the mountainsides. These fractures have greater spacing between them commonly in the range of meters. Sets II and IV seem to be the most common fractures. Their distribution and orientation vary with the acute angle either parallel or perpendicular to the fold axis (Figure 4.14).

Thrusts

Subvertical thrusts cut steeply dipping beds with a low angle to the bedding in the backlimb of the major anticline. Several small thrusts are also seen in the core of this major M2-fold. These thrusts were measured and comprise mainly one set (set C) that strikes NW-SE (figure 4.12; figure 4.13). These thrusts have not been restored because the bedding is near horizontal where the thrusts were measured.

4.3.3 Subarea M3-a

The fracture distribution in subarea M3-a is mainly dominated by perpendicular fracture sets (figure 4.11D). In addition, there are some non-systematic fractures that occur in the backlimb.

Perpendicular fractures

The fractures in subarea M3-a were measured in unit 10 and 21 of the Kapp Starostin Formation (figure 3.1, table 4.1). The backlimb bedding dips about 40° to the WSW where the fractures have been collected. A fracture pattern similar to the fractures collected in subarea M2-b was found. Set I strikes NNW-SSE (near parallel to the fold axis), set II strikes NNE-SSE and set III strikes NE-SW (the two latter sets are perpendicular to the major fold axis), and set IV strikes NW-SE. All fracture sets are steep to sub-vertical relative to the bedding. Set II and IV are apparent conjugate sets with the acute bisecting angle parallel to the fold axis. The dominating fracture sets are I, II and III, however, the pattern of fracture occurrence for each set seems to be similar to the forelimb of subarea M2-b, where set I and II are dominating (figure 4.11).

Mainly two major fracture sets (set II and IV) were found in the hinge zone of the macroscopic fold, but another two less pronounced sets have been identified. The sets are all steep to subvertical to the bedding that dips on average 40° to the ENE. Set II strikes N-S and set IV strikes E-W. There is an indication of set I, striking NW-SE parallel to the fold axis, and set III, striking NE-SW perpendicular to the fold axis. Both sets have subvertical fractures. Sets I and IV are seemingly conjugate sets, where the bisecting axis strikes parallel to the fold axis. Set II and IV are numerous and dominate the fracture occurrence in the hinge zone (figure 4.11).

Fractures of subarea M3-a are usually open, straight and planar shaped. They are commonly smooth but also locally occur as rugged. Either conjugate fracture sets or thrust sets were measured in this subarea.

4.3.4 Subarea M3-b

The fractures are distributed between the different populations. All sets and populations occur within subarea M3-b (figure 4.11E).

Perpendicular fractures

Fractures were measured in the backlimb unit 21 of the Kapp Starostin Formation. Similarly unit 2, 3 and 4 were studied in the backlimb hinge and forelimbs (figure 3.1, table 4.1). These fracture sets partly differ in geometry and orientation from fractures in the other subareas (figure 4.11).

The backlimb bedding dips on average 45° to the SW. It reveals three major fracture sets. Set I strikes NNW-SSE and is parallel to the fold axis, set II strikes NNE-SSW, whereas set III strikes ENE-WSW and is perpendicular to the fold axis. All three sets are perpendicular to the bedding. Set II is absent (figure 4.11).

The bedding of the hinge zone is subhorizontal and reveals four major fracture sets. Set I strikes NW-SE, set II strikes NNE-SSW, set III strikes NE-SW, and set IV strikes ENE-WSW. They are all steeply dipping and subvertical. Set I is parallel and set III is perpendicular to the fold axis. Sets II and IV seem to be a conjugate pair with the acute angle perpendicular to the fold axis (figure 4.11).

The bedding in the forelimb has an average NW-SE strike and dip angle of about 70° to the NE. The forelimb consists of similar fracture sets as the backlimb. Set I strikes NW-SE, set II strikes NNE-SSW, set III strikes ENE-WSW and set IV strikes ESE-WNW. Set I is parallel and set III strikes perpendicular to the fold axis, whereas set II and set IV are apparent conjugate sets with the bisecting acute angle perpendicular to the fold axis (figure 4.11). Compared to the lidar interpretation of fractures, similar sets can be found (figure 4.14). All three sets cut steeply and are perpendicular to the near-horizontal bedding.

The majority of the studied fractures are open and planar, cutting through the whole bed. Throughgoing fractures that cut several beds are common, especially in the forelimb. A few fractures are rugged or listric shaped, bending off towards the bed boundaries. No fractures have calcite filling.

Conjugate fractures

Steeply dipping conjugate sets with their acute angle perpendicular to bedding were found both in the backlimb and hinge. Three steep angle fracture sets have been measured in the backlimb, where set **q** strikes NNE-SSW, set **w** strikes ENE-WSW and set **x** strikes ESE-

WNW. Similar fractures were found in the forelimb, where set **w** strikes ENE-WSW and set **x** strikes ESE-WNW. They all dip steeply with an average angle of about 70° in proportion to the bed orientation. En-échelon fractures were observed in the backlimb at locality M3-3 with (set **q**) NE-SW strike, dipping 30° to NW (figure 4.12).

Thrusts

Several small-scale thrust faults or imbricate thrusts are seen in the backlimb, hinge and forelimb of the Kapp Starostin Formation strata, similar to those mentioned for subarea M2-b. Several of the thrust faults end blindly in folds. In particular, one meso-scopic fault-propagation fold with related minor thrust faults is observed (figure 4.8D). The faults have a common planar geometry and easterly transport direction, and on either limb of the macro-fold they seem to be rotated within the major fold (figure 4.7). In present position there are two sets in the backlimb; set A strikes to the NNE-SSW and set C strikes to NW-SE. The hinge comprises only one set; set C strikes NW-SE. All sets cut the bedding with a low angle. In this case as well, these thrust faults have been restored through rotating the bedding back to horizontal. In restored position, set A strikes NE-SW and set C strikes NW-SE. They appear as both fore- and back-thrusts, and may therefore represent conjugate sets with the bisecting acute angle parallel to the bedding (figure 4.13).

4.3.5 Subarea M3-c

The fracture distribution consists mainly of perpendicular fracture sets, but also thrusts and conjugate fractures occur (figure 4.11F).

Perpendicular fractures

Units 3, 5 and 10 (figure 3.1, table 4.1) were studied for fracture measurements in the Kapp Starostin Formation. Four fracture sets were recognized in the backlimb (figure 4.11F); Set I strikes NNW-SSE (parallel to the fold axis), set II strikes NNE-SSW, set III strikes ENE-WSW and (perpendicular to the fold axis), and set IV strikes to the NW-SE. All sets dip steeply and are nearly perpendicular to the bedding plane, which has an average dip of 60° to the SW. Set II and IV seem to be apparent conjugate fracture sets with the acute bisecting angle parallel to the fold axis.

Three fracture sets are found in the hinge; set I strikes NNW-SSE and is parallel to the fold axis, set III strikes ENE-WSW and is perpendicular to the fold axis, set IV strikes ESE-WNW. Set II is absent. All fractures are perpendicular to the bedding, which is sub-

horizontal. In light of observations from other subareas, set IV may be part of a conjugate fracture set (with set II) (figure 4.11).

Fractures observed in field are for the most part straight, planar and open. Throughgoing fractures cutting through several beds are abundant in the forelimb, but are rare in the hinge and backlimb. Calcite filled fractures occur infrequently.

Conjugate fractures

Conjugate fractures with the acute bisecting angle perpendicular to the bedding were measured in the backlimb. Two fracture sets were found; set **q** strikes NNE-SSW whereas set **x** strikes NW-SE. They both dip steeply with the average dip between 65°-80° to the bedding (figure 4.11). The fractures show commonly a smooth surface, but are also sometimes rough. They are layer bound and in many cases terminate within the bed.

Thrusts

Similarly to subarea M3-b, several meso-scopic imbricate thrusts cut the backlimb, hinge and forelimb of the major fold. In this subarea the thrust faults produce complex structures in the forelimb and hinge zone, e.g. a duplex is observed in the backlimb (figure 4.9). The thrust faults indicate in present position that two sets exist in the backlimb and two sets in the hinge. In the backlimb set A strikes NNE-SSW and set C strikes NW-SE. In the hinge set B strikes E-W whereas set C strikes NNW-SSE. These thrusts all dip with a low-angle to the bedding. When the thrusts are restored with the bedding back to horizontal, two sets are prominent. Set A strikes NE-SW and set C strikes NW-SE. (figure 4.13). Calcite filling and slickensides are often found on the shear fracture surfaces (faults). Two slickensides were measured, and both show the displacement towards NE.

4.3.6 Subarea G-a

Most fracture populations are present at subarea G-a (figure 4.11G). However, the perpendicular fractures are more numerous.

Perpendicular fractures

Fracture data have been measured in units 7 and 10 (figure 3.1, table 4.1) of the Kapp Starostin Formation. The bedding in the backlimb is in average dipping 50° to the SSE, and in this limb four main fracture sets were found. Set I strikes NNW-SSE and is parallel to fold axis, set II strikes NNE-SSW, set III strikes NE-SW and is perpendicular to fold axis, and set IV strikes ENE-WSW. All fracture sets are oriented perpendicular to the bed surface. Set III

and set IV are apparent conjugate sets. Fractures interpreted on photographs taken in the field show the same pattern as for the dataset on measured fractures (figure 4.11; figure 4.14).

The hinge zone shows three fracture sets that are all sub-vertical to the sub-horizontal bedding. Set I strikes NNW-SSE and is parallel to the fold hinge, set II strikes NE-SW, and set IV strikes E-W. Set III is absent. Sets III and IV have a slightly different strike compared to other subareas. Further they are probably conjugate sets with the acute angle nearly perpendicular to the fold axis (figure 4.11).

Fracture sets measured in this subarea are similarly oriented to the sets observed elsewhere. Their character is also similar in that they are open, planar, and straight fractures. Some are rugged, but they are most often smooth. Throughgoing fractures are less common than short fractures terminating at the bed boundaries.

Conjugate fractures

Conjugate fractures with their acute bisecting angle perpendicular to bedding are only found in the backlimb. They consist mainly of two sets; set **q** strikes NNW-SSE and set **x** strikes WNW-ESE. They cut the bedding with an average angle of 72°, and dips to the WSW and SSW (figure 4.11). These fractures are mainly smooth, but can also be rugged. The fractures are rarely throughgoing.

Thrusts

The low-angle-to-bedding thrust faults crosscutting the beds of Kapp Starostin Formation are here found to have a slightly different strike compared the other thrust domains. The sets seem similar, but are possibly oriented clockwise with approximately 40°. In the present fold-position, the backlimb and hinge each consist of one fracture set. The backlimb comprises set A that strikes N-S, whereas the hinge reveals set C, which strikes NW-SE. When restored with the bedding back to horizontal position, two major fracture sets occur. Set B strikes WNW-ESE and set C strikes NNW-SSE. The fault planes are commonly throughgoing, showing displacements between 1 and 10 meters. They are usually filled with calcite and are coated slickensides. Two slickenside surfaces were measured, and associated slip-lines show displacement towards NW and WNW (figure 4.13). Evidence for a possible pre-folding stage of the thrust faults is here seen at locality GT-1, where the fault cuts through the hinge zone and is folded all the way around with the bedding, before it terminates in the backlimb (figure 4.10). Spectacular examples of such splay faults crop out near the Gavltinden peak, seen as internal deformation of the forelimb of a syncline-anticline pair (figure 4.3; figure 4.6).

4.4 Fracture intensity

This chapter presents the intensity of fracturing that has been recorded in each structural domain (forelimb, backlimb and hinge). The fracture frequency will be considered briefly and then compared with the fracture orientations. The fracture intensity depends highly on the bed thickness, and the following descriptions are made from only three subareas (M2-b, M2-c and M3-b), were the same bed and same bed thickness could be traced between the structural domains of the macro-fold (forelimb, backlimb and hinge).

A characteristic 15 cm thick bed of the Vøringen Member was followed through the backlimb, hinge and forelimb in subarea M2-b. The measurements were taken from the same bed both beneath and above the through-cutting M2-thrust (figure 4.4). When comparing the separate domains (backlimb, hinge and forelimb) above and underneath the M2-thrust, there are some differences (figure 4.15). The fracture intensity measured in the backlimb *above* the thrust is low, 6 fractures per meter. The intensity increases from 6 to 10 fractures per meters in the direction of the hinge area. In comparison, the fracture intensity in the backlimb *beneath* the thrust is higher, 13 to 20 fractures per meter. The fracture intensity in the hinge is very high; fractures are present up to 28 times per meter. The intensity of the forelimb is fairly low, with frequencies increasing from 4 to 12 fractures per meters towards the hinge zone. In subarea M3-c the fracture intensity was recorded in a bed with thickness of 53cm. The hinge zone has an average of 15 fractures per meters, and has significantly higher fracture intensity than the backlimb, which has 6 fractures per meters (figure 4.15). The fracture intensity can be compared between the hinge and backlimb of subarea M3-b, in a 32 cm thick bed. In this case the fracture data shows slightly higher frequency in the backlimb than in the hinge zone; where the backlimb has an average of 6 fractures per meter in comparison to the hinge, which has only 4, 3 fractures per meters.

Bed thickness versus fracture frequency is analyzed in figure 4.16 that shows a diagram where absolutely all the numbers of fractures per meter is plotted towards the bed thickness. The plots show linear trends, suggesting a general higher fracture intensity in the hinge zones. The backlimb and forelimb can not be clearly distinguished, because of their crossing lines, but in general display larger variations and lower intensities.

The final analysis addresses the large throughgoing fractures cut across more than one bed, compared to the short fractures terminating in the bed or at the bed boundary. When comparing fractures in the limestone with the dark spiculites (figure 3.2), the throughgoing fractures are observed with several meters spacing. When comparison is made between the

two lithologies, it is clear that 30% of the measured fractures in the carbonate beds are

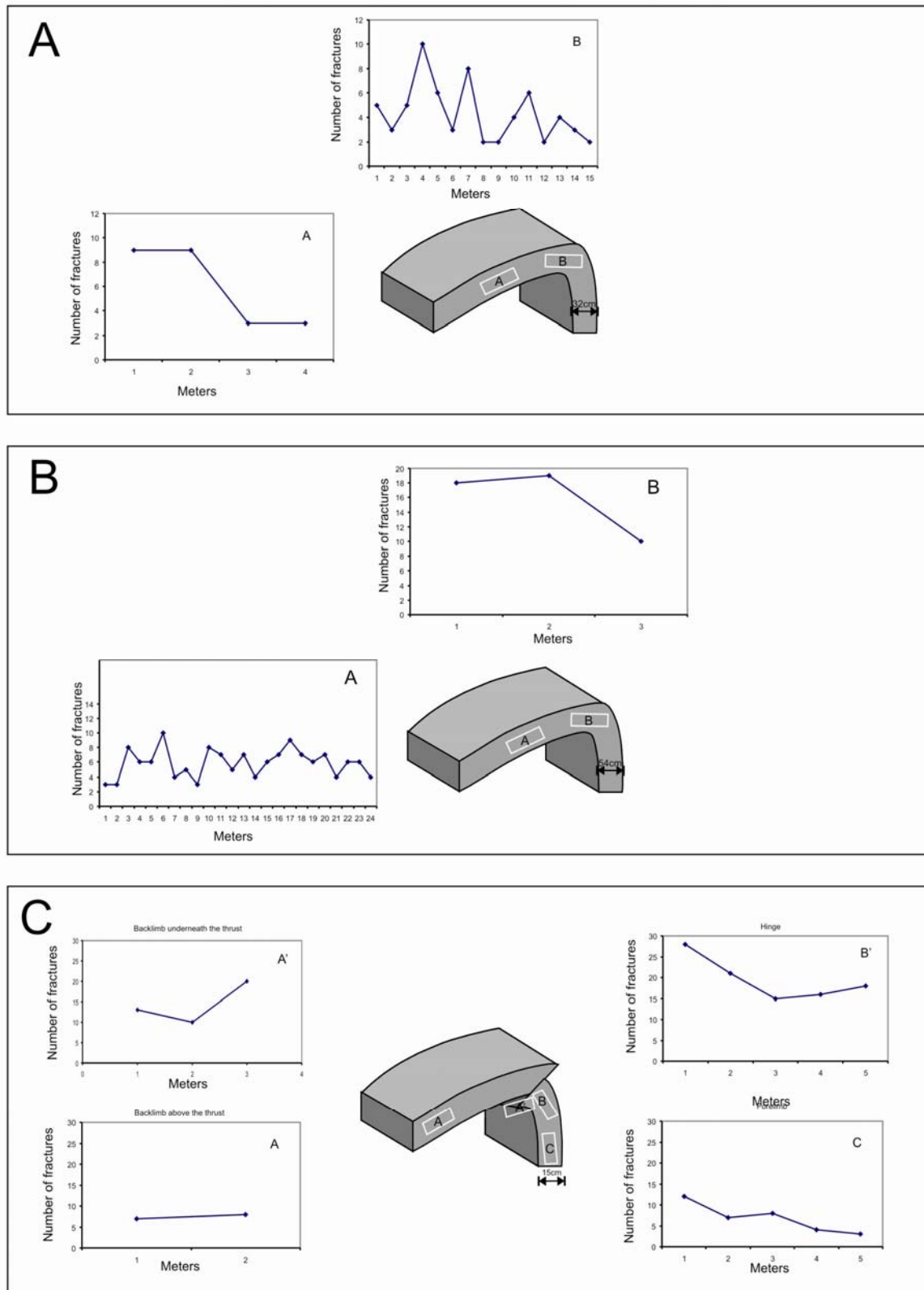


Figure 4.15: Fracture intensity measured in different fold domains by following in the same bed with the same thickness. A: A 32cm thick bed followed in backlimb and hinge in subarea M3-b. B: A 53 cm thick bed was followed through the backlimb and hinge in subarea M3-c. C: A 15cm thick bed from the Vøringen member was

measured in subarea M2-b. The bed was studied in the forelimb, hinge and backlimb underneath the thrust and in the backlimb above the thrust.

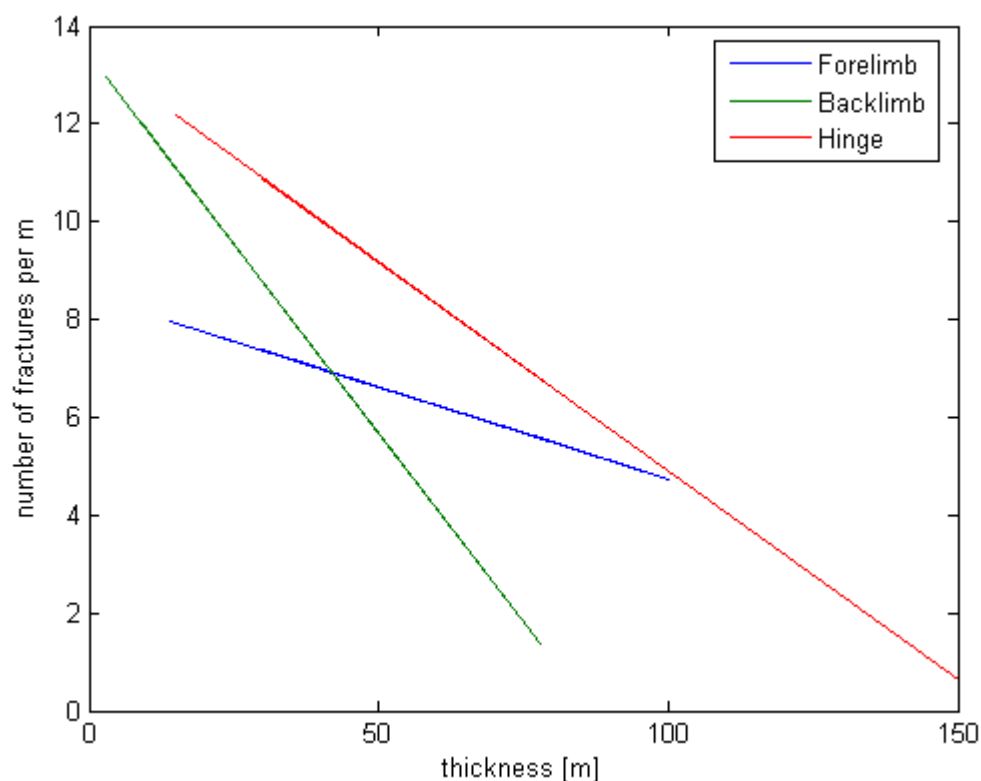


Figure 4.16: Numbers of fractures per meter versus bed thickness. All collected data are plotted. Note the red line, which shows that the hinge has overall higher fracture intensity. Mean square error of linear regressions are 16,6 (backlimb), 2,8 (forelimb) and 26,6 (hinge).

through going, however, only 4% of the measured fractures are observed to be throughgoing in the dark spiculite. The throughgoing fractures seem to have the same orientation as the short fractures. When comparing the fold domains, the throughgoing fractures constitute of all measured fractures; 31% in the backlimb, 26% in the hinge and 43% in the forelimb, whereas the short fractures comprises 69% in the backlimb, 74% in the hinge and 56% in the forelimb.

4.4.1 Tentative interpretation

Many similarities can be determined between both the thrust domains and subareas. Three fracture categories can be distinguished. On the background of these observations the following interpretations are made:

Four bedding-perpendicular fracture sets striking more or less systematic to the fold axis are found in nearly all the thrust domains; set I, II, III and IV (figure 4.17; 4.18). Set I

strikes between NW-SE and N-S and are parallel to the fold axis. These fractures are interpreted as tensile fractures within the b- and c-axis (Turner and Weiss, 1963; Hancock, 1985). However, many may have been reactivated as shear fractures (see discussion chapter 5). Set III strikes between NE-SW and E-W and are perpendicular to the fold axis. This set is interpreted to be tensile fractures within the a- and c-axis (Turner and Weiss, 1963; Hancock, 1985); again reactivation is possible. Set II strikes between N-S and NE-SW and set IV strikes between E-W and NW-SE. They are together interpreted as conjugate $hk0$ shear fractures with the enclosing acute angle perpendicular or parallel to the b-axis (Price, 1967; Hancock 1985).

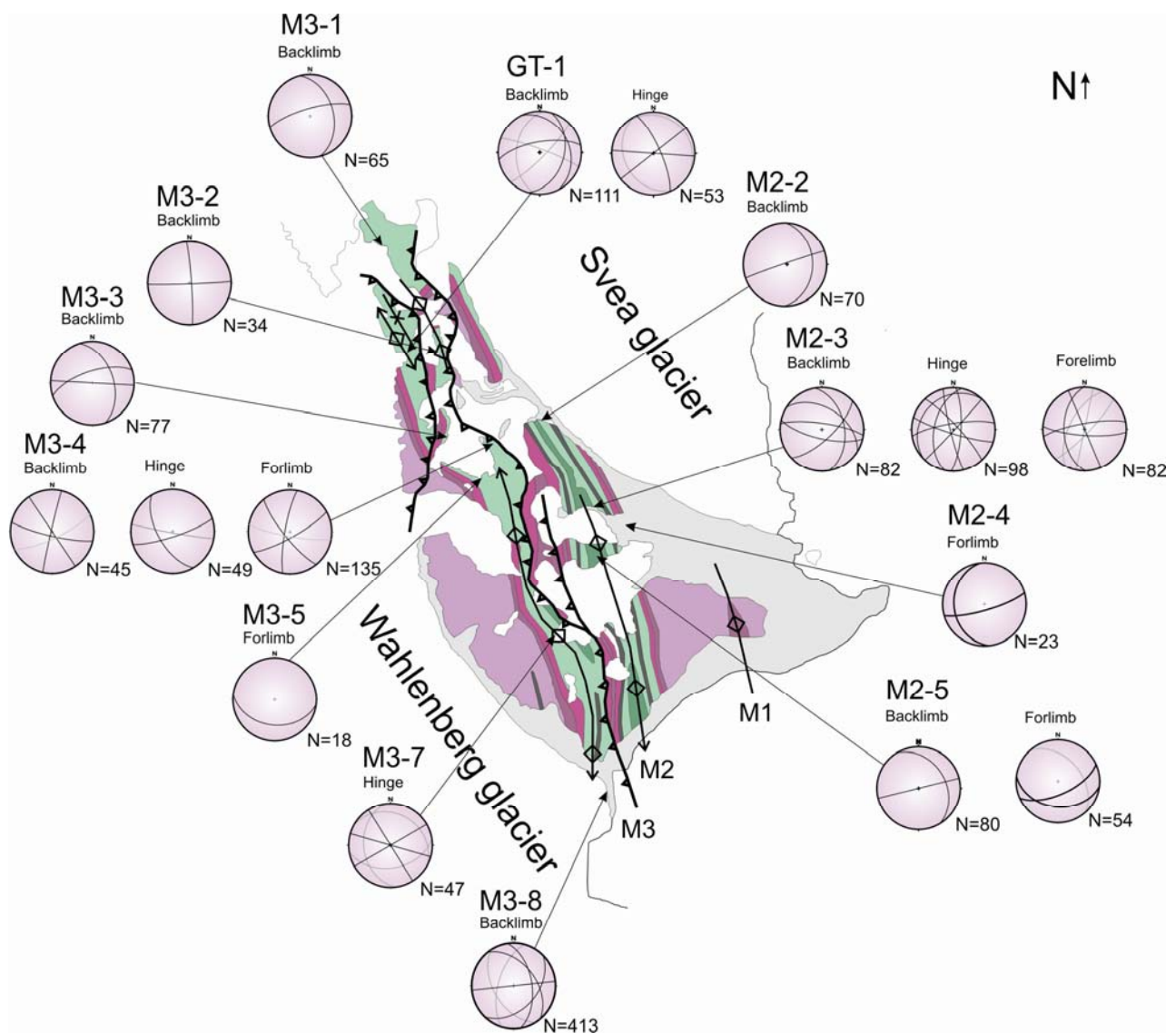


Figure 4.17: Along-strike variations showing the dominating sets including all populations. See figure 4.1 for legend of bedrock map.

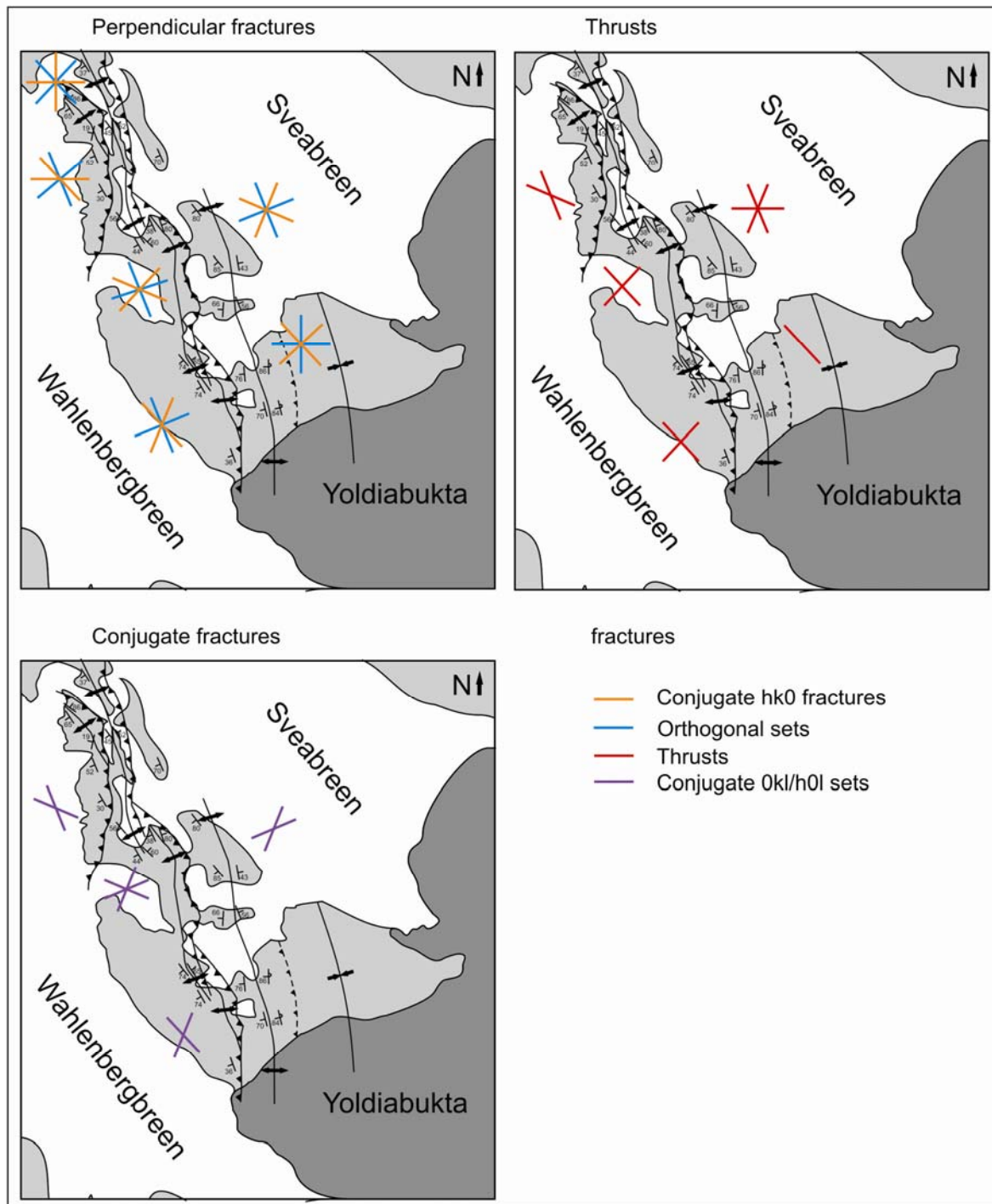


Figure 4.18: An overview map of the Mediumfjellet displaying the strike orientations of the three fracture populations

Three conjugate sets with the acute angle perpendicular to the bedding are found, striking mainly in three directions; Set **q** strikes NNE-SSW, set **x** strikes WNW-ESE to NW-SE, and set **w** strikes ENE-WSW. These fractures do not seem to have developed symmetrically with

the macro-folds. However they are still interpreted to be conjugate $h0l/0kl$ sets with the enclosing acute angle about the c-axis (Hancock, 1985).

The low-angle-to-bedding thrust faults/ shear fractures and their associated fractures are both analyzed in present orientation and restored with the bedding back to horizontal. In order to further consider whether they are pre-folding or syn-folding fractures. Three sets are found in their outcrop orientation. Set A strikes between NNE-SSW to N-S, set B strikes WNW-ESE to W-E, and set C strikes NNW-SSE to NW-SE. When restoring the fractures, three sets are also identified, but with slightly different strikes. Set A strikes NNE-SSW to NE-SW, set B strikes W-E to WNW-ESE, and set C strikes NNW-SSE to NW-SE. These fractures dip in two directions opposite of each other and are therefore interpreted to be conjugate $h0l/0kl$ sets with the acute angle about the a- or b-axis (parallel to the bedding) (Hancock, 1985).

Fracture intensity is interpreted to be in general higher in the hinge zone, although examples of higher intensities in the forelimb also are present. When comparing limestones and spiculites, the throughgoing fractures are more common in the limestones.

4.5 Summary

This chapter will give a brief summary of the structural elements and the fractures linked to the fold-and-thrust domains. The area has been divided into four domains; three domains associated with the in-sequence thrusts (M1, M2, M3), where the oldest is placed to the NE (M3) and youngest to SW (M1), and one domain linked to the younger out-of-sequence (G). Each thrust domain consists of several subareas. A short constellation of the subareas will follow (see table 4.2 for composite summary of all data).

The M1-thrust is assumed to be a footwall flat underneath the M2-fold and is laterally poorly exposed (figure 4.8). The thrust marks the cut-off of the overlaying M2 anticlinal forelimb. No fractures were possible to determine in this thrust domain.

The M2-thrust is laterally exposed as a tipline in the core of the M2-fold. At locality M2-b, the M2-thrust cuts slightly through the fold hinge. The orientation of the fold axis curves southwards in a clockwise direction from a NNW-SSE to a N-S trend (from 160° to 177°). Southwards, the fold also tightens and develops a moderate plunge (figure 4.8). The fractures in the M2-thrust domain show a throughgoing similarity. Four fracture sets perpendicular to the bedding are found; set I strikes NNW-SSE, set II strikes NNE-SSW, set III sets ENE-WSW and set IV strikes WNW-ESE. Of these sets I and III are interpreted to be extensional fractures, and sets II and IV are conjugate $hk0$ shear fractures (Hancock, 1985).

The fracture system seems to be more complex where the thrust cuts through the fold hinge. The perpendicular to bedding fractures do also show general clockwise rotation southwards. The conjugate sets with the acute angle perpendicular to the bedding consist of two major sets; set **w** strikes ENE-WSW and set **q** strikes NNE-SSW. These sets are interpreted to be h0l/0kl fractures (Hancock 1985), but are without symmetric relationship to the fold axis. The low-angle-to-bedding thrust faults display three sets, both in present position and when restored. However, they show some minor differences. In present positions, set A thrusts strike NNW-SSE, set B strikes between WNW-ENE and NW and set C strikes between NNW-SSE and NW-SE. The restored fractures reveal three sets; set A strikes NNE-SSW, set B strikes E-W, set C strikes between NNW-SSE, and NW-SE. In both in-situ and restored cases, set C is the most prominent fracture set. These fractures are interpreted to be h0l/0kl thrust faults with the bisecting acute angle about the a- or b-axis (Hancock, 1985).

The major M3-thrust appear as a relative flat lying thrust in subarea M3-a. However, the thrust seems to develop a prominent oblique ramp in subarea M3-b, before the thrust again flattens laterally southwards on a higher stratigraphic level. The lateral ramp is identified along strike, where it seems to climb southwards in a flat-ramp-flat geometry (figure 4.8). The M3-anticline is fairly small to the N, developing into a NNW plunging, major fold towards the ramp-area, and further into two smaller anticlines above faults (branching) in the south. The fold axes have a relatively stable orientation. In subarea M3-c, the orientation of the fold axis is similar to the M2-thrust, showing a mild bend southwards (from 324 to 339). The restored fractures in the M3 domain have great similarities to the M2-thrust domain. Four mutual, major perpendicular fracture sets are found. These occur with greater variations than in domain M2, in that set I strikes between NNW-SSE and NW-SE, set II strikes between NNE-SSW and NE-SW, set III strikes between ENE-WSW and NE-SW, and set IV strikes between ESE-WNW and ENE-ESE. Of these, sets I and II are interpreted to be extensional fractures parallel and perpendicular to the fold axis and sets III and IV are interpreted to be conjugate hk0 sets (Hancock, 1985). The larger variations are found in connection to localities near the oblique ramp (subarea M3-b). There, the conjugate sets with the acute angle perpendicular to bedding display three orientations, where set **q** strikes NNE-SSW, set **w** strikes ENE-WSW, and set **x** strikes WNW-ESE. These fractures are interpreted to be h0l/0kl fractures with the bisecting angle about the c-axis (Hancock, 1985), but are not systematic with the fold axis. The low-angle-to-bedding thrust faults consist of three sets in their present positions. Set A strikes NNE-SSW, set B strikes E-W, and set C strikes between NNW-SSE and NW-SE. When restored, they appear as only two sets, where set A strikes NE-SW and set

C strikes NW-SE. Set C is also here the most prominent set for both present and restored positions. These fractures have been interpreted to be low angle $h0l/0kl$ thrust faults (Hancock, 1985), similar to those in thrust domain M2.

The Gavltinden thrust (GT) is a steeply dipping thrust, observed to cut down section into the Kapp Starostin Formation strata. The thrust has a small curvature in map view, bending in both directions towards Wahlenbergreen. The fold is extremely tight and plunges steeply to the NW at the northern end, which could indicate a small oblique ramp in this area. The fold is straightening up southwards and seemingly plunges to the SE at the south side (no measurements). The fracture sets of the Gavltinden area are similar to the fractures measured in the M2- and M3-thrust domains; set I strikes NNW, set II strikes NNE-SSW, set III strikes NE-SW, and set IV strikes ENE-WSW. Sets I and III are interpreted to be extensional fractures parallel or perpendicular to the fold axis, whereas sets II and IV are interpreted to be conjugate $hk0$ sets (Hancock, 1985). Conjugate sets with the acute angle perpendicular to the bedding exhibit two sets, where set **q** strikes NNE-SSW and set **x** strikes NW-SE. These fractures are interpreted after Hancock (1985) to be conjugate $h0l/0kl$ fractures with the bisecting angle parallel to the c-axis. The low-angle-to-bedding thrust faults are slightly different in this thrust domain compared to M2- and M3- domains. Two sets are documented both in-situ, and restored positions. In observed position, set A strike N-S and set C strikes NW-SE, whereas in restored position set B strikes WNW-ESE and set C strikes NNW-SSE. Set C is also here the most prominent, but compared to the two previous thrust domains, these thrusts are oriented slightly anticlockwise. The fractures are also here interpreted to be low angle $h0l/0kl$ thrust faults (Hancock, 1985).

The fracture intensity is in general higher in the fold hinge zones. However, evidences for higher intensities are locally also present in the fold limbs (figure 4.15). Large throughgoing fractures are observed to be more common in the limestones than in the spiculites. Further more, the throughgoing fractures are representing the same orientations as the short fractures. When comparing throughgoing fractures to the fold domain, they are in general more common in the forelimb (43% of total measured fractures in the forelimb) than in the hinge (26%) and the backlimb (31%).

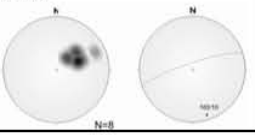
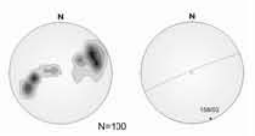
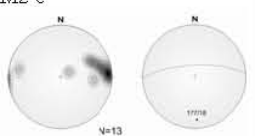
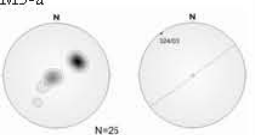

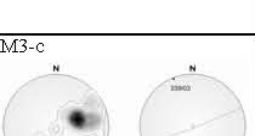
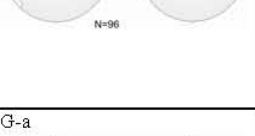
	Subarea		Shear fractures			Dilatational fractures	
			Conjugate Okl or h0l fractures (hybrid)	Low-angle Okl or h0l thrust faults	Conjugate hk0 fractures	Perpendicular to foldaxis	Parallel to foldaxis
M2	M2-a	 <ul style="list-style-type: none"> - Only the backlimb is exposed 	No fractures collected	No fractures collected	No fractures collected	No fractures collected	No fractures collected
	M2-b	 <ul style="list-style-type: none"> - Backlimb, hinge and forelimb are well exposed. - M2-thrust cuts the fold hinge - Fold axis strikes NNW-SSE - Forelimb is thinned - Scan-line is taken in the forelimb, hinge and backlimb. 	Forelimb: - Set w: ENE-WSW Backlimb: - Set q: NNE-SSW	<u>Present position</u> Forelimb: - Set A: NNE-SSW - Set C: NW-SE Backlimb: - Set A: NNE-SSW - Set B: WNW-ESE - Set C: NNW-SSE <u>Restored</u> - Set A: NNE-SSW - Set B: E-W - Set C: NNW-SSE	Backlimb: Set II and IV strikes NW-SE and NNE-SSW with the acute, bisecting angle more or less parallel to the fold axis. Hinge: Set II strikes N-S and IV strikes WNW-ESE, with the acute angle parallel to the fold axis. Forelimb: Set II strikes NNE-SSW and set IV strikes WNW-ESE, with the bisecting angle parallel to the fold axis.	Backlimb: Set III strikes ENE-WSW. Hinge: Set III strikes NE-SW. Forelimb: Set III strikes ENE-WSW.	Backlimb: Set I striking NNW-SSE. Hinge: Set I strikes NNW-SSE. Forelimb: Set I strikes NNW-SSE.
	M2-c	 <ul style="list-style-type: none"> - Backlimb, hinge and forelimb are well exposed. - Fold axis strikes N-S - Fold is tight and overturned - Fractures are interpreted on the lidar scan 	No fractures collected	<u>Present position</u> Hinge: - Set C: NNW-SSE <u>Restored</u> - Set C: NW-SE	Forelimb: Set II strikes NE-SW and IV strikes NW-SE.	Forelimb: Set III strikes E-W	Forelimb: Set I strikes N-S
M3	M3-a	 <ul style="list-style-type: none"> - Backlimb and hinge are well exposed - The stratigraphic beds seem to be thinner. - Fold is tight and overturned - Scan-line is taken in the hinge and backlimb 	No fractures collected	No fractures collected	Hinge: Set II strikes N-S, and a set IV strikes E-W. Backlimb: Set II strikes NNE-SSW and IV strikes NW-SE.	Hinge: Set III strikes NE-SW. Backlimb: set III strikes NE-SW.	Hinge: Set I striking NW-SE. Backlimb: Set I strikes NNW-SSE.
	M3-b	 <ul style="list-style-type: none"> - Backlimb, hinge and forelimb are well exposed - Thrust ramp or fault intersection - Fold axis strikes NW-SE - Tight overturned fold including a smaller open anticline-syncline pair. - Small fault-propagation fold - Scan-line collected in forelimb, hinge and backlimb 	Forelimb: - Set w: ENE-WSW - Set x: WNW-ESE Backlimb: - Set q: NNE-SSW - Set w: ENE-WSW - Set x: WNW-ESE	<u>Present position</u> Hinge: - Set C: NW-SE Backlimb: - Set A: NNE-SSW - Set C: NW-SE <u>Restored</u> - Set A: NE-SW - Set C: NW-SE	Forelimb: set II strikes NNE-SSW might be one part of a conjugate hk0 fracture set. Hinge: Set II strikes NNE-SSW and set IV strikes ENE-WSW Backlimb: Set II strikes NNE-SSW might be one part of a conjugate hk0 fracture set.	Forelimb: set III strikes to the ENE-WSW Hinge: Set III NE-SW Backlimb: set III strikes to the ENE-WSW	Forelimb: Set I strikes NW-SE Hinge: Set I strikes NW-SE Backlimb: Set I strikes NNW-SSE
	M3-c	 <ul style="list-style-type: none"> - Backlimb, hinge and forelimb are well exposed - Thrust ramp and fault intersection - Fold axis strikes NNW-SSE - Tight and overturned fold - Scan-line was taken in the backlimb and hinge 	Backlimb: - Set q: NNE-SSW - Set x: NW-SE	<u>Present position</u> Hinge: - Set B: E-W - Set C: NNW-SSE Backlimb: - Set A: NNE-SSW - Set C: NW-SE <u>Restored</u> - Set A: NE-SW - Set C: NW-SE	Hinge: Set IV strikes ESE-WNW and may be part of a conjugate hk0 set (with set II). Backlimb: Set II strikes NNE-SSW and set IV strikes to the NW-SE.	Hinge: Set III strikes ENE-WSW Backlimb: Set III strikes ENE-WSW.	Hinge: Set I strikes NNW-SSE Backlimb: Set I strikes NNW-SSE.
G	G-a	 <ul style="list-style-type: none"> - Backlimb, hinge and forelimb are well exposed - Extremely tight and overturned fold - Fold axis strikes NW-SE - Out-of-sequence fault - Scan-line was recorded in the hinge and backlimb 	Backlimb: - Set q: NNW-SSE - Set x: WNW-ESE	<u>Present position</u> Backlimb: - Set A: N-S - Set C: NW-SE <u>Restored</u> - Set B: WNW-ESE - Set C: NNW-SSE	Hinge: Set II strikes NE-SW, set IV strikes E-W Backlimb: Set II strikes to the NNE-SSW and IV strikes to the ENE-WSW.	Backlimb: Set III strikes to the NE-SW	Hinge: Set I strikes NNW-SSE Backlimb: Set I strikes NNW-SSE

Table 4.2: Summary table, with fold orientations, fold characteristics, conjugate sets, thrust orientations, hk0 shear fractures and dilatational fractures.

Chapter 5

Structural analysis and discussion

5.1. Introduction

This chapter includes an analysis and the related interpretation of the structural elements described in chapter 4, with the main focus on the fracture system of the study area. The interpretation leads to the discussion including a 2 stages fracture model, followed by the relevance of the fracture system for fluid flow.

The focus of the study is on the fracture geometry. However, in order to understand the fracturing, the influence or link to the large structural elements is of great importance. The chapter is split into 3 parts. The discussion firstly addresses the macro-scopic structural elements in chapter 5.2 and, secondly, the fracture distribution within the fold-and-thrust system of Mediumfjellet (chapter 5.3). Certain observations regarding the fold geometry, fold evolution and the fracture distribution will then be addressed in chapter in context of the regional kinematics including the two stage fracture model. Subsequently, chapter 5.4 will discuss how the fold mechanics influences the fracturing, before the model is compared similar petroleum regions in the world, and discussed with permeability and porosity occurrence at Mediumfjellet.

5.2 Fold and thrust geometry

Fracturing is well known to be kinematically closely related to folding and thrusting, and the knowledge of the fold and thrust evolution can to a certain degree be used to predict the occurrence of fold-related fractures (e.g. Fischer and Wilkerson, 2000). The discussion of the fold-and-thrust system geometry of Mediumfjellet forms the foundation for further debating the fracture development at the field sites.

Summarized, the field area of Mediumfjellet is divided into three in-sequence thrust domains (M1, M2, and M3) and one out-of-sequence thrust domain (G) (figure 4.1). The M1 thrust is poorly exposed and can not easily be followed, but seems to be a footwall low-angular thrust cutting the forelimb of the M2 fold-propagation fold. The M2 thrust splays from the M1 thrust and forms a macro-scopic anticline, where the M2 thrust basically terminates in the core of the fold. The anticline is tight, with an overturned eastern limb and

locally is cut by the thrust. In the north, the fold plunges to the south. Southwards it tightens and the fold axis rotates clockwise near Yoldiabukta. The M3 thrust domain similarly consists of a tight and overturned anticline, in this case in the NW of the M3-thrust, but the fold seems to have greater lateral variations. The fold changes southwards from a small and tight anticline in the north, to a major, overturned, NW-plunging anticline with a smaller frontal syncline, and then splits into two folds above two thrusts southwards near Yoldiabukta. The Gavltinden thrust domain (G) is characterized by a steeply dipping thrust that is observed to cut down-section through the strata. The hanging wall of the G displays a very tight and partly overturned, NW-plunging anticline that changes to a southwards plunge in the south. A bend in the thrust and the steep fold plunge in the north may indicate variations in thrust displacement.

When analyzing the thrusts in more detail, the admissible cross-sections show that the M1 thrust cut the foot-wall with a low angle and is most likely a hanging wall flat close above a thrust ramp resulting in the hanging wall M2 anticline. The thrust truncation of the M2 fold core towards the north and the clockwise rotation of the M2 fold towards the south could imply that the M2 thrust displacement decreases southwards. The lateral variations in the M3-thrust system is interpreted to reflect two thrust linkages, probably resulting in oblique ramps or ridges (figure 4.8), whereas the out-of-sequence Gavltinden thrust is superimposed on earlier structures.

This study suggests that the thrust system is a forward propagating in-sequence imbricate fan where the M3-thrust is the oldest and the M1-thrust is the youngest. The fold-and-thrust system consists of low-angle-to-footwall-bedding thrusts and fault-propagation folds or transported fault propagation folds (see McClay, 1992). The Gavltinden thrust is thought to be an out-of-sequence thrust, transporting an older, truncated anticline. This is so because of the tight fold shape and the locally down-section-cutting thrust. These interpretations are based on the following observations: 1) fault geometry, 2) fold geometry, and 3) the lidar scan interpretation. See chapter 4 for detailed description of the lateral changes of the three sub-domains and their accompanying subareas, and chapter 1 for a brief description of previous work and models presented from the field area.

The model of the fold-and-thrust geometry suggested in this study is in accordance with several other interpretations of this and nearby areas (e.g. Bergh and Andresen, 1990; Wennberg et al., 1993; Bergh et al., 1997; Braathen et al., 1999a; Braathen et al., 1999b; Ingebrigtsen, 1994 and Haabet, 1995), but has some minor differences. These differences are identified because this study has made it possible to see the structural geometry and the

associated lateral variations in a completely different way. The collected laser-scan of the mountain-ridge has been analyzed in a computer based 3D-model (e.g. figure 4.8), which visualize the entire Mediumfjellet fold-and-thrust system. There are several benefits of the computer based analysis. For example, Berg and Andresen (1990) refer to the M3-thrust as one throughgoing thrust along the Mediumfjellet ridge. Interpretations made in the presented model shows that the M3 thrust surface has significant lateral variations, in that the thrust surface shows two ENE-WSW directional ridges, separated by large concave trajectories (figure 4.8). These ridges are located in subareas M3-b and M3-c. Such furrowed or fluted surface-patterns have been described by Ray (2006) as a common shape of thrust growth and subsequent fault linkage in fold-and-thrust belts. This study suggests that the three M3 segments are linked in these two subareas, which is added by the observations of two fault segments that appear on different stratigraphic levels, and that the associated folds plunge in the linkage direction, implying less displacement (chapter 5).

Berg and Andresen (1990) suggest that the lateral changes prove that the fold mechanism is interchangeable between a fault-propagation fold mechanism (e.g. Jamison, 1987) and fault-bend fold mechanism (e.g. Suppe, 1983; see chapter 2). However, neither of the two fold models explains the fold geometry of the Mediumfjellet properly, as discussed in the continuation.

Based on the observations of thinned forelimbs and thickened hinges, Bergh and Andresen (1990) also suggested that the folding is caused by shear folding. These observations are confirmed in the present study. However, evidences for flexural slip folding (Twiss and Mores, 1992; see chapter 2) has also been observed in the field, which is further supported by earlier described flexure slip folding from the Vermlandrygg anticline (Ingebrigtsen, 1994; Haabet, 1995). The questions of structural style and folding mechanism are further discussed in chapter 5.5.2 and 5.5.3; however, in this case the discussion is in relation to the fracture distribution.

5.3 Kinematics and chronology of fractures

The fracture characteristics of Mediumfjellet suggest a complicated fracture history. Three main fracture populations are documented, the so-called; 1) perpendicular fractures (sets I-IV), 2) conjugate fractures (sets **q**, **w** and **x**), and 3) thrust faults (sets A, B and C) (see chapter 4). The fracture distribution is further discussed in section 5.4, but is here discussed as the main criteria for the fracture chronology. These criteria are based on, firstly the symmetric relationship of the fracture orientations to the fold axis and, secondly rotated positions within the major fold.

The perpendicular and conjugate fractures are interpreted to be related to the folding event, whereas the thrusts are interpreted to be related to an early stage of contraction that most likely occurred prior to folding. This suggests a 2 stage fracture model (figure 5.1), with a pre-folding fracture event indicating a NE-SW shortening direction and a syn-folding fracture event suggesting a NE-SW to E-W shortening. The fractures are described with their tentative interpretations in chapter 4. Braathen et al., (1999) describe a 5-stage kinematic model for the Spitsbergen fold-and-thrust belt as a whole, of which two events affected the central zone including Mediumfjellet (Bergh and Andresen, 1990). This is outlined in chapter 1. The suggested 2 stage model in the present study proposes a third stage in addition to the model presented earlier from the central zone (explained as stage 1 in the suggested 2 stage fracture model).

The suggested 2 stage fracture model in the present study (figure 5.1), is supported by earlier studies made in the Spitsbergen fold-and-thrust belt (e.g. Kleinspehn et al., 1989; Wennberg et al., 1994; Braathen and Bergh 1995; Bergh et al., 1997; Braathen et al., 1999). Bergh & Andresen (1990) introduce a 2 stage kinematic model from the Mediumfjellet and Lappdalen thrust front starting with an in-sequence and a subsequent out-of-sequence stage. Braathen et al. (1999) shows that the in-sequence thrusting are characterized by folding-and-thrusting in an ENE direction (stage 2 and 3; chapter 1), and the following out-of-sequence folding and thrusting is in a NE direction (stage 4; chapter 1). These two stages are part of the 5 stage model of whole Spitsbergen fold-and-thrust belt, which Braathen et al., (1999) summarize from earlier work. However, stage 1 and stage 5 are not shown to exist in the central zone of the thin skinned deformation province (Braathen et al, 1999). The two fracture stages will here be discussed in light of the earlier suggested five stages.

5.3.1 Pre-folding fracturing (stage 1)

As well established above, the fracture system has been split into three main populations; fractures perpendicular to bedding (extensional and shear fractures), conjugate h0l/0kl (hybrid) fractures, and thrusts. A fourth population is the so called unknown fractures. The fractures have been described in detail and interpreted in chapter 4. Earlier conceptual models from similar studies are described in chapter 2.

The low angle thrust faults are interpreted to be conjugate h0l/0kl fractures with the acute bisecting angle parallel with the bedding (Hancock, 1985). Three sets are observed.; Set A strikes between NNE-SSW to N-S, set B strikes WNW-ESE to W-E and set C strikes NNW-SSE to NW-SE. The restored (back-rotated with bedding) fractures consist similarly of three sets, showing some minor differences in orientation. Set A strikes NNE-SSW to NE-SW, set B strikes WNW-ESE to W-E and set C strikes NNW-SSE to NW-SE. Set C is the most dominating in both cases. Because of the similarity in style/orientation, the sets will hereafter be referred to as restored fracture when they are mentioned. The fractures dip in opposite directions between 15° and 40°. In an interpretation as conjugate shear fractures, the largest principal stress direction is parallel to the bedding and perpendicular to the strike direction (see chapter 2) (Hancock, 1985; Price 1966), which implies a WNW-ESE (set A), NNW-SSE (set B) and ENE-WSW orientation of stress. These fractures are interpreted to have developed prior to the folding event; however, some aspects regarding the fracture distribution will be discussed here.

The indication for a pre-fold fracture event is sustained by the following observations; i) the low-angle-to-bedding thrusts strike preferably with a NW-SE to NNW-SSE orientation, which indicates a NE-SW to ENE-WSW shortening axis. ii) Slickensides on the fault planes trend in a NW-SE direction. iii) Fault planes are rotated or even folded within the major folds indicating that they developed before folding (see chapter 4). Finally, iv) the thrust faults orientation is consistent when restored with bedding (bedding back to horizontal position). When restoring the thrusts, they all seem to have the same dip (between 15° and 40°), which is the mechanical expectation for a pre-folding thrusts position. Additionally calcite filling on most of the thrust surfaces and perpendicular fractures terminating at the faults surface can be mentioned, but there are not enough data to be conclusive. Two of the evidences (ii and iii) are discussed under, related to the kinematics and the fracture chronology.

In the light of the kinematics established for the fold-and-thrust belt, the this population of fractures (sets A, B and C) are thought to be developed at an early stage of the fold-and-thrust

belt evolution. Early developed thrusts, which later have been folded, would appear as rotated within the fold system. Several rotated thrust-related structures (thrust faults or small fault propagation folds) are observed in many of the subareas (e.g. figure 4.7). The evidence for rotation is that the thrusts seem to have a consistent fault angle to the bedding regardless of the bed orientation. Butler (1992) shows, similarly, that low-angle fractures to the bedding most likely have developed prior to folding. He demonstrates this theory by restoring the low-angle-to-bedding fractures (unfolds the beds back to horizontal). He points out that low-angle fracturing caused by folding would rather develop near parallel to the main thrust and cause shearing and thinning in the forelimb of the fold (discussed in chapter 5.4). These fractures are in this present study interpreted to have developed prior to folding.

Looking at the low-angle-to-bedding thrust faults from field observations in the thin-skinned deformation zone represented by Mediumfjellet, the present study tentatively presents evidence for an early initial contractional stage (stage 1 in Braathen et al., 1999; chapter 1). This deformation phase is characterized by fairly mild NE-SW shortening, by small thrusts at Mediumfjellet, in contrast to the intense deformation reported from areas in the west (Braathen et al. 1999). Similar conclusions have been reached from work in the western basement-involved deformation zone (Nordenskiöldland; Braathen and Bergh, 1995, and Brøggerhalvøya; Bergh et al., 2000), which proposes an initial stage characterized by NNE–SSW to N-S shortening.

There are however minor differences between the kinematics of earlier work and the pre-folding fractures at Mediumfjellet. Firstly, the thrusts documented at Mediumfjellet have a slightly clockwise rotated orientation compared to that reported from the western thick-skinned deformation zone at Nordenskiöldland (Braathen and Bergh, 1995). A possible explanation could be that Mediumfjellet is located in proximity to the Isfjorden-Ymerbukta fault zone, a transfer fault in the fold-and-thrust belt (see previous work, chapter 1; Braathen et al., 1999a; Karlsen, 2000). The strain partitioning of the thrust sheets caused by this transverse structure might have rotated the stress field slightly as indicated by the bend in the M2- and M3-fold axes to the south. This theory is supported by Karlsen (2000) who also reports low-angle-to-bedding thrust faults with ENE-WSW to ESE-WNW shortening direction. These thrusts are interpreted to pre-date the later major thrusting.

Secondly, several of the restored thrust faults also have strikes prominently between E-W and ENE-WSW, indicating N-S directed shortening orientations. Similar thrust directions were reported by Hansen (1991) (see also Wennberg, 1994) from the Lappdalen area north of Mediumfjellet. There are several possible explanations for these structures; i)

they may be caused by the folding event (syn-folding structures) and should in such a case not be restored; ii) they may be caused by local and lateral variations of the stress field such as around lateral ramps, which will rotate the stress field (Aptoria, 1992); iii) they may represent reactivation of pre-existing structures, in this case suggesting that even earlier fracture imprint may exist. In the latter context, it is worth mentioning the technical picture established at Brøggerhalvøya (Bergh et al., 2000), where N-S shortening is pronounced at an early stage. The few observations at Mediumfjellet opens for that those structural trends are more widespread.

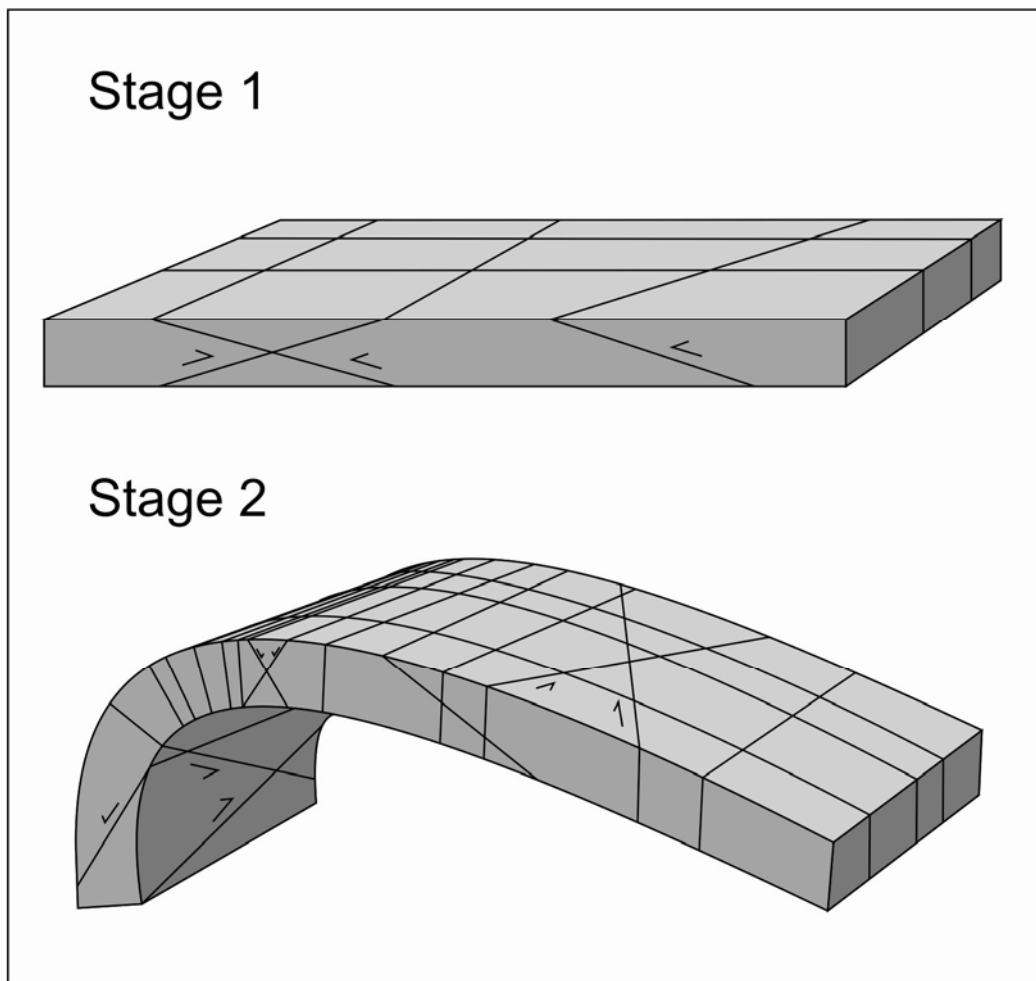


Figure 5.1: The present study suggested two-stage model of fracturing in Mediumfjellet. Stage one suggests generation of low-angle-to-bedding thrusts and possible extensional fractures, whereas stage two displays the rotated low-angle-to-bedding thrust truncated by superimposed perpendicular fractures and conjugate hybrid fractures (see text for explanation).

5.3.2. *Syn-folding fracturing (stage 2)*

Two fracture populations are recognized with a symmetric relationship to the fold; both subvertical and conjugate hybrid fractures.

Looking into the perpendicular fractures, there are striking similarities between the thrust domains and the subareas. Four fracture sets can principally be determined; set I, II, III and IV (figure 4.11). All four fracture sets strike in directions which are interpreted to be in systematic around the fold axis (figure 4.18) and, hence, are here suggested to be related to the folding event (e.g. Fischer and Wilkerson, 2000), as clarified above. As described earlier, set I strikes between NW-SE and N-S, set II strikes between N-S and NE-SW, set III strikes between NE-SW and E-W, and set IV strikes between E-W and NW-SE. Set I and III is interpreted to be extensional orthogonal sets (e.g. Kulander et al., 1979), where set I is parallel and set III perpendicular to the fold axis. Set II and IV are interpreted to be hk_0 shear fracture sets (e.g. Hancock, 1985), which both occur with the intersecting acute angle parallel or perpendicular to the fold axis.

Similar fracture patterns have been reported from other studies (e.g. Stearns, 1968; Hancock, 1985; Bergbauer and Pollard, 2004; Bellhansen et al., 2006; Cooper, 2006). These conceptual models show the distribution of fracture orientations that can be expected from thrust-related folds. In general they all separate into three different populations; dilatational fractures, shear fractures and hybrid fractures (e.g. Hancock, 1985). In some models, the fracture system connects to cylindrical (e.g. Price, 1966) or symmetric folds (e.g. Stearns, 1968), while others argue for fracturing in more complex non-cylindrical (e.g. Stearns and Friedman, 1972) and asymmetric folds (see chapter 2 for more information). In any case several differences can be noted when comparing published results with those presented herein.

Firstly, cylindrical fold models can not explain the fracturing associated with the lateral ramps and fault segments. In these subareas (M3-b and G-a), where the fold plunges similar to the ramp, the fractures seem to be oriented nearly angular to fractures elsewhere. This is well illustrated in subarea M3-b and GT-a, where the hk_0 fractures are oriented perpendicular to the fold axis (acute bisecting angle around the a-axis). With the basis in the literature, previous studies considering non-cylindrical fold (e.g. Stearns and Friedman, 1972) explain how the fracture orientations changes around the fold as the fold axis varies in plunge (figure 2.4). This suggests lateral variations of fracturing in relation to non-cylindrical element.

Secondly, the fractures which were measured and interpreted to be hk_0 fractures (Hancock, 1985) in the study area are mainly oriented with the intersecting acute angle parallel to the fold axis (b-axis). This fracture set is described as infrequent by Price and Cosgrove (1990) (figure 2.4). Yet, Stearns (1968) pointed to that such hk_0 shear fractures

(with the enclosing angle about the b-axis; Hancock 1985), can be related to the more common hk0 fractures (with the enclosing acute angle about the a-axis). In the case when a given fold has developed a neutral surface (figures 2.4), the principal axis of stress and strain are known to position across this neutral surface (figure 2.3; chapter 2). This means that conjugate fracture sets with the acute angle about the a-axis underneath the neutral surface, may change to conjugate fracture sets with the acute angle about the b-axis above the neutral surface. This kind of hk0 fracturing has also been reported from the Alpine external southwest Pyrenees (Hancock, 1985). The present study at Mediumfjellet suggests a neutral surface folding mechanism

Thirdly, the orthogonal fracture system consists of dilational fractures both parallel and perpendicular to the fold axis. However, the most commonly occurring fracture of the M2- and M3- thrust systems are the fractures striking perpendicular to the fold axis. Hancock (1985) showed that this fracture orientation develop parallel with the direction of the highest principal stress. Contrary to the other subareas, such fractures are basically absent in subarea G-a. In this case, the extensional fracture set parallel to the fold axis is the most prominent. This might be related to the out-of-sequence thrust-related folding, where the layers have been folded extremely tight and therefore experienced layer parallel, fold-axis perpendicular stretching.

There are also identified three sets of conjugate fractures (hybrid fractures) with the acute bisecting vector perpendicular to the bedding. These h0l and 0kl fractures are also called hybrid fractures and develop as extensional shear fractures where the maximum stress (σ_1) is perpendicular to bedding (see chapter 2). Set **q** strikes NNE- SSW to NE-SW, set **x** strikes WNW-ESE to NW-SE and set **w** strikes ENE-WSW. See chapter 4.3 for detailed description of these fractures or chapter 4.5 for a brief summary.

Hybrid fractures have been described by several authors (e.g. Jaeger and Cook, 1979; Ramsey and Chester, 2004). Hancock (1985) points out that these fractures can be present in a fold but will form symmetrically around the fold axis, either parallel or perpendicular to the axis. The sets **q** and **x** fractures collected at Mediumfjellet can easily be related to the fold symmetry as both set **q** and **x** strike obliquely to the fold axis. However, set **w** is perpendicular to the fold axis. The orientations of these fractures can be explained in several ways, as addressed below.

The fractures could be extensional features developed in relation to folding. In this case, the fractures will develop perpendicular to the direction of the least principal stress; if

the greatest principal stress is vertical to the bedding (e.g. Peacock and Sanderson, 1992). Set **w**, perpendicular to the fold-axis, suggests that extension along the fold axis may have occurred. As the fold geometry is not cylindrical in the study area, local strain fields may have developed. Alternatively, changes in fracture orientations could be related to fold plunges and associated lateral ramps (e.g. Stearns and Friedman, 1972), as discussed earlier with perpendicular fractures. However, these **w**-set fractures do not occur frequently in areas where major folds plunge significantly (in subarea G-a and M3-b; see chapter 4). Another explanation of these hybrid fractures related to the folding event is that they may be the formation as en échelon fractures. This can be explained by shearing between two controlling fractures. Set **q** and **x** both strikes oblique to the fold axis, although together they are oriented symmetric compared to the fold axis with crosscutting relationship. Their bisecting acute angle strikes parallel to the extensional fractures. Their interpretation can be supported by the work of Florez-Niño (2005), who shows that shearing between extensional fractures oriented perpendicular to the fold axis may produce oblique fractures. In this case, shearing between the extensional fractures perpendicular to the fold axis has not been observed. However, en échelon fractures (set **q**) were observed in subarea M3-b, which supports the theory. Perpendicular extensional fractures oriented normal to the fold-axis at Mediumfjellet are also seen as large, pronounced and throughgoing fractures which could have caused shearing between them.

A second explanation for the hybrid fractures is that they are pre-existing features developed prior to folding. Several studies have shown that such fractures to be common for flat-lying sedimentary strata (e.g. Peacock and Sanderson, 1992)

In a regional context, three fracture populations (sets I-IV and **q**, **w** and **x**) have been interpreted to have developed synchronously with the folding event; i) extensional fractures parallel and perpendicular to the fold axis (sets I and III), ii) conjugate $hk0$ (Hancock, 1985) shear fractures with the acute bisecting angle parallel to the bedding and parallel or perpendicular to the fold axis (sets II and IV), and iii) conjugate $h0l/0kl$ (Hancock, 1985) fractures with the acute bisecting angle perpendicular to bedding, and orientations symmetric with respect to the fold axis (sets **q**, **w** and **x**) (see discussion in chapter 5.4 for more information of the these fracture types and the distribution). The evidence for temporally interacting folding and fracturing is based on the symmetric relationships with the fold geometry, suggesting a link between these two deformation mechanisms. Such a linked small and large scale deformation style is reported by numerous authors (e.g. Price, 1966; Stearns

1968; Stearns and Friedman, 1972; Price and Cosgove, 1990; Bergbauer and Pollard, 2004). However, McClay (2000) argues that the fracture chronology and orientations may vary with the changing slip and stress/strain orientations. Following McClay's (2000) view; two theories for fracture development and evolution will be discussed (figure 5.2); i) fractures developed in relation to the major folds, or ii) extensional fractures developed in an orthogonal pattern prior to folding and have later been reactivated as shear fractures during folding.

The first theory include the three fold related fracture populations mentioned above. The dilatational (extensional) fractures found at Mediumfjellet are both parallel and perpendicular to the fold axis (chapter 4). These fractures have their axis of least principal stress perpendicular to their strike direction and the axis of greatest principal stress perpendicular to bedding or parallel to the strike direction. In a folding event, the maximum horizontal stress is most likely parallel to the strike of the fractures (Hancock, 1985) (see chapter 2). The direction of the greatest horizontal stress is here found to strike between NE-SW to NNE-SSW for Mediumfjellet. The conjugate hk_0 (Hancock, 1985) shear fractures found at Mediumfjellet have an acute bisecting angle both parallel and perpendicular to the fold axis, of which the most common fracture population has the acute angle parallel to the fold axis. This study suggests that these fractures have developed in accordance to local stress fields during the folding event, by extension along the trend of the fold axis and by local shearing, basically by developing en-échelon fractures between the dilatational fractures. Therefore, they are not related to the regional kinematics

The second theory is based on that the perpendicular fractures may have developed as extensional orthogonal sets in two directions prior to the major folding event, first in a NW-SE initial contractional stage possibly related with the low-angle-to-bedding thrusts (stage 1; Braathen et al., 1999), followed by a new set within a NNE-SSW contractional stage (stage 2; Braathen et al., 1999). In this model the early developed extensional fractures have been reactivated in the major folding event as shear fractures (figure 5.2). Of special interest in this context is the work by Engelder and Geiser (1980) and Engelder (1982), which show that extensional fractures parallel to the maximum horizontal stress in the Appalachian Plateau (New York) are the first fractures to develop in a contractional regime. Such fractures may even develop far ahead of the advancing thrust front. Further these authors argue that even if several fracture sets occur with a crosscutting relationship, they are extensional fractures that have developed in a changing stress field, reflecting the orientation of the maximal horizontal stress at any given time that the fracturing stress is reached.

The interpreted stress axes for the three aforementioned fracture populations suggests a general NE-SW to E-W orientation, which is in accordance to what has earlier been suggested (e.g. Braathen et al., 1999). Fractures that do not fit into this syn-fold model are thought to be fractures developed in accordance with local stress/strain fields such as the mentioned lateral ramps, or have developed prior to folding. Based on the close symmetrical relationship between the major folds and fractures, this study suggests that the syn-folding fracture event best explains the vast majority of the fracture data.

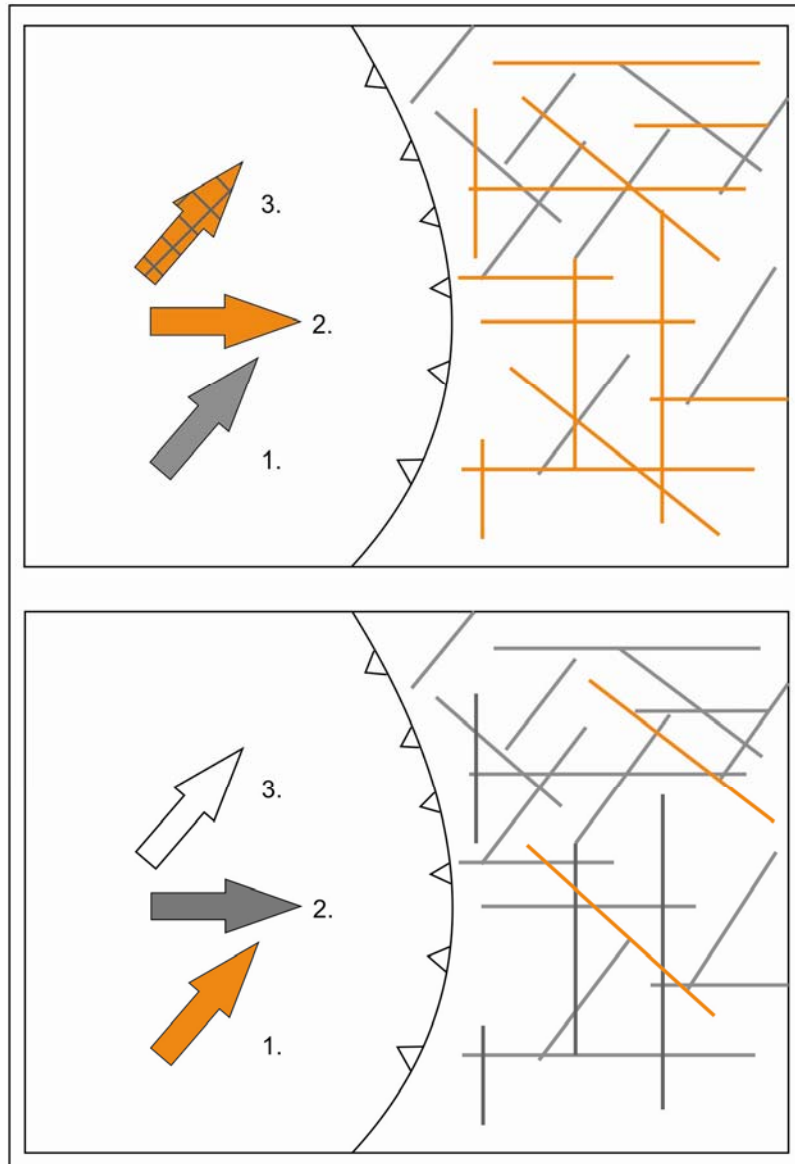


Figure 5.2: Two models for chronological fracture development at Mediumfjellet. The uppermost figure suggests three stages of pre-folding fracturing (1 and 2) and one syn-folding stage (3) with reactivation of previous fractures (from 2) as conjugate hk_0 shear fractures. The lowermost figure displays pre-folding fracturing initiated as thrusts (1) and syn-folding fractures (2). It is concluded that the latter, is the most likely model in this study.

5.3.3 Out-of-sequence fracturing (stage 3?)

A third possible stage of fracturing may potentially exist in the area, related to the out-of-sequence thrusting. In order to address this option, a comparison between fracture development within the in-sequence thrust domains and the out-of-sequence thrust domain was conducted. No major variations were found. The fractures of the out-of-sequence thrust domain are thus suggested to have developed synchronous with the in-sequence fracturing and subsequently likely been reactivated during the out-of-sequence fold-and-thrust event.

5.3.4 Non-systematic fractures

The non-systematic fractures do not show any orderly relationship to the fold axis or to each other. These fractures can not be interpreted to have developed synchronously or prior to folding. They may be preexisting fractures or fractures caused by local stress fields within the complex fold-and-thrust system. Similarly, Hancock (1985) interprets fractures that do not have any symmetric relationship with the fold axis to be developed prior to or after the folding event, or be caused by local stress fields within the fold systems. Fischer and Wilkerson (2000) interpreted them to be induced by fold-related strain.

5.4 Fold growth linked to fracturing

Most of the existing fracture models do not consider the temporal evolution of the folding, such as fold migration, hinge rotation or influence of pre-existing fractures (e.g. Price, 1966; Stearns, 1968; Hancock, 1985). By connecting the fold geometry (discussed in chapter 5.2) and the fracture distribution (discussed in chapter 5.3), these topics can now be further considered.

Fracturing within the two fault-related folds of current interest (fault-bend fold and fault-propagation fold) depends on several factors regarding the kinematics and temporal evolution of the fold. Numerous studies highlight the different aspects in the development of these two fold types (e.g. Suppe, 1983; Jamison, 1987; Saffar, 1992; Erslev and Mayborn, 1996; Salvini and Storti, 2000; Suppe et al., 2004; Hardy and Connors, 2005; Tavani et al., 2006). These studies are in general regarding the interaction between fold and fault growth, i.e. the fault propagation, in light of ramp angles (e.g. Almendinger, 1998), limb rotation (e.g. Erslev, 1991), hinge migration (e.g. Suppe, 1983), and fold mechanisms (shear or flexural slip folding) (e.g. Colman-Sadd, 1978; Suppe 1983 and Erslev, 1991). In the following sections, fold and fracture aspects of the present study will be discussed by combining the relationship between fracturing, the folding and bed properties. The background theory is already described in chapter 2.

Generally speaking, the thrust-related fold geometry depends on the ramp angle, as discussed by Suppe and Medwedeff (1990). High thrust ramp angles produce open and upright folds, whereas low thrust-ramp angles produce tight and overturned folds. This is interesting since tight folds in general will develop higher fracture intensities in the hinge zone than open, upright folds. In this study, very tight folds are observed both in subarea M2-c and G-a. Subarea M2-c reveals a low-angle thrust fault, whereas the subarea G-a with the upright Gavltinden thrust anticline is thought to be tight because of the two generations of folding and thrusting (out-of-sequence) imposed on the rocks. In a broader perspective, several authors have found strong correlations between fold-hinge curvature and fracture intensities (e.g. Pearce et al., 2006). This study supports this correlation by showing that the hinge zone has higher fracture intensity than the backlimb and forelimb (figure 4.16; see chapter 4). On the contrary, Mynatt et al., (in press) found that fractures do not necessarily relate to the fold curvature. Salvini and Storti (2000) support that by inferring that the deformation depends on the time and space distribution of the fold evolution.

Limb rotation or fixed limbs are two typical models for explaining the fold evolution of thrust related folds. They are commonly explained in relation to if the fold hinges are migrating or fixed (e.g. Salvini and Storti, 2001; figure 5.3). Fold-propagation folds are commonly regarded to develop with a fixed hinge and rotating limbs (Mosar and Suppe, 1992). Contrary, a fold-bend fold has hinge migration and fixed limbs (Suppe, 1983). In addition, a transported fault-propagation fold forms as a mixture of these two fold mechanism. In a non-migrating hinge zone (fixed hinge zone), the deformation will basically concentrate at the hinges and decrease towards the limbs and will be more or less constant during fold growth, except the forelimb, which go through some deformation (e.g. Erslev, 1991). Contrary, the deformation in a hinge-migrating fold will be higher in the fold limbs, and constantly deforming as the fold propagates over the ramp (e.g. Suppe, 1983). The fractures are largely influenced by the deformation in the fold, where a relationship between fold mechanism and the fracture intensity are established. Figure 4.16 shows the overall fracture intensity in number of fractures per meter versus the bed thickness. It is clear the fold hinges in Mediumfjellet in general has significant higher fracture intensity than the forelimbs and backlimbs. In accordance with the discussion above, this may indicate a fixed hinge for the development of the Mediumfjellet folds, proposing fold-propagation folding (see figure 5.3). However, local variations show that the intensities can also be higher in the forelimb in this case suggesting either a fault-bend fold or transported fault propagation fold deformation. Limb rotations occur only within a fault-propagation fold or a transported fault-propagation folding. In this model, the forelimb continuously changes the dip, and may even be vertical or overturned (Shaw et al., 2005).

The three folds presented above may all be present in Mediumfjellet. They could be induced by two possible fold mechanisms; i) shear folding or ii) flexural-slip folding (see chapter 2 for descriptions). Shear folding mechanism may be present in both fault-propagation folding and fold-bend folding (Shaw et al., 2005). A fault-propagation fold is characterized by a triangular (trishear) zone of shearing propagating from the thrust tip (Erslev, 1991), which produces thinning in the forelimb and thickening in the hinge. It has earlier been alluded that the folding mechanism in the study area has developed partly by shear folding, because of the thickened hinge zones and observed thinning of the limbs (Bergh and Andresen, 1990). This has also been observed in the present study. However, other observations rather suggested an input of a forced folding mechanism (flexural-slip folding), because of the following two observations; Firstly, shear surfaces between the stratigraphic layers has been observed near the hinge zone, for example at locality M3-7

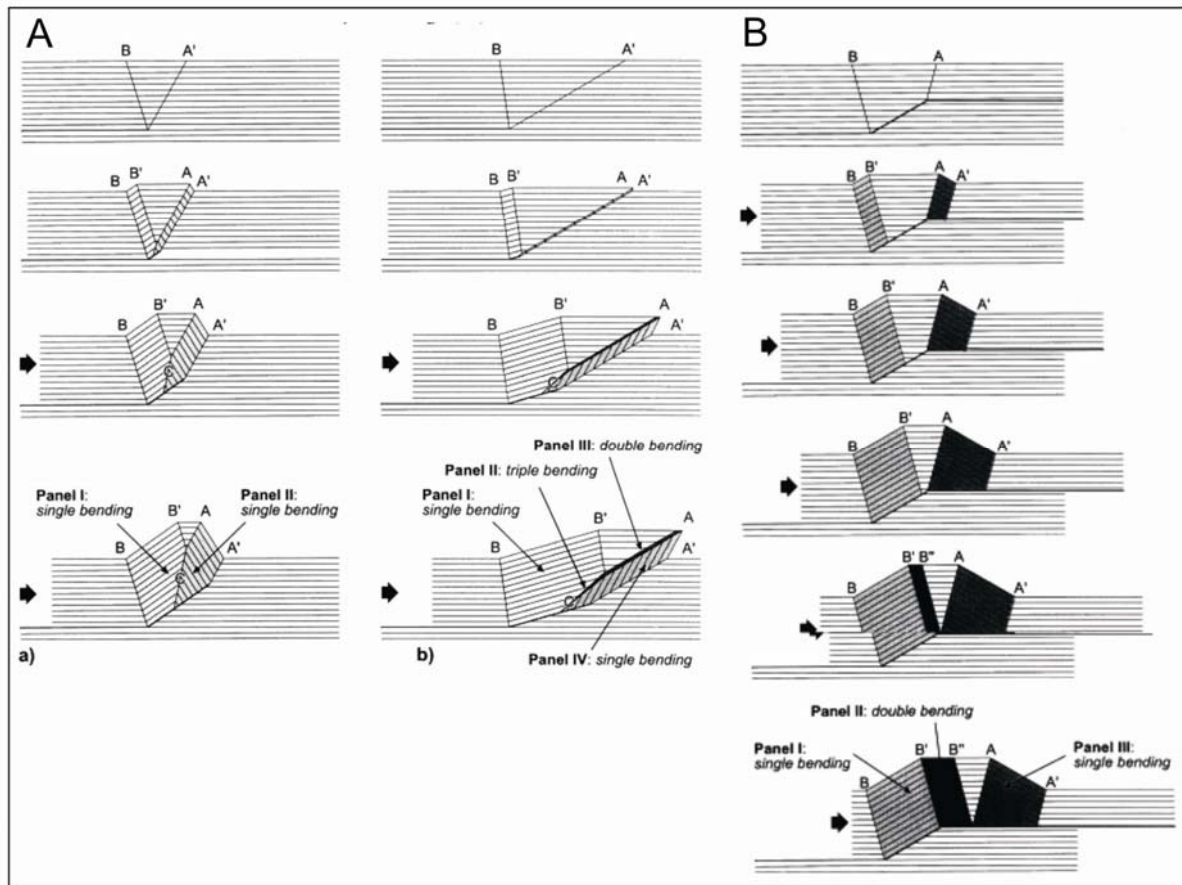


Figure 5.3: Deformation panels of fault-propagation folds (A) and fault-bend fold (B). A) Constant thickness (a) and overturned (b) fault-propagation fold. Note that deformation for the overturned fault-propagation fold is high in the hinge zone and low in the fold limbs B) Simple step fault-bend fold with migrating fold hinges. The highest deformation is located in the limbs (modified from Salvini and Storti, 2001).

(figure 4.12) and, secondly, M and Z meso-scopic fold geometries are observed for example in subarea M3-b. These structures are commonly associated with flexural-slip folding or neutral surface folding (Davis and Reynolds, 1996).

The present study thus proposes a relationship between the fracture intensity in the fold domains (forelimb, hinge and backlimb) and the fold mechanism. The intense fracturing in the hinge zone, combined with observations such as overturned (limb rotation) and thinned forelimbs (trishear) suggest that the Mediumfjellet thrust stack most likely consist of fault-propagation folds and transported fault-propagation folds formed by both shear folding and flexural-slip folding. This study thus suggests local lateral variations between these two mechanisms.

5.5 Fold-and-thrust belts and fracture reservoirs

Zagros fold and thrust belt is located at the northeaster part of the Arabian plate. The fold-and-thrust belt is a result from a collision between the Arabian plate and the central Iran plate starting in the late Cretaceous until present (e.g. Stocklin, 1968). Similarly to Spitsbergen fold-and-thrust belt, the Zagros fold-and-thrust belt consist of several levels of weak strata and detachment horizons interbedded with stronger competent beds (Fard et al., 2006). The lithologies consist mainly of limestones interbedded with sand, evaporites and shales (Rudkiewicz et al., 2007). Emphasis has been on the Asmari Formation, which has been investigated for fracture development (Wennberg et al., 2006; Ahmadhadi et al., 2007). Similar to the present study of Mediumfjellet, Wennberg et al., (2006) analyzed orthogonal fracture sets with the most prominent set parallel to the fold axis. However, no shear fractures where documented. Wennberg et al., (2006) further compared the fracture intensity to the bed mechanics. Contrary, in the study of Ahmadhadi et al. (2007) the fracture orientation in several anticlines is oblique to the fold axis. Thus, the derived interpretation is that controlling pre-existing fractures were reactivated during the folding event. The Zagros fold-and-thrust belt is today highly productive on hydrocarbon resources (Wennberg et al., 2006; Ahmadhadi et al., 2007; Rudkiewicz et al., 2007), in many cases producing from fracture reservoirs.

The South Pyrenean fold-and-thrust belt is located between Spain and France and is a result of a continental collision of the European plate and the Iberian plate. Collision occurred between early Eocene to late Oligocene. The orogeny is double-verging in that it consists of two foreland fold-and-thrust belts, one on each side of the collision suture (e.g. Puigdefàbregas et al., 1992). Main lithologies involved in the deformation are red sand at the base overlain by carbonate rocks interbedded with salt, gypsum and shale, again overlain by turbiditic siliclastic rocks. Salt is making up the detachment horizon (Travé et al., 2007). Major folds are formed by thrusts ramping up from the weak detachment surface (Travé et al., 2007). Similarly to the present study at Mediumfjellet, Tavani et al., (2006) studied the relationship between folding mechanism, mechanical stratigraphy and spatial evolution of meso-scale structures. They suggest that the frequency of pressure solutions cleavage displays a spatial distribution in relation to the fold position, whereas joints and veins are not systematic in a similar way. In another publication from the same fold-and-thrust belt, Travé et al. (2007) address, factors controlling the fluid flow, and suggested that the fracture properties are controlling the flow. In this case as well, the South Pyrenees represents an example of a present hydrocarbon producing field, with productive fracture reservoirs.

As obvious from the two mentioned fold-and-thrust belts, fractures play a major role as fluid flow pathways (e.g. Odling, 1992; Aydin, 2000; Odling et al., 2004) and for increasing porosity. Major through going fractures are important for the migration, whereas the shorter fractures are valuable for the porosity, especially for impermeable strata such as those occurring in the Kapp Starostin Formation.

This section will first discuss the rock properties in the Kapp Starostin Formation, before comparing the carbonate strata to the fracture development in the fold domains, proposing a 2D porosity-permeability model.

The rock-properties and their related diagenetic history may be an important factor of fracturing. Six sedimentary lithologies are sub-divided in the Kapp Starostin Formation at Mediumfjellet; siliceous shale, bryozoan shale, brachiopod limestone, bryozoan limestone, light-colored spiculite and dark spiculite (see description chapter 3). All the stratigraphic layers were considered as potential strata for a possibly carrier rock or rock with reservoir properties. These six lithologies can be subdivided into three mutual characteristic categories based on the fracture properties; 1) limestone, 2) silica rich mudstone or shale, and 3) paper shale.

Carbonates are common strata for fractured reservoirs (e.g. Normann Wellsfield, NTW, Canada; Val d'Agri Fields, Italy; La Paz field, Venezuela). Limestones are characterized as a hard and competent rock. Tsang (1984) pointed out that these rocks produce clear and tall fractures. Fractures observed in the carbonate rich strata (unit 1, 2, 3, 6, 9 and 20; figure 3.1) at Mediumfjellet are commonly running through the whole bed terminating at the layer boundary. This makes them easy to be determined and measured. However, up to 30% of all the fractures observed in field are through-going (running through more than one bed). The through-going fractures usually also have the same orientations as the shorter fractures.

Compared to the silica rich strata at the Mediumfjellet, the fractures in the silica-rich shale are commonly characterized by very thin hairline fractures often filled with calcite and appear in untidy fracture patterns (figure 3.2). One explanation for this could be that when siliceous ooze compacts and heats, the rock mass contracts and fractures. This happens when the silica transform from opal A to opal C/T (see chapter 2) (Davies, 2005; Davies et al., 2008).

This study suggests the following permeability and porosity model. The model is based on fractures collected in the carbonate beds (units 1, 2, 3, 6, 9 and 20; figure 3.1). The assumption is built on that the throughgoing fractures benefit the permeability and that the

short fractures are important for the porosity. The backlimb consist of 31% throughgoing fractures and 69% short fractures, which is the area with a general high porosity and permeability. The hinge zone is dominated by the short fractures (69%), which suggest a low permeability and high porosity. Whereas the forelimb have the highest occurrence of throughgoing fractures (43,5%), implying moderate permeability and porosity. Consequently, the forelimb with the general highest amount of throughgoing fractures will together with the

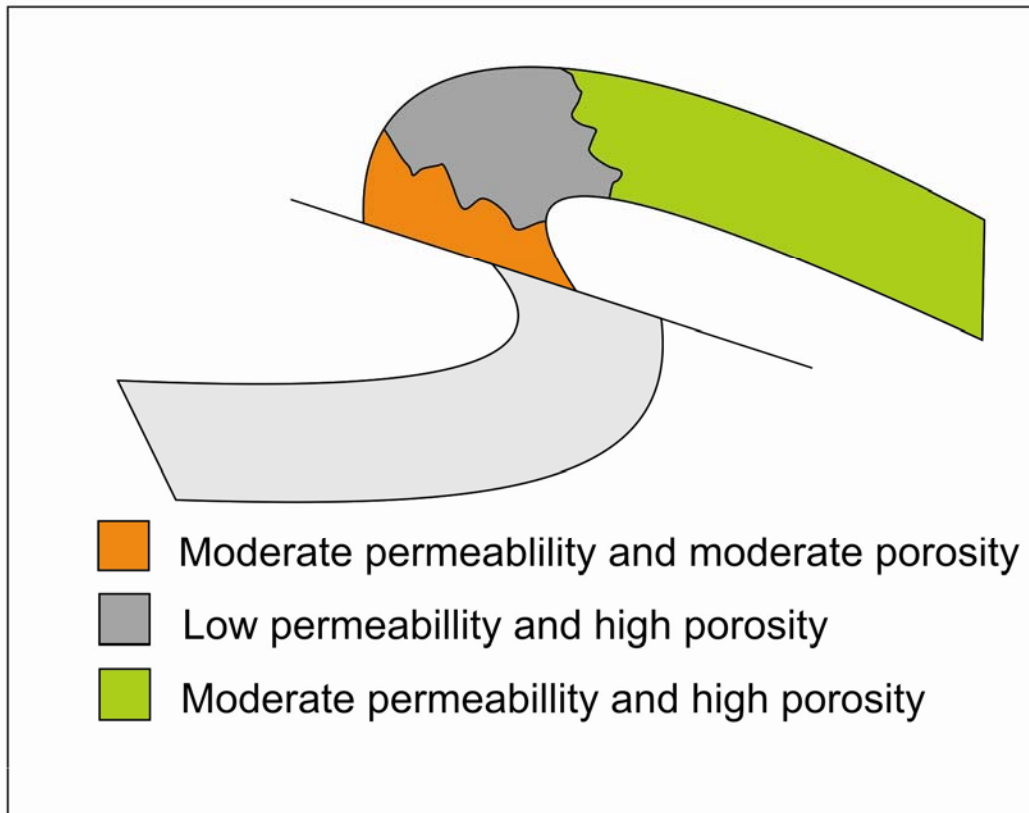


Figure 5.4: A theoretical permeability and porosity model based in fracture characteristic and their appearance in domain. Good porosity and permeability properties can in general be found in Mediumfjellet. In this model moderate permeability makes up 30% and 60% of the area, low permeability is less than 30 %, moderate porosity is between 30% and 60%, whereas high porosity makes up more than 60% of the area. The percentage is estimated from the total fractures collected in the domain.

relative high fracture intensity (see above), result as a good carrier rock for fluid transportation. The hinge zone, which is characterized by relative good porosity and high fracture intensity, will work as the domain with the best reservoir properties. The Backlimb will probably be insignificant for a fluid model.

This study suggests a model, assumed that the thrust fault is open for fluid flow but sealed at the top (Triassic shales), with fluid migration along the thrust fault into, and through the forelimb and thereafter into the hinge zone.

Chapter 6

Conclusion and future work

6.1. Conclusion

Based on the descriptions and discussions made of the thesis, the following conclusions can be drawn:

1. Based on Lidar scan data, 3D field modelling, and fracture analysis, the geometry of the Mediumfjellet thrust stack is documented to have variations along strike. The thrust geometry varies along-strike with examples including thrust intersections, possible thrust displacement gradients and oblique ramp faults and folds. This likely relates to lateral variations between fault-propagation folding and transported fault-propagation folding. The fold geometry is also controlled by the folding, as suggested by observations of both shear folding and flexure-slip folding.
2. Three fracture populations are interpreted to exist in the Mediumfjellet thrust stack; i) perpendicular fractures, ii) hybrid fractures, and iii) thrust fractures. The perpendicular fractures consist of a conjugate shear fracture system (set II and IV) and an orthogonal extensional fracture set (set I and III). The hybrid fractures consist of three steeply dipping fracture sets (set **w**, **x** and **q**), and are suggested to be local extensional features or en-échelon fractures indicating local shearing. The thrust fractures (sets A, B and C) are conjugate shear fractures indicating bedding-parallel contraction.
3. The discussed fracture development at Mediumfjellet suggests a 2-stage fracture model, where the folded and thereby rotated thrusts within the major folds indicate a pre-folding stage. The geometrical relationship between the perpendicular fractures, conjugate hybrid fractures and the fold-axis is consistent with a syn-folding fracture event. The 2 stage fracture model suggests an initiation stage of thrust fracturing and extension fracturing reflecting NE-SW shortening and later a syn-folding event consistent with NE-SW to E-W contraction.

4. Non-systematic fractures are interpreted to result from variations in the local stress fields, such as in areas hosting lateral ramps. Alternatively, they are pre-existing fractures developed prior to folding and in cases reactivated during later deformation
5. General higher fracture intensity in the fold hinges suggests folding with fixed hinges and rotating forelimbs, as commonly ascribed to fault-propagation folding. Local variations occur, with more deformation in the forelimb, suggesting effects associated with transported fault-propagation folding.
6. High fracture intensities and a general higher number of short fractures in the fold hinge zones confirm the hinge as a good fractured carbonate reservoir. Additionally, the forelimb and the areas around the major thrusts will probably work as better pathways for fluid migration as the forelimb reveals more throughgoing fractures compared to the hinge zone and backlimb. The backlimb will be less significant as a reservoir and for fluid flow.

6.2. Future work

This fracture study has been carried out in a large area, made up of complex fold-and-thrust structures. In order to cover such a large area, it is important to understand the value of data gathered in smaller areas, especially of fracturing. More detailed single-fold case studies should be carried out in order to further understand the detailed links between fractures and folding.

The 3D modelling and modelling software applied in this work opens for an enormous range of possibilities. It is possible to make fold curvature maps, where fracture intensity and fold curvature may be compared. It is possible to give each bed in the strata different fracture properties. A fractured layer model may be generated and fluid flow models from porosity/permeability input could be used to address the lateral variations in the fluid flow. It should also be possible to establish a trend between fracture intensity and bedding thickness. This trend can be used as a conditioning factor for all the layers in the numerical model. This could further be conditioned to the model, which in the end would result in an advanced 3D fractured model

References

- Ahmadhadi, F., Lacombe, O., and Daniel, J.-M., 2007, Early reactivation of Basement Faults in Central Zagros (SW Iran): Evidence from Pre-folding Fracture Populations in Asmari Formation and Lower Tertiary Paleogeography: In: Thrust Belts and Foreland Basins, Lacombe, O., Lavé, J., Roure, F. and Vergès (Eds.), p. 205-228.
- Almendinger, R. W., 1998, Inverse and forward numerical modelling of trishear fault-propagation folds: *Tectonics*, v. 17, p. 640–656.
- Andresen, A., Bergh, S. G., and Haremo, P., 1994, Basin inversion and thin skinned deformation associated with the Tertiary transpressional belt West Spitsbergen orogen: Proceeding from International Conference on Arctic Margins, Anchorage.
- Aydin, A., 2000, Fractures, faults and hydrocarbon entrapment, migration and flow: *Marine and Petroleum Geology*, v. 17, p. 797-814.
- Bellhansen, N., Fiore, P., and Pollard, D. D., 2006, The role of Fractures in the structural interpretation of sheep Mountain Anticline, Wyoming: *Journal of Structural Geology* (in press), p. 1-18.
- Bergbauer, S., and Pollard, D. D., 2004, A new conceptual fold-fracture model including prefolding joints, based on the Emigrant Gap anticline, Wyoming: *GSA Bulletin*, v. 116, p. 294-307.
- Bergh, S., Maher, H. D., and Braathen, A., 2000, Tertiary divergent thrust directions from partitioned transpression, Brøggerhalvøya, Spitsbergen: *Norsk Geologisk tidsskrift*, v. 80, p. 63-82.
- Bergh, S. G., and Andresen, A., 1990, Structural development of the Tertiary fold-and thrust belt in east Oscar II land, Spitsbergen: *Polar Research*, v. 8, p. 217-236.
- Bergh, S. G., Braathen, A., and Andresen, A., 1997, Interaction of Basement-Involved and Thin-Skinned Tectonism in the Tertiary Fold-Thrust Belt of Central Spitsbergen, Svalbard: *AAPG Bulletin*, v. 81, p. 637-661.
- Birkenmajer, K., 1975, Caledonides of Svalbard and plate tectonics: *Geological Society of Denmark*, v. 24, p. 1-19.

- Birkenmajer, K., 1981, The geology of Svalbard, the western part of the Barents Sea, and the continental margin of Scandinavia. In: A. E. M. Nairn, N. Churjin and F. G. Stehli (Ed.), The ocean basins and margins. New York Plenum Publishing Cooperation: 265-322.
- Boyer, S. E. and Elliott, D. 1982. Thrust systems. American Association of Petroleum Geologists Bulletin, 66, 1196-1230.
- Braathen, A., Bergh, S., and Maher, H. D., 1997, Thrust kinematics in the central part of the Tertiary transpressional fold-thrust belt in Spitsbergen: Norges Geologiske Undersøkelse Bulletin, v. 433, p. 32-33.
- Braathen, A., and Bergh, S. G., 1995, Kinematics of Tertiary deformation in the basement-involved fold-thrust complex, western Nordenskiöld Land, Svalbard: tectonic implications based on fault-slip data analysis: Tectonophysics, v. 249, p. 1-29.
- Braathen, A., Bergh, S. G., Karlsen, F., Maher Jr, H., Andresen, A., Hansen, A.-I., and Bergvik, A., 1999, Kinematics of the Isfjorden-Ymerbukta Fault Zone: a dextral oblique-thrust ramp in the Tertiary fold-thrust belt of Spitsbergen: Norsk Geologisk tidsskrift, v. 79, p. 227-240.
- Braathen, A., Bergh, S. G., and Maher Jr., H. D., 1999, Application of a critical wedge taper model to the Tertiary transpressional fold-thrust belt on Spitsbergen, Svalbard: GSA Bulletin, v. 11.
- Buchan, S. H., Challinor, A., Harland, W. B., and Parker, J. R., 1965, The Triassic stratigraphy of Svalbard: Norsk Polarinstitutt Skrifter, v. 135, p. 1-92.
- Buckley, S. J., Vallet, J., Braathen, A., and Wheeler, W., 2008, Oblique helicopter-based laser scanning for digital terrain modelling and visualisation of geological outcrops: Commission IV/4.
- Butler, R. W. H., 1982, The terminology of structures in thrust belts: Journal of Structural Geology, v. 4, p. 239-245.
- Colman-Sadd, S. P., 1978, Fold Development in Zagros Simply Folded Belt, Southwest Iran: AAPG Bulletin, v. 62.
- Robert R. Compton, 1985, Geology in the Field, John Wiley & Sons
- Cooke, M. L., Simo, J. A., Underwood, C. A., and Rijken, P., 2006, Mechanical stratigraphic controls on fracture patterns within carbonates and implications for groundwater flow: Sedimentary Geology, v. 184, p. 225-239.

- Cooper, S. P., Goodwin, L. B., and Lorenz, J. C., 2006, Fracture and fault patterns associated with the basement-cored anticlines: The example of Teapot Dome, Wyoming: AAPG Bulletin, v. 90, p. 1903-1920.
- Cutbill, L. J., and Challinor, A., 1965, Revision of the stratigraphical scheme for the Carboniferous and Permian rocks of Spitsbergen and Bjørnøya: Geological Magazine, v. 102, p. 418-439.
- Dalman, W. K., 1999, Lithostratigraphic Lexicon of Svalbard.
- Davies, R. J., 2005, Differential compaction and subsidence in sedimentary basins due to silica diagenesis: A case study: GSA Bulletin, v. 117, p. 1146-1155.
- Davies, R. J., Goult, N. R., and Meadows, D., 2008, Fluid flow due to the advance of basin-scale reaction zones: GSA Bulletin, v. 120, p. 195-206.
- Davis, G. H., and Reynolds, S. J., 1996, Structural Geology of rocks and regions: John Wilsley and Sons Inc, v. (second edition).
- Ehrenberg, S. N., Pickard, N. A. H., Henriksen, L. B., Svånå, T. A., Gutteridge, P., Macdonald, D. I. M., and Anonymous, 2001, A depositional and a sequence stratigraphic model for cold-water, spiculitic strata based on the Kapp Starostin Formation (Permian) of Spitsbergen and equivalent deposits from the Barents sea: American Association of Petroleum Geologists and Society of Economic Paleontologists and Mineralogists, v. 2001, p. 56.
- Engelder, T., 1982, Reply: Tectonics, v. 1, p. 465-470.
- Engelder, T., and Geiser, P., 1980, On the use of regional joint sets as trajectories of paleostress fields during the development of the Appalachian Plateau: Journal of Geophysical Res., v. 85.
- Erslev, E. A., 1991, Trishear fault-propagation folding: Geology, v. 19, p. 617-620.
- Erslev, E.A., Mayborn, K.R., 1997. Multiple geometries and modes of fault-propagation folding in the Canadian thrust belt. Journal of Structural Geology 19, 321–335.
- Ezaki, Y., Kawamura, T., and Nakamura, K., 1994, Kapp Starostin Formation in Spitsbergen: A sedimentary and faunal record of Late Permian paleoenvironments in an Arctic region: Canadian Society of Petroleum Geologist Memoir, v. 17, p. 647-655.

- Faleide, J. I., Tsikalas, F., Breivik, A. J., Mjelde, R., Ritzmann, O., Engen, Ø., Wilson, J., and Eldholm, O., 2008, Structure and evolution of the continental margin off Norway and the Barents Sea: Episodes, v. 31, p. 82-91.
- Fard, R. A., Braathen, A., Mokhtari, M., and Alavi, S. A., 2006, Interaction of the Zagros Fold-thrust Belt and the Arabian type, deep-seated folds in the Ababan Plain and the Dezful Embayment, SW Iran: Petroleum Geoscience, v. 12, p. 347-362.
- Fisher, M. P., and Wilkerson, M. S., 2000, Predicting the orientation from joints from fold shape; results from pseudo-three-dimensional modelling and curvature analysis: Geology, v. 28, p. 15-18.
- Fleuty, M. J., 1964. The description of folds. Geologists Association, London, 75 (4): 461-492.
- Florez-Niño, J.-M., Aydin, A., Mavko, G., Antonellini, M., and Ayaviri, A., 2005, Fault and fracture systems in a fold and thrust belt: An example from Bolivia: AAPG Bulletin, v. 89, p. 471-493.
- Fossen H. and Gabrielsen, R. H., 2005. Strukturgeologi, Fagbokforlaget Vigmostad Bjørke AS.
- Gee, E. R., Harland, B., and McWhae, J. R. H., 1953, Geology of Central Vestspitsbergen; Part 1. Review of the Geology of Spitsbergen, with Special References to Central Vestspitsbergen Trans. Roy. Soc. Edinb., v. 63, p. 299-256.
- Gross, M. R., 1993, The origin and spacing of cross joints: Examples from the Monterey Formation, Santa Barbara coastline, California, J. Struct. Geol., 15, 737 – 751.
- Gross, M. R., and Eyal, Y., 2007, Throughgoing fractures in layered carbonate rocks: GSA Bulletin, v. 119, p. 1387-1404.
- Grundvåg, S.-A., 2008, Facies analysis, sequence stratigraphy and geochemistry of the middle-upper Permian Kapp Starostin Formation, central Spitsbergen: Master Thesis in Sedimentary Geology, Department of Geology, University of Tromsø.
- Haabet, T., 1995, Strukturell analyse av småstrukturer i den tertiære underlagsinvolverte Vermlanrygg-antiklinalen, Tygghamna, Spitsbergen: Masteroppgave i geologi, Universitetet i Tromsø.
- Hancock, P., 1985, Brittle microtectonics: principles and practice: Structural Geology, v. 7, p. 437-458.

- Hansen, S. P. J., 1991, En strukturgeologisk analyse av Foldete og skjøvne enheter i Perm-Trias ved Ekmanfjorden, i sentrale deler av vest-Spitsbergens Tertiære folands folde- og skyvebelte: Hovedfagsoppgave i Geologi.
- Hardy, S., and Connors, C. D., 2006, Short note: A velocity description of shear fault-bend folding: *Journal of Structural Geology*, v. 28, p. 536–543.
- Harland, W. B., 1969, Contribution of Spitsbergen to understanding of tectonic evolution of North Atlantic region: In: M. Kay (Ed.), *North Atlantic Geology and Continental Drift. AAPG Memoir*, v. 12, p. 817-851.
- Harland, W. B., Anderson, L. M., Manasrah, D., and Butterfield, N. J., 1997, *The Geology of Svalbard: Geological society Memoir*, v. 17.
- Harland, W. B., and Horsefield, W. T., 1974, West Spitsbergen orogen: In: Data for orogenic studies, A. M. Spencer (Ed.), *Geological society of London Special report*, p. 747-755.
- Huang, Q., and Angelier, J., 1989, Fracture spacing and its relation to bed thickness *Geological Magazine*, v. 126, p. 355-362.
- Ingebrigtsen, A. J., 1994, Geometrisk og Kinematisk analyse av Vermlandryggantiklinalen, en Tertiær underlagsinvolvert makrofold ved Trygghamna, vest Spitsbergen; - Deformasjoen påvirket av preeksisterende heterogeniteter: Masteroppgave i Geologi, Universitetet i Tromsø.
- Jaeger, J. C., and Cook, N. G. W., 1979, *Fundamentals of Rock mechanics*: Chapman & Hall, London.
- Jamison, W. R., 1987, Geometric analysis of fold development in overthrust terranes: *Journal of Structural Geology*, v. 9, p. 207-220.
- Karlsen, F., 2000, Structural development of the Isfjorden-Ymerbukta Fault Zone at Bohemansflya, Spitsbergen: a transverse structure in the Tertiary fold-thrust belt: Master thesis.
- Kleinspehn, K. L., Pershing, J., and Teyssier, C., 1989, Paleostress stratigraphy: A new technique for analyzing tectonic control on sedimentary-basin subsidence: *Geology*, v. 17, p. 253-256.
- Kulander, B. R., Barton, C. C., and Dean, S. L., 1979, The application of fractography to core and outcrop fracture investigations: Tech. Rep. U.S. Dept. Energy METC/SP-79/3, Morgantown Energy Technology Center, p. 1-174.

- Lacazette, A. 2000, Natural Fracture Nomenclature, Disk 1, 13 pages, in L.B. Thompson (ed.) Atlas of Borehole Images, AAPG Datapages Discovery Series 4, American Association of Petroleum Geologists, Tulsa (2 compact disks).
- Lauritzen, Ø., 1981, Development pattern of gypsum/anhydrite in Lower Permian sediments of central Spitsbergen - a suggested classification: Norsk Polarinstitutt Årbok, v. 1973, p. 5-21.
- Lowell, J. D., 1972, Spitsbergen Tertiary orogenic belt and the Spitsbergen fracture zone: Geological Society of America Bulletin, v. 83, p. 3091-3102.
- Lyberis, N., and Manby, G. M., 1993, The origin of the West Spitsbergen Fold Belt from geological constraints and plate kinematics: Implications for the Arctic: Tectonophysics, v. 224, p. 371-391.
- Maher, H., Bergh, S., Braathen, A., Manby, G. M., and Lyberis, N., 1991, Discussion on pre-ocean opening compression of the Northwestern Atlantic margin: evidence from eastern Greenland Journal of the Geological Society, v. 157, p. 707-710.
- Maher, H. D., and Welbon, A. I., 1992, Influence of the Carboniferous structures on Tertiary tectonism at St. Jonsfjorden and Bellsund Western Svalbard: Norsk Geologisk tidsskrift, v. 72, p. 67-75.
- Maher, H. D. J., Bergh, S. G., Dalman, W. K., and Harland, W. B., 1995, Tertiary or Cretaceous age for Spitsbergen's fold-thrust belt on the Barents shelf: Tectonics, v. 14, p. 1321-1326.
- Maher Jr., H. D., Bergh, S., Braathen, A., and Ohta, Y., 1997, Svartfjella, Eidembukta, and Daudmannsodden lineament: Tertiary orogen-parallel motion in the crystalline hinterland of Spitsbergen's fold-thrust belt: Tectonics, v. 16, p. 88-106.
- Malkowski, K., and Hoffmann, A., 1979, Semi-quantitative facies model for the Kapp Starostin formation (Permian), Spitsbergen: Acta Palaeontologica Polonica, v. 24, p. 217-230.
- Marshak, S., Wilkerson, M. S., and Hsui, A. T., 1992, Generation of curved fold-thrust belts: Insight from simple physical and analytical models: in: Thrust Tectonics, McClay (Ed.), p. 83-93.
- McCann, A. J., and Dalman, W. K., 1995, Reactivation of the long-lived Billefjorden Fault Zone in north central Spitsbergen, Svalbard.: Geol. Mag., v. 133 (1), 1996.

- McClay, K. R., 1992, Glossary of thrust tectonics terms: Department of Geology, Royal Holloway and Bedford New College, University of London, Egham, Surrey, England, TW20 OEX.
- , 2000, The Mapping of Geological Structures: John Wilsley and Sons Ltd., Chichester, England, p. 161.
- Mosar, J., and Suppe, J., 1992, Role of shear in fault-propagation folding: In: Thrust Tectonics, McClay, K. R. (Ed.), p. 123-132.
- Myhre, A. M., Eldholm, O., and Sundvor, E., 1982, The margin between Senja and Spitsbergen fracture zones: implications from plate tectonics: *Tectonophysics*, v. 89, p. 33-50.
- Mynatt, I., Hilley, G. E., Kaven, J. O., and Pollard, D. D., (in press), Geometric and mechanical models of fault, fold and fracture development for Raplee Ridge, UT.
- Mynatt, I., and Pollard, D. D., 2008, Fracture initiation, development and reactivation in folded sedimentary rocks at Raplee Ridge, UT: *Structural Geology* (in press).
- Mørk, A., and Borøy, 1984, Mesozoic source rocks on Svalbard. In *Petroleum Geology of the North European Margin: Norwegian Petroleum Society* (Graham and Trotman, 1984), p. 371-382.
- Mørk, A., Embry, A. F., and Weitschat, W., 1989, Triassic transgressive-regressive cycles in the Sverdrup Basin, Svalbard and the Barents shelf: In: *Correlation in hydrocarbon exploration*. Norwegian Petroleum Society, Graham and Trotman, London, p. 113-130.
- Nathorst, A. G., 1910, Beiträge zur Geologie der Bäreninsel. Spitzbergen und des König-Karl-Landes: *Bulletin Geologiska Institutionen Universitetet i Upsala*, v. 10, p. 261-416.
- Nøttvedt, A., Cecchi, M., Gjeldberg, J. G., Kristensen, S. E., Lønøy A., Rasmussen, A., Skott, P. H., and van Veen, P. M., 1993, Svalbard-Barents Sea correlation: a short review. In Vorren, T.O. et al. (eds.), *Arctic Geology and Petroleum Potential*. NPF Special Publication: Elsevier Scientific Publications, v. 2, p. 363-375.
- Odling, N. E., 1992, Permeability of natural and simulated fracture patterns: *NPF Special Publication*, v. 1, p. 365-380.
- Odling et al., 2004. Permeability scaling properties of fault damage zones in siliclastic rocks. *Journal of Structural Geology*. v26. 1727-1747.
- Peacock, D. C. P., and Sanderson, D. J., 1992, Effects of layering and anisotropy on fault geometry: *Journal of the Geological Society*, v. 149, p. 793-802.

- Pearce, M. A., Jones, R. R., Smith, S. A. F., McCaffrey, K. J. W., and Clegg, P., 2006, Numerical analysis of fold curvature using data acquired by high-precision GPS: *Journal of Structural Geology*, v. 28, p. 1640-1646.
- Poblet, J., and McClay, K., 1996, Geometry and kinematics of singlelayer detachment folds: *American Association of Petroleum Geologists Bulletin*, v. 80, p. 1085–1109.
- Price, N., 1966, *Fault and Joint Development in Brittle and Semi-Brittle Rock*: Pergamon Press, Oxford, p. 176.
- Price, N., and Cosgrove, J., 1990, *Analysis of geological structures.*: Cambridge University Press, Cambridge, p. 502.
- Price, R. A., 1967, The tectonic significance of mesoscopic subfabrics in the southern Rocky Mountains of Alberta and British Columbia: *Can. Journal of Earth Science*, v. 4, p. 39-70.
- Puigdefàbregas, C., Muñoz, J. A., and Vergés, J., 1992, Thrusting and foreland basin evolution in the Southern Pyrenees, In: *Thrust Tectonics*, McClay, K. R. (Ed.), p. 247-254.
- Ramsey, J. M., and Chester, F. M., 2004, Hybrid fracture and the transition from extension fracture to shear fracture: *Nature*, v. 428, p. 63-66.
- Ray, S. K., 2006, Scaling properties of thrust fault traces in the Himalayas and inferences on thrust fault growth: *Journal of Structural Geology*, v. 28, p. 1307-1315.
- Rudenkiewicz, J. L., Sherkati, S., and Letouzey, J., 2007, Evolution of Maturity in Northern Fars and the Izeh Zone (Iranian Zagros) and Link with Hydrocarbon Prospectivity. In: *Thrust Belts and Foreland Basins From Fold Kinematics to Hydrocarbon Systems*, Lacombe, O., Lavé, J., Roure, F. and Vergés, J. (Eds.), p. 229-246.
- Salvini, F., and Storti, F., 2001, The distribution of deformation in parallel fault-related folds with migrating axial surfaces: comparison between fault-propagation and fault-bend fold: *Journal of Structural Geology*, v. 23, p. 25-32.
- Shaw, J. H., Connors, C., and Suppe, J., 2005, *Seismic Interpretation of Contractional Fault-Related Folds: An AAPG Seismic Atlas*, *Studies in Geology*, v. 53.
- Siedlecka, A., 1975, The petrology of some Carboniferous and Permian rocks from Bjørnøya, Svalbard: *Norsk Polarinstitutt Årbok*, v. 1973, p. 53-72.
- Skaloud, J., Vallet, J., Keller, K., Veyssièrè, G., and Kölbl, O., 2006, An eye for Landscapes - Rapid Aerial Mapping with Handheld Sensors: *GPS World*, v. 17, p. 26-32.

- Stearns, D. W., 1968, Certain aspects of fractures in naturally deformed rocks: *Rock Mechanics Seminar*. R. E. Riecker, Bedford, Terrestrial Sciences Laboratory, p. 97-118.
- Stearns, D. W., and Friedman, M., 1972, Reservoirs in fractured rocks.: In: King, R. E (ed). *Stratigraphic oil and gas fields - Classification exploration methods, and case histories: AAPG Memoir 16, Society of Exploration Geophysics Special Publication, v. 10, p. 82-106.*
- Steel, R., Gjelberg, J., Helland-Hansen, W., Kleinspehn, K., Nøttvedt, A., and Rye-Larsen, M., 1985, The Tertiary Strike-slip basins and Orogenic belt of Spitsbergen.
- Steel, R. J., and Worsley, D., 1984, Svalbard post Caledonian strata- an atlas of sedimentological patterns and paleogeographic evolution: *Petroleum Geology of the North European Margin*, p. 109-135.
- Stöcklin, J., 1968, Structural history and tectonics of Iran; a review: *American Association of Petroleum Geologists Bulletin*, v. 59, p. 509-526.
- Suppe, J., 1983, Geometry and kinematics of fault-bend folding: *American Journal of Science*, v. 283, p. 684-721.
- , 1985, *Principles of Structural Geology*: Prentice Hall, Eaglewood Cliffs, New Jersey, p. 537.
- Suppe, J., Connors, C. D., and Zhang, Y., 2004, Shear fault-bend folding. In: K.R. McClay, Editor, *Thrust Tectonics and Hydrocarbon Systems: AAPG Memoir*, v. 82, p. 303-323.
- Suppe, J., and Medwedeff, D. A., 1984, Fault-propagation folding: *Geological Society of America Abstracts with programs*, v. 16, p. 670.
- Suppe, J., and Medwedeff, D. A., 1990, Geometry and kinematics of fault-propagation folding: *Eclogae Geologicae Helvetica*, v. 83, p. 409-454.
- Talwani, M., and Eldholm, O., 1977, Evolution of the Norwegian - Greenland Sea: *Geological Society of America Bulletin*, v. 88, p. 969-999.
- Tavani, S., Storti, F., Fernández, O., Muñoz, J. A., and Salvini, F., 2006, 3-D deformation pattern analysis and evolution of the Aníscolo anticline, southern Pyrenees: *Journal of Structural Geology*, v. 28 p. 695–712.
- Tavani, S., and Storti, F., 2006, Fault-bend folding as an end-member solution of (double edge) fault-propagation folding: *Terra Nova*, v. 18, p. 270-275.

- Travé, A., Labaume, P., and Vergés, J., 2007, Fluid systems in Foreland Fold-and-Thrust Belts: An Overview from the Southern Pyrenees: In: Thrust Belts and Foreland Basins, Lacombe, O., Lavé, J., Roure, F. and Vergès (Eds.), p. 93-115.
- Tsang, Y. W., 1984, The effect of tortuosity on fluid flow through a single fracture: *Water Resources Research*, v. 20, p. 1209-1215.
- Turner, F. J., and Weiss, L. E., 1963, *Structural Analysis of Metamorphic Tectonites*: McGraw-Hill, New York.
- Twiss, R. J., and Moore, E. M., 1992, *Structural Geology*, W.H. Freeman, New York, p. 532.
- Welbon, A., and Maher, H. D., 1992, Tertiary tectonism and basin inversion of the St. Jonsfjorden region, Svalbard: *Journal of structural geology* v. 14, p. 41-55.
- Wennberg, O. P., 1990, En geometrisk og kinematisk analyse av østmarginen til det tertiære foldebeltet nord for Isfjorden, Oscar II land, Spitsbergen, Masters thesis, University of Oslo
- Wennberg, O. P., Andresen, A., Hansen, S., and Bergh, S. G., 1994, Structural evolution of a frontal ramp section of the West Spitsbergen, Tertiary fold and thrust belt, north of Isfjorden, Spitsbergen: *Geological Magazine*, v. 131 (I), p. 67-80.
- Wennberg, O. P., Svånå, T., Azizzadeh, M., Aqrawi, A. M. M., Brockbank, P., Lyslo, K. B., and Ogilvie, S., 2006, Fracture intensity vs. mechanical stratigraphy in platform top carbonates: the Aquitanian of the Asmari Formation, Khaviz Anticline, Zagros, SW Iran *Petroleum Geoscience*, v. 12, p. 235-246.
- Wilkerson, M. S., Apotria, T., and Farida, T., 2001, Interpreting the geologic map expression of contractional fault-related fold terminations: lateral/oblique ramps versus displacement gradients *Journal of Structural Geology* v. Volume 24, p. 593-607.
- Worsley, D., 1986, *The geological history of Svalbard*: Det norske stats oljeselskap, p. 121.

Appendix I

Unit-description of Kapp Starostin Formation

Rock-description of Kapp Starostin Formation	
1	Grey colored, highly silicified shale. Individual laminae are about 3-5 cm thick, in total making up 3 m of unit thickness. No lithoclasts from Gipshuken formation is found. Similar beds are not described from the type section at Festningen [Dalmann 1999], but are here interpreted to belong to the Kapp Starostin formation.
2	Grey bedded limestone with patches of yellow weathering relief. Various layers are between 15 and 50 cm thick, summarizing to a total thickness of about 3,5 meters. It is very coarse grained and contains large (>10cm) fragments of brachiopods, sponges and crinoids.
3	Medium grey colored, coarse grained packstone to wackestone with coarse sandy matrix of medium grey color with scattered yellow weathering. The unit has a gradual contact to the underlying strata because of slope scree. Individual beds are competent and from 0,5m to 2 m thick. The fabric consists of Abundant macrofossils i.e. whole brachiopods, shell fragments and spicules. The unit is interpreted to be the Vøringen member.
4	Medium grey colored, cliff forming mudstones, which are more light grey colored towards the top. The beds vary from 10cm to 30cm in thickness together reaching a total unit thickness of 12 meters. They are highly silicified and recrystallized. Individual beds can be seen to be bioturbated, with nodular and undulating boundaries. They often contain black elongated chert concretions up to 10 cm in length. Partly dissolved macrofossils and scattered whole fossils and fragments are present.
5	Alternating grey, highly silicified shale and dark grey soft shale. total thickness of the unit is 15 meters thick. The grey silicified shale has an upward thickening trend from 10-15 cm at the bottom to more than 50 cm at the top. In contrast, the dark shales are upwards thinning trend from about 10 cm to a few cm. They are both very bioturbated.
6	Grey limestone layers with patches of yellow weathering. Each layer is about 50 cm

	thick and has a total thickness of 3 meters. It is very coarse grained made up of big closely spaced whole brachiopods, sponges and crinoids (packstone).
7	Light gray, strongly silicified beds with slightly nodular bed boundaries. The bed thickness varies between 0,5m and 1 meter. The total thickness of the unit is about 2,8m thick. It reveals partly silicified lamination and elongated chert nodules. There are also up to 20 cm abundant silicified bioclasts occurring. At the top with a sharp contact to unit 8, it occurs a 0,5 m thick bed with silicified shale.
8	Intercalations between grey, fine grained cliff forming beds with nodular bedding and darker, weathered out soft shale. The total thickness of the unit is about is 2,4 meters thick. The competent beds are about 20 to 50 cm thick, and have an upwards thinning trend. The soft shale layers are up to 5 cm thick. Scattered bioclasts and abundant spicules occur, but no obvious macrofossils.
9	Cliff forming, light grey bioturbated limestone beds, with an upwards thinning trend. The unit has a total thickness of 3,7 meters. The beds range from thicknesses of 50 cm to less than 10 cm thick. The beds have a characteristic yellow weathering color. The bed boundaries are smooth between the thick beds and more rugged between the thinner beds. Towards the top there are some scattered to abundant macrofossils, the latter seen as whole brachiopods sponges, shell fragments and crinoids. Dark burrows occur at top of- and sometimes within the bedding. About 30 cm of soft weathered out shale towards unit 11.
10	Fine grained, dark grey, cliff forming and silicified mudstone beds with platy shale intercalations. The total thickness of the unit is 3 meters. The bed boundaries are rugged and slightly nodular. Sponge spicules and scarce scattered silicified bioclasts occur.
11	Slopeforming, soft, weathered bryozoan paper shale. The total thickness is about 20 meters mainly of slopescree.
12	Bioturbated dark grey to black shale with two major upwards fining and thinning cycles. A distinct yellow weathered bed occurs on top of each cycle. The total thickness of the unit is 15 meters. The thickness of each bed decreases from 80 cm to 40 cm thicknesses. They are intercalated with 2-10 cm platy shale, decreasing in frequencies towards the top. The bed boundaries are rugged and nodular bedding is common above just above the shales. Abundant spicules and scattered bioclasts can be found.
13	Silicified dark grey mudstone with shaly intercalations with a total thickness of the bed is 3,5 meters. The beds are heavily bioturbated.

14	Grey, cliff forming rock, with light grey, yellow to white weathering color. The total thickness of the bed is 10 meters. Mudstone beds are intercalated with shale at the bottom. The middle part consists of thicker and more massive beds with elongated sandstones, bedding parallel strong veining and a possible sedimentary breccia. There are abundant silicified bioclasts and heavy bioturbation further. The upper part of the unit contains partly laminated cliff forming mudstone intercalated with shale.
15	Bioturbated, dark grey, fine grained silicified mudstone. Abundant spicules and scattered bioclasts occur. The total thickness of the bed is 3,5 meters.
16	Three upwards fining packages of fine grained competent dark silicified shale reaching a total thickness of 16 meters. The three packages have a total overall fining upwards trend. The bedding is nodular and contains abundant spicules. The middle part has a bit of yellow weathering color and is more competent and more bioclasts occur. The top part is very fine grained with strong nodular bedding and contains rounded red chert nodules. The content of spicules and bioclasts are also higher.
17	Bioturbated, dark grey to grey silicified mudstone with rugged bedding boundaries. No obvious macrofossils occur. Total bed thickness is 3,5 meters.
18	Highly nodular, bioturbated, dark silicified shale. The nodules have a black inner part and a grey coating. The total bed thickness is 2 meters.
19	Dark silicified cliff forming mudstone, with a total thickness of 1,5 meters. The beds contain bedding parallel lamination with dark elongated pebbles and sandy slingers. The beds are heavily bioturbated and contain dark scattered shell fragments.
20	Dark silicified, highly nodular shales with a total thickness of the unit is 8 meters. A distinct intercalated competent yellow weathered bed, can be several meters thick or totally pinch out laterally.
21	15 meters of massive, light grey silicified cliff forming mudstone. The unit has a very characteristic yellow weathering colour, the same as seen in unit 3, 7 and 10. The contact to the underlying unit is very sharp.
22	Silicified, nodular, cliff forming mudstone beds. With a total thickness of 2,5 meters. This unit is the topmost of Kapp Starostin Formation and lay conformly underneath the Triassic Vardebukta Formation. This boundary is a regional hiatus marked by the great mass-extinction in Perm.

Appendix 2

Locality: 2e
 GPS Coordinates: ?

Thrust System: OOST
 Structural Position: Backlimb
 Scanline Number: 2e-1
 Lithological Unit: 10
 Bed Thickness: 50 cm
 Scanline Trend: 015

UNIT	BED ORIENTATION	DISTANCE	FRACTURE FREQUENCY	STRIKE	DIP	INTER / INTRA	SURFACE	COMMENTS		
0-1m	150/51	3	7	20	43	IR	S			
		24		340	26	IA	S			
		40		340	22	IR	S			
		52		334	27	IR	R			
		61		328	20	IR	R			
		74		270	5	IR	R			
		80		10	30	IR	S			
		1-2m		147/55	17	6	320	30	IA	S
18	5	43	IR		S					
45	340	21	IR		S					
68	21	40	IR		S					
80	250	70	IR		S					
85	266	65	IR		S					
2-3m	154/60	42	6		327		30	IA	S	
50		327			30		IA	S		
83		1		60	IA	R				
91		354		21	IA	S				
94		340		34	IR	R				
99		350		35	IA	S				

3-4m	153/57	28	5	293	20 IA	S		
		38		260	68 IR	S		
		59		315	27 IA	S		
		74		318	35 IR	S		
		81		260	70 IA	S		
4-5m	154/54	2	6	278	45 IA	S		
		10		315	28 IA	S		
		21		265	70 IR	S		
		40		320	30 IR	S		
		51		20	2 IA	S		
5-6m	130/52	68	7	354	35 IR	S		
		8		260	70	IR	R	RHR corrected
		30		328	20	IR	S	values
		45		262	70	IR	S	prominent
		65		310	30	IR	S	prominent
6-7m	154/48	70	5	250	70	IR	S	
		80		350	40	IR	S	
		90		0	40	IR	S	
		0		270	70	IR	S	
		40		184	40	IR	S	
7-8m	-	70	2	60	90	IR	S	prominent
		80		340	42	IR	S	
		100		85	80	IR	S	
		70		88	70	IR	R	
		100		196	55	IR	S	prominent

Locality: 2e
GPS Coordinates: 33 X 0479748
 8719772
Thrust System: OOST
Structural Position: Backlimb
Scanline Number: 2e-2
Lithological Unit: 10
Bed Thickness: 50 cm
Scanline Trend: 015

UNIT	BED ORIENTATION	DISTANCE	FRACTURE FREQUENCY	STRIKE	DIP	INTER / INTRA	SURFACE	COMMENTS
0-1m	166/45	13	4	18	40	IR	S	
		28		348	41	IR	R	
		48		354	37	IR	R	
		84		12	40	IR	S	
1-2m	147/51	8	5	293	37	IA	S	
		19		21	36	IR	S	
		36		14	45	IR	R	
		90		5	50	IR	S	
		90		346	34	IR	S	
2-3m	145/55	29	5	275	63	IR	R	
		29		320	46	IR	S	
		32		340	32	IR	S	
		33		11	43	IR	S	
		80		20	43	IR	S	
		96		258	67	IR	S	
3-4m	150/54	14	3	335	30	IA	S	
		22		335	30	IA	S	
		22		20	43	IR	S	
4-5m	153/55	21	3	327	20	IR	R	
		52		20	41	IR	S	
		98		335	25	IA	S	

Locality: 2e
GPS Coordinates: N 7832527
 E 1405192
Thrust System: OOST
Structural Position: Backlimb
Scanline Number: 2e-3
Lithological Unit: 10
Bed Thickness: 40cm
Scanline Trend: 040

UNIT (m)	BED ORIENTATION	DISTANCE	FRACTURE FREQUENCY	STRIKE	DIP	INTER / INTRA	SURFACE	COMMENTS
0-1m	158/52	28		291	45	IA	Rough	
		39		28	43	IR	Smooth	
		57		30	14	IA	Rough	
		73		30	14	IA	Rough	
		86		10	45	IR	Rough	
		92		328	30	IA	Smooth	
1-2m	152/50	9		346	36	IR	S	
		52		343	42	IR	R	
		68		20	42	IR	S	
		72		342	41	IR	R	
		85		330	46	IR	R	
2-3m	145/50	25		21	43	IR	S	
		35		351	64	IR	S	
		58		352	30	IA	R	Conjugate set
		62		291	84	IR	R	Conjugate set
		65		352	30	IR	R	Conjugate set
		72		291	84	IA	R	Conjugate set
		83		7	35	IR	R	
3-4m	150/50	89		291	84	IA	R	Conjugate set
		4		320	43	IR	S	
		14		14	36	IA	S	
		44		327	65	IR	R	
		81		20	45	IR	R	
		98		164	47	IR	R	

4-5m	146/50	13	343	25	IA	R	
		33	20	25	IR	S	
		36	343	25	IR	R	
		38	343	25	IR	S	
		59	5	53	IR	R	
5-6m	160/50	66	328	40	IR	R	
		2	354	45	IR	S	
		16	325	50	IR	S	
		57	355	45	IR	S	
		78	324	36	IR	S	Conjugate set
6-7m	148/48	100	46	80	IR	S	Conjugate set
		19	358	45	IR	R	
		23	310	20	IR	R	
		34	358	45	IA	R	
		60	355	38	IR	R	
7-8m	140/50	73	358	45	IR	R	
		96	325	35	IR	S	
		6	355	35	IR	S	
		46	45	40	IR	S	
		68	46	80	IR	S	Conjugate
		84	0	30	IR	R	
		87	330	35	IR	R	

Locality: 3b
GPS Coordinates: 33X 0480301
 8718424
Thrust System: M3
Structural Position: Backlimb
Scanline Number: 3b-1
Lithological Unit: 21
Bed Thickness: ?
Scanline Trend: 330

UNIT	BED ORIENTATION	DISTANCE	FRACTURE FREQUENCY	STRIKE	DIP	INTER / INTRA	SURFACE	COMMENTS
0-1m	126/44	0	12	274	78	IR	S	conj?
		1		238	30	IA	S	conj?
		6		253	64	IA	S	
		10		238	30	IA	S	conj?
		18		238	30	IR	S	conj?
		24		260	83	IA	S	
		29		265	87	IA	S	
		38		203	13	IR	S	Conjugate set
		38		136	73	IR	S	Conjugate set
		40		270	66	IR	S	
		52		7	60	IA	S	
		61		155	45	IA	S	Conjugate
		1-2m		126/41	36	2	252	70
42	267		62		IA		R	
2-3m								Covered
3-4m	133/55	0	5	323	40	IR	S	
		14		354	82	IR	R	
		30		255	41	IR	S	
		63		240	62	IA	S	
		78		241	65	IA	S	
4-5m	133/55	5	13	232	52	IA	S	
		18		320	70	IR	S	
		28		255	65	IR	S	
		43		236	65	IR	S	

		55		254	65	IA	S	
		61		265	62	IA	S	
		68		262	70	IR	S	
		74		256	63	IA	S	
		80		270	50	IA	S	
		82		270	50	IA	S	
		83		270	50	IA	S	
		86		263	36	IR	S	
		100		250	75	IR	S	
5-6m	140/65	49	6	256	75	IA	S	
		51		292	50	IR	R	
		68		12	60	IR	S	
		68		260	70	IR	S	
		83		67	61	IR	S	
		99		250	70	IA	S	
6-7m	140/65	42	3	235	30	IA	S	Conjugate
		44		235	30	IA	S	Conjugate
		46		235	30	IA	S	Conjugate
7-8m	-	6	11	325	08	IA	S	
		8		241	65	IR	S	
		16		250	60	IA	S	
		21		250	50	IA	S	
		35		163	34	IA	S	Conjugate
		53		248	76	IA	S	
		54		248	76	IR	S	
		56		340	54	IA	S	
		78		267	50	IA	S	
		80		253	69	IA	S	
		97		235	75	IA	S	Conjugate

Locality: 3b
GPS Coordinates: 33X 0480389
 8718658
Thrust System: M3
Structural Position: Backlimb
Scanline Number: 3b-2
Lithological Unit: 21
Bed Thickness 30 cm
Scanline Trend: 348

UNIT	BED ORIENTATION	DISTANCE	FRACTURE FREQUENCY	STRIKE	DIP	INTER / INTRA	SURFACE	COMMENTS	
0-1m	150/42	0	12	68	64	IR	S	Conjugate set	
		1		250	70	IR	S	Conjugate set	
		4		250	70	IR	S		
		5		75	78	IR	S		
		5		342	46	IA	S		
		20		92	90	IA	S	conj?	
		22		345	70	IA	S		
		47		295	60	IR	S		
		55		274	88	IR	S	conj?	
		58		274	88	IR	S	conj?	
		67		272	85	IR	S	conj?	
		100			218	60	IR	S	
		1-2m		162/60	9	13	158	88	IA
10	345		50		IA		S		
20	348		44		IR		S		
20	276		88		IR		S	conj?	
30	270		62		IA		S		
30	20		58		IA		S		
40	258		60		IR		S		
40	342		50		IR		S		
65	314		60		IR		S		
70	314		60		IR		S		
80	272		62		IR		S		
85	325	40	IR	S					

90

272

62

IR

S

Locality: 3c
GPS Coordinates: N 7832062
 E 1409016
Thrust System: M3
Structural Position: (forelimb) - hinge - (backlimb)
Scanline Number: 3c-1
Lithological Unit: 2
Bed Thickness: 30 cm
Scanline Trend: 030

UNIT	BED ORIENTATION	DISTANCE	FRACTURE FREQUENCY	STRIKE	DIP	INTER / INTRA	SURFACE	COMMENTS
0-1m	281/12	16	5	197	85	IA	R	Backlimb
		18		197	85	IR	R	
		29		172	82	IR	R	
		65		172	82	IR	R	
		82		200	67	IR	S	
1-2m	281/12	20	6	190	89	IR	S	Backlimb
		23		190	89	IR	S	
		40		150	73	IR	R	
		60		140	79	IR	R	
		71		159	84	IR	S	
2-3m		100	8	144	90	IR	S	Backlimb
		13		202	90	IR	S	
		16		144	90	IR	S	
		27		130	14	IA	S	
		30		144	90	IR	S	
		57		354	87	IR	S	
		60		217	87	IR	S	
3-4m		70	7	153	85	IR	R	Backlimb
		100		202	80	IR	R	
		6		151	80	IR	R	
		13		143	81	IR	R	
		33		155	86	IR	S	
	70	160	87	IR	R			
	78	193	76	IR	S			

		92		325	88	IR	S	
		98		307	23	IR	S	
4-5m		1	10	137	72	IA	R	Hinge
		5		155	75	IA	R	
		36		138	80	IR	R	
		55		138	80	IA	R	
		71		148	82	IR	S	
		72		181	73	IR	S	
		73		181	73	IR	S	
		80		192	80	IR	S	
		90		82	65	IR	R	
		100		194	75	IR	S	
5-6m	267/20	4	3	153	82	IR	S	Hinge
		19		326	84	IR	R	
		67		138	87	IR	R	
6-7m		17	3	120	62	IR	R	Hinge
		35		73	85	IR	R	
		67		290	42	IR	S	
7-8m		1	9	130	90	IA	R	Forelimb
		14		65	81	IR	R	
		22		100	87	IA	R	conj?
		29		100	87	IA	R	conj?
		36		100	87	IA	R	conj?
		55		72	56	IR	R	
		70		72	56	IA	R	
		85		72	56	IA	R	
		94		146	60	IR	R	
8-9m	285/45	1	8	34	54	IA	S	Forelimb
		12		72	69	IA	S	
		16		138	61	IA	R	
		30		70	72	IR	S	
		33		70	72	IR	S	
		76		92	62	IA	S	
		78		130	60	IR	S	
		100		79	81	IR	S	

Locality: 3c
GPS Coordinates: N 7832050
 E 1409032
Thrust System: M3
Structural Position: Hinge
Scanline Number: 3c-2
Lithological Unit: 2
Bed Thickness: 150 cm
Scanline Trend: 030

UNIT	BED ORIENTATION	DISTANCE	FRACTURE FREQUENCY	STRIKE	DIP	INTER / INTRA	SURFACE	COMMENTS
0-1m		no fractures	0					
1-2m	-	0	6	256	88	IR	S	
		16		194	78	IR	S	listric shape
		18		194	78	IR	S	listric shape
		65		175	84	IA	S	
		80		192	82	IR	S	
		84		192	82	IR	S	
2-3m	268/23	43	2	352	89	IR	S	
		58		352	89	IR	S	
3-4m	201/18	85	1	344	84	IR	S	
4-5m	234/34	no fractures	0					
5-6m	256/12	45	3	150	70	IR	S	
		62		188	80	IR	S	
		100		180	68	IR	S	

Locality: 3c

GPS Coordinates: ?

Thrust System: M3

Structural Position: Forelimb - (Hinge)

Scanline Number: 3c-3

Lithological Unit: 3

Bed Thickness: 60 cm

Scanline Trend: 310

UNIT	BED ORIENTATION	DISTANCE	FRACTURE FREQUENCY	STRIKE	DIP	INTER / INTRA	SURFACE	COMMENTS			
0-1m	323/60	4	8	60	85	IA	R	Hinge			
		10		60	85	IA	R				
		24		70	85	IA	R				
		47		70	85	IA	S				
		67		70	85	IR	S				
		84		76	83	IR	S				
		86		65	75	IA	R				
		96		65	75	IR	S				
		1-2m		340/78	4	6	65		75	IA	S
					33		65		75	IA	S
43	65		75		IA		S				
60	55		76		IA		R				
78	65		75		IA		R				
89	65		75		IA		R				
2-3m	336/74	8	4	60	75	IA	R				
		75		63	80	IA	S				
		80		60	80	IA	R				
		86		65	80	IA	R				
3-4m	326/74	3	7	58	80	IR	S				
		19		58	80	IA	R				
		29		58	80	IA	S				
		40		58	80	IR	S				
		47		58	80	IA	R				
		52		43	85	IA	R				

4-5m	325/76	83	3	58	79	IR	R	
		20		60	78	IR	S	
		41		60	80	IR	R	
5-6m	320/75	68	8	58	79	IR	R	
		5		86	84	IR	S	
		19		60	75	IR	S	
		41		60	75	IA	R	
		59		53	76	IR	S	
		66		53	76	IR	R	
		70		53	76	IR	S	
6-7m	330/70	86	7	53	76	IR	S	
		97		60	79	IR	S	
		10		60	79	IA	S	
		20		60	79	IA	S	
		27		75	75	IR	S	
		38		58	79	IR	S	
		65		55	82	IR	S	
7-8m	339/80	77	4	235	2	IR	R	
		98		75	80	IA	S	
		10		75	80	IR	S	
		30		67	85	IR	S	
		84		72	78	IA	R	
		99		80	79	IR	S	

Forelimb

Forelimb

Locality: 3c
GPS Coordinates: 33 X 0481154
 8718178
Thrust System: M3
Structural Position: Forelimb - Hinge
Scanline Number: 3c-4
Lithological Unit: 3
Bed Thickness: 50 cm
Scanline Trend: 030

UNIT	BED ORIENTATION	DISTANCE	FRACTURE FREQUENCY	STRIKE	DIP	INTER / INTRA	SURFACE	COMMENTS				
0-1m	260/17	1	11	176	82	IR	R	Hinge				
		12		148	66	IR	R					
		28		75	75	IA	S					
		37		75	75	IA	S					
		45		95	79	IA	S					
		50		260	85	IR	R					
		60		310	79	IA	S					
		65		165	84	IA	S					
		74		195	89	IR	S					
		79		147	79	IR	S					
		99		189	81	IR	S					
		1-2m		258/19	24	7	85		85	IR	S	Hinge
					30		187		80	IR	S	
					40		90		86	IR	S	
57	185		85		IR		S					
75	160		79		IR		R					
77	185		85		IR		S					
2-3m	253/21	93	7	193	82	IR	R					
		22		193	71	IR	R					
		45		193	71	IR	R					
		52		168	78	IR	R					
		72		261	86	IA	S					
		74		261	86	IA	S					
83	261	86	IA	S								

3-4m	284/19	96	8	267	87	IR	S	Forlimb
		7		170	78	IA	S	
		32		145	80	IR	R	
		43		296	90	IA	S	
		51		140	75	IA	R	
		66		10	85	IR	S	
		90		174	74	IR	R	
		96		174	74	IR	S	
4-5m	330/22	100	7	275	89	IR	S	
		18		186	60	IA	S	
		37		200	60	IR	R	
		56		160	72	IA	S	
		64		130	77	IA	S	
		72		170	70	IR	S	
		89		190	80	IR	S	
		97		105	70	IA	S	
5-6m	330/29	3	13	105	70	IA	S	
		14		115	84	IA	S	
		26		163	75	IR	R	
		39		88	65	IR	R	
		44		256	89	IR	S	
		55		209	70	IR	S	
		56		145	15	IA	S	
		59		145	15	IA	S	
		78		145	15	IA	S	
		83		173	64	IA	S	
		90		145	15	IA	S	
		92		173	64	IA	S	
		99		280	72	IR	R	
6-7m	325/32	29	6	150	59	IR	S	
		50		150	59	IR	S	
		51		275	75	IR	S	
		90		150	59	IR	S	
		96		150	64	IR	S	
7-8m	325/34	100	9	150	64	IA	S	
		7		150	64	IA	S	

24	150	42	IR	S
32	80	88	IR	R
40	160	50	IR	R
47	325	54	IA	R
58	211	71	IA	S
74	147	65	IA	S
91	160	67	IA	S
95	160	67	IA	S

Locality: 3c
GPS Coordinates: 33 X 0481141
 8718180
Thrust System: M3
Structural Position: Backlimb
Scanline Number: 3c-5
Lithological Unit: 3
Bed Thickness: 30 cm
Scanline Trend: 030

UNIT	BED ORIENTATION	DISTANCE	FRACTURE FREQUENCY	STRIKE	DIP	INTER / INTRA	SURFACE	COMMENTS				
0-1m	150/19	0	8	295	85	IR	R	Backlimb				
		11		336	65	IA	R					
		35		15	85	IR	S					
		40		103	80	IA	R					
		42		103	80	IA	S					
		44		103	80	IA	S					
		45		103	80	IA	S					
		60		286	60	IA	R					
		1-2m		174/15	8	11	190		85	IR	S	
					21		190		85	IA	S	
27	65		75		IA		S					
30	65		75		IA		S					
45	293		2		IR		R					
51	276		82		IA		S	conj?				
55	276		82		IR		S	conj?				
61	337		60		IA		S					
66	337		60		IA		S					
79	337		60		IR		R					
99	80	85	IR	R								

Locality: 3c

GPS Coordinates: ?

Thrust System: M3

Structural Position: Forelimb - Hinge

Scanline Number: 3c-6

Lithological Unit: 4

Bed Thickness: 80 cm

Scanline Trend: 030

UNIT	BED ORIENTATION	DISTANCE	FRACTURE FREQUENCY	STRIKE	DIP	INTER / INTRA	SURFACE	COMMENTS
0-1m	072/28	0	13	58	88	IA	S	Hinge
		10		172	76	IR	R	
		20		180	79	IA	R	
		43		98	78	IA	R	
		43		234	86	IA	S	
		53		234	86	IA	S	
		58		134	76	IA	S	
		71		162	77	IA	S	
		71		96	76	IA	S	
		82		55	90	IA	S	
		94		179	68	IR	S	
		98		187	88	IA	S	
		100		185	76	IA	S	
		1-2m		054/28	76	2	94	
100	165		52		IR		S	
2-3m	058/27	20	3	170	65	IR	S	
		25		118	86	IA	R	
		33		167	82	IA	S	
3-4m	052/26	17	6	170	70	IR	S	Forlimb
		27		170	70	IR	S	
		57		184	60	IR	R	
		65		78	80	IA	S	
		90		134	82	IR	R	
		100		134	82	IR	R	

Locality: 3e
GPS Coordinates: 33 X 0482892
 8712910
Thrust System: M3
Structural Position: Backlimb
Scanline Number: 3e-1
Lithological Unit: 3
Bed Thickness: 70 cm
Scanline Trend: 340

UNIT	BED ORIENTATION	DISTANCE	FRACTURE FREQUENCY	STRIKE	DIP	INTER / INTRA	SURFACE	COMMENTS
0-1m	160/35	60	1	283	80	IR	R	
1-2m	160/35	2	6	330	67	IR	S	conj?
		25		240	87	IA	S	
		35		335	70	IR	R	conj?
		44		250	81	IR	S	
		57		70	85	IR	S	
		64		50	33	IR	S	
2-3m	160/33	51	2	67	98	IA	R	
		98		255	78	IA	S	
3-4m	160/37	7	4	250	90	IR	S	
		21		42	45	IA	S	
		36		248	89	IA	R	
		94		256	90	IR	S	
4-5m	160/34	62	1	266	85	IR	R	
5-6m	158/34	35	3	58	75	IR	S	
		50		273	82	IR	R	
		95		260	80	IA	S	
6-7m	158/36	4	2	138	45	IA	R	
		91		260	80	IR	S	
7-8m	147/32	53	2	246	80	IA	S	
		56		246	80	IA	S	
8-9m	153/30	19	3	265	84	IR	S	
		49		253	67	IA	S	
		68		288	80	IA	R	

9-10m	160/34	12	5	264	80	IA	R				
		30		235	80	IR	R				
		50		12	60	IA	S				
		54		96	80	IR	S				
		79		80	89	IR	S				
10-11m	163/26	18	3	285	76	IR	R				
		40		314	68	IR	R				
		67		287	80	IA	S				
11-12m	167/34	7	8	290	63	IA	S				
		16		264	72	IR	S				
		18		264	72	IA	S				
		19		264	72	IA	S				
		24		264	72	IA	S				
		40		28	66	IR	S				
		77		236	45	IA	R				
		83		254	86	IA	S				
		12-13m		165/45	9	11	278	80	IR	S	
					12		278	80	IA	S	
15	278		80		IA		S				
30	242		82		IA		S				
36	275		80		IA		S				
50	242		82		IA		S				
60	242		82		IA		S				
61	265		86		IA		S				
63	265		86		IA		S				
82	242		82		IA		S				
13-14m	163/35	8	3	80	70	?	?	Covered			
		31		40	80	?	?	Covered			
		46		260	75	?	?	Covered			
14-15m	160/35	15	3	287	75	IA	R				
		21		60	78	IR	R				
		75		254	57	IA	S				
15-16m	160/40	13	5	56	85	IR	S				
		46		273	70	IA	S				
		50		250	34	IA	S				

		63		270	81	IR	S	
		99		270	81	IR	S	
16-17m	148/30	77	1	50	72	IA	R	
17-18m	158/34	18	2	265	80	IR	R	
		80		260	84	IA	S	
18-19m	145/30	3	3	48	89	IR	S	
		57		60	78	IA	S	
		97		280	90	IR	S	
19-20m	165/25	88	1	280	89	IR	S	
20-21m	165/36	83	1	242	45	IR	S	
21-22m	165/36	5	3	110	78	IA	S	
		15		246	75	IA	S	
		39		266	85	IA	S	
22-23m	160/35	24	3	90	75	IR	R	
		45		90	75	IR	R	
		99		255	65	IR	R	
23-24m	150/40	75	2	40	55	IR	R	
		81		275	75	IR	S	
24-25m			0					no fractures
25-26m	145/32	9	1	268	75	IR	S	
26-27m	152/45	5	3	260	76	IR	R	
		94		275	85	IR	S	
		98		275	85	IA	S	
27-28m	160/44	2	5	16	50	IA	S	
		27		230	82	IA	S	
		42		230	86	IA	S	
		66		82	89	IR	R	
		92		270	90	IA	S	
28-29m	160/35	15	2	270	70	IR	R	
		76		263	67	IR	R	
29-30m	160/35	7	8	265	68	IR	R	
		13		265	68	IA	S	
		22		60	76	IR	S	
		23		263	76	IR	S	
		25		60	76	IR	S	
		44		263	76	IR	S	

87
97

270
273

77
80

IR
IR

S
S

Locality: 3e
GPS Coordinates: 33 X 0482872
 8712668
Thrust System: M3
Structural Position: Backlimb
Scanline Number: 3e-2
Lithological Unit: 10
Bed Thickness: (1) 50 cm, (2) 42 cm
Scanline Trend: 340

UNIT	BED ORIENTATION	DISTANCE	FRACTURE FREQUENCY	STRIKE	DIP	INTER / INTRA	SURFACE	COMMENTS
0-1m	190/75	55	3	82	86	IR	S	Bed: 1+2
		75		300	60	IA	R	1
		85		270	85	IR	S	1
1-2m	175/65	10	3	80	85	IA	S	2
		33		78	86	IA	S	2
		68		320	43	IR	S	1+2
2-3m	170/66	7	8	250	70	IA	S	1
		12		260	87	IA	R	2
		29		263	84	IR	S	1
		36		20	40	IR	S	1
		40		290	36	IA	R	2
		62		75	88	IR	R	1
		66		290	36	IA	R	2
		86		95	30	IR	R	1
3-4m	170/52	5	6	80	86	IR	S	2
		38		80	86	IA	S	2
		59		255	80	IR	S	1
		68		305	60	IR	S	2
		74		265	85	IA	S	2
		90		290	60	IR	S	1
4-5m	167/55	38	6	82	85	IR	S	2
		53		323	45	IR	S	1
		73		70	82	IR	R	2
		73		260	86	IR	S	1

		80		232	67	IR	S	1
		85		330	50	IA	S	1
5-6m	170/70	12	10	85	84	IR	S	1
		19		85	89	IR	S	2
		30		85	84	IA	S	1
		41		298	60	IR	S	1
		43		74	80	IR	S	2
		53		295	64	IA	R	1+2
		63		15	40	IA	S	1
		63		269	89	IA	R	2
		70		320	50	IR	S	2
		85		70	89	IR	S	1+2
6-7m	170/50	0	4	314	40	IR	S	1+2
		28		252	85	IR	R	1
		65		268	80	IR	S	2
		98		258	88	IR	S	1+2
7-8m	169/59	4	5	290	60	IR	S	1
		20		148	45	IR	S	2, conjugate set
		47		268	82	IR	R	2
		75		78	88	IR	S	1+2
		100		6	48	IR	S	1+2, conjugate set
8-9m	170/38	0	3	255	82	IR	S	2
		42		318	58	IR	S	1+2
		80		104	82	IR	R	1+2
9-10m	169/66, 170/54	12	8	272	82	IA	R	2
		14		272	82	IR	R	1
		34		265	80	IA	S	1
		37		265	80	IR	S	2
		60		260	85	IA	R	1
		63		160	54	IA	S	1, prominent, 1.50m
		66		260	85	IA	R	1
		98		335	40	IA	R	2
10-11m	168/58	7	7	272	65	IR	R	1
		12		95	86	IR	R	2
		20		165	62	IR	S	1, conjugate
		27		90	80	IA	R	2, conjugate

		61		250	88	IR	S	1
		64		244	89	IR	S	2
		100		320	38	IR	R	2
11-12m	174/54	10	5	234	34	IR	R	1+2
		22		95	89	IR	S	2
		35		320	44	IR	S	+2
		54		265	88	IR	S	1+2
		78		305	55	IA	R	1
12-13m	170/60	25	7	70	75	IR	S	1+2
		29		70	75	IR	S	1
		62		262	80	IA	R	1
		76		262	80	IA	S	1
		94		70	82	IR	R	2
		98		70	82	IR	S	1
		100		324	40	IR	S	2
13-14m	172/42	3	4	250	82	IR	S	2
		27		262	86	IR	S	1+2
		53		302	60	IR	S	1+2
		75		86	85	IR	S	1+2
14-15m	175/64	25	6	320	42	IR	S	1+2, conjugate
		55		322	48	IR	S	2, conjugate
		72		85	82	IA	S	1+2
		75		135	68	IR	S	1+2
		85		72	78	IR	S	1
		93		322	48	IR	S	2
15-16m	175/60	35	7	260	88	IR	S	1+2
		50		268	80	IR	S	1
		55		268	80	IR	S	2
		66		310	50	IA	S	2
		74		314	44	IR	S	2
		90		318	54	IR	S	2
		100		65	80	IR	S	1+2
16-17m	168/55	0	9	150	52	IR	S	2
		5		70	90	IR	S	1+2
		14		250	86	IR	S	1
		15		148	50	IR	S	1+2, conjugate

		21		270	82	IA	R	1
		48		270	82	IA	S	1
		66		328	44	IA	S	1
		84		75	90	IR	S	2
		91		75	90	IR	S	1
17-18m	170/40	15	7	72	90	IA	S	2
		25		68	82	IR	S	1+2
		60		305	48	IR	S	2
		70		188	60	IR	S	2
		76		260	82	IR	S	1
		100		146	54	IR	S	1+2, conjugate
		100		268	82	IR	S	1
18-19m	170/38	30	6	252	88	IR	S	1
		58		325	45	IR	S	1
		59		260	86	IR	S	2
		72		318	40	IA	S	2
		95		328	46	IR	S	1
		100		24	40	IR	S	2
19-20m	178/48	21	7	256	80	IR	S	1+2
		35		325	40	IA	S	1
		40		260	80	IA	S	2
		63		325	52	IR	S	2
		75		310	50	IR	S	2
		80		78	82	IR	R	1
		90		310	50	IR	R	1
20-21m	168/55	10	4	318	40	IR	S	1
		70		80	90	IR	S	1
		95		72	82	IR	S	1+2
		100		20	40	IR	S	1+2
21-22m	168/52	1	6	310	44	IR	S	1+2
		27		70	98	IR	S	1+2
		48		256	88	IR	S	1+2
		84		252	80	IR	S	1+2
		85		268	86	IR	S	1+2
		96		268	86	IR	S	1+2
22-23m	170/44	10	6	260	82	IR	S	1+2

		48		320	50	IA	S	1
		54		70	80	IR	R	1+2
		70		78	80	IR	S	1+2
		95		314	50	IR	S	2
		96		264	86	IR	S	1
23-24m	172/40	24	4	322	50	IR	R	2
		40		252	84	IR	S	1+2, prominent
		75		318	52	IR	S	1+2
		92		262	80	IR	S	1+2, major

Locality: 3g
GPS Coordinates: 33 x 0480373
 8719528
Thrust System: M3
Structural Position: Hinge
Scanline Number: Hinge
Lithological Unit: 10
Bed Thickness: 32 cm
Scanline Trend: 025

UNIT	BED ORIENTATION	DISTANCE	FRACTURE FREQUENCY	STRIKE	DIP	INTER / INTRA	SURFACE	COMMENTS
0-1m	330/09	13	9	336	83	IA	S	
		29		0	85	IR	S	
		41		16	80	IA	S	
		42		16	80	IA	S	
		52		33	85	IR	S	
		52		303	87	IR	S	
		62		33	85	IR	S	
		89		3	85	IA	R	
		99		354	87	IA	R	
		1-2m		330/09	9	9	352	85
11	12		88		IR		S	
15	357		63		IA		S	
20	357		63		IA		S	
22	0		90		IR		S	
48	357		63		IA		S	
53	355		85		IR		S	
77	355		85		IR		S	
100	355		85		IR		S	

Locality: 3g
GPS Coordinates: 33 x 0480392
 8719704
Thrust System: M3
Structural Position: Hinge
Scanline Number: 3g-2
Lithological Unit: 10
Bed Thickness: 32 cm
Scanline Trend: 125

UNIT	BED ORIENTATION	DISTANCE	FRACTURE FREQUENCY	STRIKE	DIP	INTER / INTRA	SURFACE	COMMENTS	
0-1cm	358/10	0	3	65	80	IR	S		
		30		273			88	IR	S
		67		267			89	IA	S
1-2m	340/04	15	3	267	87	IA	S		
		49		276			90	IA	S
		71		72			83	IR	S

Locality: 3g
GPS Coordinates: 33 X 0480375
 8719792
Thrust System: M3
Structural Position: Hinge
Scanline Number: 3g-3
Lithological Unit: 10
Bed Thickness: 48 cm
Scanline Trend: 350

UNIT	BED ORIENTATION	DISTANCE	FRACTURE FREQUENCY	STRIKE	DIP	INTER / INTRA	SURFACE	COMMENTS	
0-1m	240/02	1	6	270	90	IR	S		
		14		230			69	IR	S
		23		283			89	IR	R
		34		84			82	IA	S
		44		70			85	IA	S
		88		270			89	IR	S
		1-2m		230/04			14	4	291
45	210	70	IR		S				
64	260	90	IR		S				
87	78	80	IR		S				

Locality: 3h

GPS Coordinates: ?

Thrust System: M3

Structural Position: Forelimb (local)

Scanline Number: 3h

Lithological Unit: 10

Scanline Trend: 160

UNIT	BED ORIENTATION	DISTANCE	FRACTURE FREQUENCY	STRIKE	DIP	INTER / INTRA	SURFACE	COMMENTS
0-1m	296/54	0	8	97	37	IR	S	conj?
		6		97	37	IA	S	conj?
		16		97	37	IA	S	conj?
		36		216	60	IA	R	
		45		97	62	IA	S	
		64		95	53	IR	S	
		86		82	50	IA	S	
		99		87	37	IA	S	
		1-2m		307/52	4	10	73	40
15	73		40		IA		S	
18	86		85		IA		S	
44	115		42		IR		R	
51	103		49		IA		S	
53	209		45		IA		S	
73	103		40		IR		S	
90	105		70		IA		S	
95	155		22		IA		S	
97	155		22		IR		S	

Locality: 3i
GPS Coordinates: 33 X 0479267
 8721403
Thrust System: M3
Structural Position: Backlimb
Scanline Number: 3i
Lithological Unit: 21
Scanline Trend: 030
 Bed thickness 34cm

UNIT	BED ORIENTATION	DISTANCE	FRACTURE FREQUENCY	STRIKE	DIP	INTER / INTRA	SURFACE	COMMENTS
0-1m	147/37	20	5	52	78	IR	S	
		29		296	45	IA	R	
		54		48	78	IR	S	
		59		252	72	IR	S	
		87		320	46	IR	S	
1-2m	142/37	4	3	26	60	IR	R	
		24		42	80	IR	R	
		89		320	55	IR	R	
2-3m	146/37	34	5	320	90	IR	R	
		42		306	57	IA	S	
		52		322	45	IR	R	
		64		247	67	IR	S	
		75		53	84	IR	S	
3-4m	137/42	9	10	5	67	IA	R	
		16		263	60	IA	R	
		36		18	59	IA	S	
		39		345	44	IR	S	
		48		65	58	IA	S	
		51		350	45	IR	S	
		56		11	50	IA	S	
		58		311	40	IR	S	
		63		352	42	IR	R	
		74		330	32	IR	S	
4-5m	140/36	1	6	322	55	IA	R	
		9		332	55	IA	S	

		11		253	73	IR	S
		21		253	73	IA	S
		24		348	45	IA	R
		37		290	45	IR	R
5-6m	140/36	18	3	312	37	IR	S
		34		307	45	IR	S
		95		20	77	IR	R
6-7m	154/42	2	8	315	85	IR	R
		22		253	80	IR	S
		35		55	82	IR	S
		58		352	43	IR	S
		64		230	88	IA	S
		66		260	76	IR	S
		79		49	88	IR	S
		90		350	42	IR	S
7-8m	150/40	49	2	245	83	IR	S
		94		342	60	IA	S
8-9m	157/40	24	2	323	48	IR	S
		32		252	75	IR	S
9-10m	154/47	21	4	303	70	IA	S
		53		320	40	IR	S
		56		302	42	IR	R
		58		145	54	IA	S
10-11m	152/40	2	6	4	70	IA	R
		10		9	69	IA	R
		20		252	78	IA	S
		27		8	50	IA	S
		67		320	50	IR	S
		90		340	44	IR	S
11-12m	146/40	20	2	312	45	IR	R
		76		232	82	IA	R
12-13m	156/40	0	4	346	42	IR	R
		43		262	70	IR	R
		63		304	39	IR	R
		92		259	80	IR	S
13-14m	144/44	6	3	342	45	IR	R

		48		342	45	IR	R
		60		340	42	IR	S
14-15m	136/42	24	2	300	42	IR	R
		30		300	42	IR	S

Locality: 4b
GPS Coordinates: 33 X 0481893
 8718550
Thrust System: M2
Structural Position: Backlimb
Scanline Number: 4b-1
Lithological Unit: 10
Bed Thickness: 32 cm (bed 1 at 4b-1 underlies bed 2 at 4b-2)
Scanline Trend: 130

UNIT	BED ORIENTATION	DISTANCE	FRACTURE FREQUENCY	STRIKE	DIP	INTER / INTRA	SURFACE	COMMENTS
0-1m	143/45	0	3	70	62	IR	S	Bed: 1
		61		240	75		S	1
		72		80	71		S	1
1-2m	144/35	24	2	240	75	IR	S	1
		98		240	82		S	1

Locality: 4b
GPS Coordinates: 33 X 0481893
 8718550
Thrust System: M2
Structural Position: Backlimb
Scanline Number: 4b-2
Lithological Unit: 10
Bed Thickness: 49 cm (bed 2 at 4b-2 overlies bed 1 at 4b-1)
Scanline Trend: 130

UNIT	BED ORIENTATION	DISTANCE	FRACTURE FREQUENCY	STRIKE	DIP	INTER / INTRA	SURFACE	COMMENTS
0-1m	143/35	25	3	260	84	IR	S	2
		69		243	76		S	
		97		260	57		S	
1-2m	144/35	42	3	250	86	IR	S	2
		53		272	60		S	
		100		265	85		S	

Locality: 4b
GPS Coordinates: 33 X 0481863
 8718738
Thrust System: M2
Structural Position: Backlimb
Scanline Number: 4b-3
Lithological Unit: 10
Bed Thickness: 48 cm
Scanline Trend: 355

UNIT	BED ORIENTATION	DISTANCE	FRACTURE FREQUENCY	STRIKE	DIP	INTER / INTRA	SURFACE	COMMENTS
0-1m	153/35	0	3	112	70	IR	R	
		42		20	80	IR	S	
		78		70	75	IA	S	
1-2m	140/35	8	3	20	63	IA	R	
		48		20	63	IA	R	
		90		23	65	IA	S	
2-3m	165/35	20	3	15	65	IR	S	
		40		84	71	IR	S	
		82		358	55	IA	S	
3-4m	157/40	2	4	358	55	IR	S	
		37		10	55	IR	S	
		75		10	55	IR	S	
		100		10	55	IR	S	
4-5m	150/45	2	6	15	67	IR	S	
		13		265	84	IA	R	
		36		30	70	IA	R	
		58		70	30	IR	S	
		69		35	56	IR	S	
		90		350	35	IR	S	

Locality: 4b
GPS Coordinates: 33X 0481727
 8718858
Thrust System: M2
Structural Position: Backlimb
Scanline Number: 4b-4
Lithological Unit: 21
Bed Thickness: 30 cm
Scanline Trend: 300

UNIT	BED ORIENTATION	DISTANCE	FRACTURE FREQUENCY	STRIKE	DIP	INTER / INTRA	SURFACE	COMMENTS
0-1m	148/60	0	9	92	90	IR	S	
		1		10	10	IR	S	
		30		352	50	IA	S	
		60		9	38	IR	S	
		68		9	38	IA	S	
		80		10	40	IR	S	
		85		10	40	IR	S	
		90		10	60	IA	S	
		100		255	88	IR	S	
		1-2m		148/68	20	10	252	85
30	25		60		IR		S	
40	8		35		IR		S	
55	15		38		IR		S	
60	270		88		IR		S	
67	15		38		IR		S	
88	258		60		IA		S	
89	258		60		IA		S	
90	260		60		IA		S	
100	264		80		IR		S	
2-3m	152/60	10	9	78	90	IA	S	
		20		245	82	IR	S	
		30		0	30	IR	S	
		40		358	38	IR	S	
		55		252	85	IA	S	

		69		348	32	IR	S
		90		348	32	IR	S
		98		345	30	IR	S
		100		242	85		
3-4m	142/62	1	12	205	50	IA	S
		5		50	90	IR	S
		7		74	90	IA	S
		8		235	50	IA	S
		30		345	30	IR	S
		35		65	90	IR	S
		40		65	90	IR	S
		50		352	30	IA	S
		65		74	90	IA	S
		70		235	50	IA	S
		80		352	30	IR	S
		90		255	82	IA	S

Locality: 4d
GPS Coordinates: 33 X 0482671
 8716568
Thrust System: M2
Structural Position: Backlimb
Scanline Number: 4d-1
Lithological Unit: 3
Bed Thickness: 78 cm
Scanline Trend: 085

UNIT	BED ORIENTATION	DISTANCE	FRACTURE FREQUENCY	STRIKE	DIP	INTER / INTRA	SURFACE	COMMENTS
0-1m	154/60	20	8	295	30	IA	S	Backlimb
		25		295	30	IA	S	
		46		340	46	IA	S	
		47		54	30	IA	S	
		48		65	81	IR	S	
		54		158	45	IA	S	
		60		290	35	IA	S	
		74		290	35	IA	S	

Locality: 4d
GPS Coordinates: 33 X 0482666
 8716646
Thrust System: M2
Structural Position: Backlimb
Scanline Number: 4d-2
Lithological Unit: 3
Bed Thickness: 70 cm
Scanline Trend: 095

UNIT	BED ORIENTATION	DISTANCE	FRACTURE FREQUENCY	STRIKE	DIP	INTER / INTRA	SURFACE	COMMENTS
0-1m	170/64	15	5	67	60	IA	S	Backlimb
		26		300	35	IA	S	Backlimb
		36		30	46	IA	S	Backlimb
		56		348	75	IR	R	Backlimb
		80		37	80	IR	S	Backlimb
1-2m	163/70	19	2	65	52	IR	R	Backlimb
		92		270	75	IR	S	
2-3m								Covered
3-4m	170/60	21	4	15	40	IA	R	
		39		17	36	IA	S	
		60		345	35	IA	R	
		95		320	40	IR	R	
4-5m	170/66	10	5	330	40	IR	S	
		30		86	84	IA	S	
		35		15	66	IR	S	
		59		350	48	IR	S	Backlimb
		99		70	55	IR	S	
5-6m								Covered
6-7m	170/66	1	5	320	34	IR	S	
		17		320	34	IR	S	
		35		53	66	IR	S	
		75		65	34	IA	S	Backlimb
		91		40	50	IA	S	Backlimb
7-8m	158/67	29	5	39	28	IR	S	Backlimb

		34		80	45	IR	S	Backlimb
		57		268	88	IA	S	Backlimb
		70		330	33	IR	S	Backlimb
		77		260	85	IA	S	Backlimb
8-9m	168/60	16	4	60	85	IA	S	Backlimb
		28		53	67	IR	S	Backlimb
		57		243	81	IR	R	Backlimb
		97		255	89	IA	R	Backlimb
9-10m	165/62	11	6	338	40	IR	R	Backlimb
		40		74	84	IR	R	Backlimb
		70		40	82	IA	R	Backlimb
		77		350	30	IA	R	
		82		8	59	IA	R	
		90		70	85	IA	R	
10-11m	150/60	13	7	350	35	IR	R	
		31		260	85	IR	S	
		76		335	45	IA	S	
		82		40	75	IA	S	
		90		50	36	IA	S	
		96		260	86	IA	S	
		99		50	36	IR	S	
11-12m	153/55	5	2	76	89	IR	S	
		35		326	35	IR	R	
12-13m	161/50	4	3	258	70	IR	R	
		10		327	33	IA	R	
		62		330	28	IR	R	
13-14m	165/60	2	6	348	18	IR	R	
		25		150	35	IR	S	
		30		20	47	IA	S	
		38		20	47	IA	S	
		40		340	86	IR	S	
		67		327	30	IA	S	
14-15m	165/60	1	10	35	60	IR	S	
		2		175	70	IA	S	
		7		35	60	IA	S	
		21		50	32	IA	S	

38	254	89	IA	S	
39	40	60	IA	S	
45	65	21	IA	S	
47	0	40	IA	S	
50	193	80	IR	S	
99	80	80	IR	S	Backlimb

Locality: 4d
GPS Coordinates: 33X 0483097
 8716888
Thrust System: M2
Structural Position: Forelimb
Scanline Number: 4d-3
Lithological Unit: 3
Bed Thickness: 80 cm
Scanline Trend: 015

UNIT	BED ORIENTATION	DISTANCE	FRACTURE FREQUENCY	STRIKE	DIP	INTER / INTRA	SURFACE	COMMENTS
0-1m	340/58	0	2	70	60	IR	S	
		50		65	72		IA	S
1-2m	322/58	15	3	74	58	IR	S	
		24		74	58		IR	S
		40		74	58		IR	S
		70		258	78		IA	S
2-3m	335/58	15	2	90	70	IR	S	
		70		258	78		IA	S
3-4m	330/65	8	4	65	80	IA	S	
		30		58	58		IR	S
		65		64	64		IR	S
		80		60	70		IA	S
4-5m	330/64	20	2	58	30	IA	S	
		98		68	62		IR	S
5-6m	340/62	14	6	68	40	IA	S	
		20		240	50		IR	S
		30		90	48		IA	S
		36		60	76		IR	S
		50		315	45		IR	S
6-7m	332/76	50	3	315	40	IR	S	
		20		80	72		IA	S
		50		38	64		IR	S
		100		305	50		IR	S
7-8m	334/65	30	4	245	80	IA	S	
		50		80	55		IA	S

70
100

305
340

82
50

IR
IR

S
S

Locality: 4d
GPS Coordinates: 33X 0483097
 8716888
Thrust System: M2
Structural Position: Forelimb
Scanline Number: 4d-3
Lithological Unit: 4
Bed Thickness: 100 cm
Scanline Trend: 015

UNIT	BED ORIENTATION	DISTANCE	FRACTURE FREQUENCY	STRIKE	DIP	INTER / INTRA	SURFACE	COMMENTS
0-1m	350/70	0	4	262	80	IR	S	
		35		140	48	IR	S	
		55		140	48	IR	S	
		60		310	62	IR	S	over several m
1-2m	345/52	5	6	142	45	IA	S	
		20		324	45	IR	S	
		30		324	45	IA	S	
		35		65	68	IR	S	
		70		135	50	IR	S	
		80		92	75	IA	S	
2-3m	335/50	25	5	130	55	IA	S	
		40		110	70	IA	S	
		45		110	70	IA	S	
		60		128	50	IR	S	
		80		88	72	IA	S	
3-4m	335/60	10	3	68	72	IA	S	
		40		132	40	IA	S	
		100		68	60	IR	S	pronounced
4-5m	328/70	0	7	20	75	IA	S	
		40		135	50	IA	S	
		50		135	40	IA	S	
		60		58	82	IR	S	
		70		130	50	IA	S	
		80		55	80	IA	S	

5-6m	338/62	100		124	40	IR	S	pronounced
		10	3	120	40	IA	S	
		60		60	62	IR	S	
		100		65	68	IR	S	pronounced

Locality: 4d
GPS Coordinates: 33 X 0482421
 8716726
Thrust System: M2
Structural Position: Backlimb
Scanline Number: 4d-5
Lithological Unit: 10
Bed Thickness: 50 cm
Scanline Trend: 090

UNIT	BED ORIENTATION	DISTANCE	FRACTURE FREQUENCY	STRIKE	DIP	INTER / INTRA	SURFACE	COMMENTS
0-1m	183/66	1	8	340	40	IR	R Backlimb	
		25		65	77	IR	S	
		33		315	15	IR	S	
		40		65	45	IA	S	
		52		65	45	IR	S	
		64		170	25	IR	S	
		85		170	25	IR	S	
		95		170	25	IR	S	

Locality: 4R (River)
GPS Coordinates: 33X 0483026
 8717112
Thrust System: M2
Structural Position: Forelimb
Scanline Number: 4R
Lithological Unit: ?
Bed Thickness: 40 cm
Scanline Trend: 290

UNIT	BED ORIENTATION	DISTANCE	FRACTURE FREQUENCY	STRIKE	DIP	INTER / INTRA	SURFACE	COMMENTS
0-1m	338/56	20	5	148	30	IR	S	
		42		72	80	IA	S	
		45		158	30	IR	S	
		66		165	40	IR	S	
		98		75	70	IA	S	
		1-2m		336/52	1	7	170	24
29	190	30	IA		S			
36	202	32	IR		S			
50	74	78	IA		S			
65	178	30	IA		S			
80	178	30	IR		S			
2-3m	330/60	96	5	178	30	IA	S	
		12		308	32	IR	S	
		30		308	32	IA	S	
		45		168	30	IR	S	
		75		142	25	IA	S	
3-4m	338/58	88	6	140	30	IA	S	
		2		0	85	IR	S	
		5		75	80	IA	S	
		40		340	80	IA	S	
		65		320	40	IR	S	
		90		74	78	IA	S	
100	172	22	IR	S				

Locality: 2e
GPS Coordinates:

Thrust System: OOST
Structural Position: Hinge
Scanline Number: 10-08
Lithological Unit: 7
Scanline Trend: 020/200
Thickness: 30cm
Date: 27/7-08

UNIT (m)	BED ORIENTATION	DISTANCE	FRACTURE FREQUENCY	STRIKE	DIP	INTER / INTRA	SURFACE	COMMENTS
0-1m	175/14	1	3	050	90	ia		
		40		336	76	ia		
		51		275	90	ir		
1-2m	192/19	20	6	278	88	ia		
		22		340	76	ia		
		35		278	88	ir		
		58		278	88	ir		
		63		278	88	ir		
		77		335	74	ia		
2-3m	192/19	48	2	256	90	ir		
		50		335	74	ir		
3-4m	192/12	23	5	243	90	ia		
		65		155	84	ir		
		67		305	17	ir	Lavvinkla	
		70		154	30	ir	Lavvinkla, ss: (tp) 154/30	
		85		280	84	ir		
4-5m	180/11	4	10	280	84	ir		
		15		280	84	ir		
		25		340	73	ia		
		45		275	90	ir		
		60		058	89	ir		
		65		058	89	ir		
		67		290	80	ir		
		74		270	90	ir		

		85		154	30	ir	
		90		065	90	ir	
5-6	172/15	40	5	275	90	ir	
		48		337	65	ia	
		75		275	90	ia	
		85		330	02	ia	Lavvinkla
		88		345	74	ir	
6-7m	172/15	17	8	340	73	ir	
		18		095	90	ia	
		22		055	76	ir	
		24		095	90	ir	
		45		337	81	ia	
		72		290	90	ir	
		80		280	90	ir	
		90		270	90	ir	
7-8m	160/12	10	6	050	88	ir	
		29		260	90	ir	
		45		260	90	ir	
		55		275	90	ir	
		76		275	90	ia	
		95		275	90	ir	
8-9m	140/13	37	3	093	88	ia	
		88		050	85	ia	
		90		332	84	ia	
9-10m	140/13	10	5	050	85	ir	
		15		268	90	ir	
		26		268	90	ir	
		46		268	90	ir	
		78		050	85	ir	

Locality: 3e

GPS Coordinates:

Thrust System: M3-backlimb

Structural Position: M3-backlimb

Scanline Number: 1-08

Lithological Unit: 3

Scanline Trend: 155

Thickness: 42cm

Date: 23/7-08

UNIT (m)	BED ORIENTATION	DISTANCE	FRACTURE FREQUENCY	STRIKE	DIP	INTER / INTRA	SURFACE	COMMENTS
0-1m	160/36	19	5	255	83	ir	s	
		56		257	84	ir	s	
		75		265	85	ir	s	
		99		260	86	ir	s	
		99		350	54	ia	s	
1-2m	160/36	27	2	255	84	ir	r	
		80		260	86	ir	s	
2-3m	160/36	72	3	270	84	ir	s	
		99		265	83	ir	s	ca
		99		350	54	ir	s	
3-4m		16	2	259	80	ir	s	ca
		64		260	80	ir	s	
4-5m		24	6	265	82	ir	s	
		62		265	82	ir	r	
		83		259	84	ir	s	
		83		350	53	ia	s	
		85		351	54	ia	s	
5-6m		85		289	55	ir	r	
		32	3	265	83	ir	s	
		73		260	80	ir	s	
6-7m		73		350	54	ia	s	
		13	3	250	54	ir	r	
		53		350	52	ia	s	
		53		268	75	ir	s	

7-8m	10 4	356	52	ia	s	
	10	263	84	ir	s	
	28	263	84	ir	s	
	60	263	84	ir	s	
8-9m	10 3	290	90	ir	r	conjugate sets
	32	315	75	ir	r	conjugate sets
	90	253	90	ir	s	
9-10m	40 3	350	54	ir	r	
	44	354	52	ir	r	
	40	256	87	ir	s	

Locality: 3e

GPS Coordinates:

Thrust System: M3-baclimb

Structural Position:

Scanline Number: 2-08

Lithological Unit: 3

Scanline Trend: 155

Thickness: 9cm

Date: 23/7-08

UNIT (m)	BED ORIENTATION	DISTANCE	FRACTURE FREQUENCY	STRIKE	DIP	INTER / INTRA	SURFACE	COMMENTS
0-1	160/36	5	6	357	50	ir	s	
		13		260	88	ia	s	
		19		288	66	ir	s	
		41		277	75	ir	s	
		59		280	66	ir	s	
		82		263	80	ia	s	
1-2m	160/36	3	10	265	85	ir	r	
		10		265	85	ir	r	
		15		263	90	ir	s	
		17		357	50	ir	s	
		40		310	60	ia	r	
		48		260	84	ir	r	
		64		255	81	ir	s	
		70		255	80	ir	r	
		76		257	80	ia	s	
2-3m	160/36	20	16	050	75	ia	s	
		27		254	84	ir	s	
		31		254	84	ir	s	
		31		254	84	ir	s	
		42		354	52	ia	s	
		45		275	80	ir	s	
		48		310	50	ir	s	
		52		52	52	ir	s	

		55		280	80	ir	s	
		59		280	68	ir	s	
		67		280	68	ir	s	
		70		280	70	ir	s	
		78		335	50	ia	s	
		95		267	82	ia	s	
		99		267	82	ia	s	Ca
		99		335	50	ia	s	
3-4m	160/36	1	10	280	85	ir	s	
		12		280	85	ir	s	
		20		280	85	ir	s	
		26		280	85	ir	s	
		26		045	67	ir	s	
		30		280	84	ir	s	
		49		005	56	ir	r	
		50		282	83	ia	s	
		75		225	81	ia	r	
		78		225	81	ir	r	
4-5m	160/63	20	13	238	80	ir	r	
		22		238	80	ir	r	
		23		238	80	ir	r	
		25		263	86	ir	s	
		39		354	60	ia	r	
		39		263	86	ir	s	
		53		354	60	ia	s	
		62		263	86	ir	s	
		67		354	60	ir	s	
		68		263	86	ir	s	
		75		262	79	ir	s	
		79		262	82	ir	s	
		85		250	82	ir	s	
5-6m	160/63	5	14	256	80	ir	s	
		10		256	80	ir	s	
		15		256	80	ir	s	
		17		256	80	ir	s	
		25		256	80	ir	s	

		25		349	51	ir	s
		43		256	80	ir	s
		46		256	80	ir	s
		55		256	80	ir	s
		63		260	82	ir	s
		73		260	82	ir	s
		76		285	80	ir	s
		85		260	82	ir	s
		98		045	88	ir	s
6-7m	160/63	5	10	330	52	ia	s
		28		330	52	ir	s
		33		330	52	ir	s
		42		330	52	ir	s
		50		330	52	ia	s
		63		260	75	ia	s
		65		330	52	ir	s
		73		331	54	ir	s
		83		332	50	ia	s
		90		343	57	ir	s
7-8m	160/63	8	9	260	52	ir	s
		14		260	52	ir	s
		18		335	70	ir	s
		20		335	70	ia	s
		50		240	85	ir	r
		75		270	85	ir	s
		80		250	85	ir	s
		95		250	85	ir	s
0-2	160/36	5	6	357	50	ir	s

Locality: 3e
GPS Coordinates:
Thickness: 3cm
Thrust System: M3
Structural Position: backlimb
Scanline Number: 3-08
Lithological Unit: 5
Scanline Trend: 155

Date: 23/7-08

UNIT (m)	BED ORIENTATION	DISTANCE	FRACTURE FREQUENCY	STRIKE	DIP	INTER / INTRA	SURFACE	COMMENTS
0-1m	170/40	2	26	37	43			
		3		315	56			
		10		37	43			
		20		315	56			
		27		233	75			
		30		198	58			
		33		233	75			
		37		295	55			
		38		198	58			
		39		320	60			
		41		295	55			
		45		198	58			
		49		280	85			
		50		37	43			
		51		315	56			
		54		315	55			
		55		37	43			
		61		275	85			
		69		275	86			
		74		298	62			
80	270	85						
81	335	52						
86	55	52						
92	335	52						

		94		45	50
		95		265	85
1-2m	170/40	1	24	045	45
		3		325	45
		4		045	45
		7		271	71
		10		310	50
		14		045	50
		18		149	63
		23		70	75
		28		251	81
		32		251	81
		34		251	80
		42		250	79
		46		251	82
		55		249	82
		58		249	82
		58		50	42
		60		325	45
		66		250	80
		71		049	43
		71		325	45
		75		250	80
		78		125	75
		83		245	80
		93		315	45

Locality: 4c
GPS Coordinates:

Thrust System: M2
Structural Position: Forlimb
Scanline Number: 4-08
Lithological Unit: 7
Scanline Trend: 130
Thickness: 47-60
Date: 25/7-08

UNIT (m)	BED ORIENTATION	DISTANCE	FRACTURE FREQUENCY	STRIKE	DIP	INTER / INTRA	SURFACE	COMMENTS			
0-1m	350/43	12	7	230	42	ir	s	ca			
		30		178			r				
		50		085			s				
		62		150			r				
		79		170			ir		s		
		81		150			74		s		
		93		025			89		ir	s	
1-2m	350/43	13	8	210	55	ir	s	cojugate set			
		22		010			85		ir	s	cojugate set
		24		210			55		ir	s	
		31		091			78		ir	s	
		40		190			72		ir	s	
		51		190			72		ir	s	
		70		085			86			s	
2-3m	350/43	70	9	342	98		s				
		10		078			86			s	
		31		165			85		ia	r	
		45		195			60		ir	s	conjugate set
		53		350			73		ir	s	
		62		015			90		ia	s	
		68		195			80		ia	s	
		86		010			90		ia	s	
		97		153			76		ia	s	
		99		206			69		ir	s	

3-4m	350/43	15	8	222	66	s		
		30		180	72	s		
		40		180	72	s		
		41		195	40	ir	s	conjugate set
		42		001	79	s	s	conjugate set
		59		180	72	s		
		70		020	78	s		conjugate set
		82		170	74	s		
4-5m	350/43	1	10	080	78	s		
		25		180	51	s		
		30		215	64	s		
		45		186	61	s		
		50		186	61	s		
		53		180	45	s		
		70		081	76	s		
		75		180	45	s		
5-6m	350/43	88	7	180	45	s		
		98		180	45	s		
		11		180	56	s		
		12		180	45	s		
		20		175	55	s		
		30		195	64	s		
		46		201	57	s		
		73		190	69	s		
6-7m	350/43	99	7	150	49	s		
		2		200	55	s		
		10		095	79	r		
		25		225	53	s		
		43		095	79	r		
		43		180	59	s		
7-8m	350/43	91	12	095	79	r		
		96		180	53	s		
		1		095	79	r		
		5		180	49	s		
		5		095	79	r		
10	180	49	s					

		15		095	79	r	
		15		145	64	s	
		30		240	97	s	
		45		180	57	s	
		60		105	73	r	
		70		045	80	s	
		70		180	53	s	
		90		155	53	s	
8-9m	350/43	5	10	220	80	s	
		8		220	80	s	
		16		170	45	s	
		20		077	86	s	
		31		170	45	s	conjugate set
		45		170	45	s	conjugate set
		55		203	32	s	conjugate set
		68		203	32	s	conjugate set
		88		180	43	s	
		99		200	65	s	
9-10m	350/43	1	14	225	48	s	conjugate set
		5		200	65	s	conjugate set
		6		225	48	s	conjugate set
		10		200	65	s	conjugate set
		20		205	45	s	conjugate set
		28		207	85	s	conjugate set
		35		216	60	s	
		35		165	60	s	
		46		230	56	s	
		70		097	75	s	
		83		212	59	s	
		91		212	59	s	
		94		212	59	s	
		99		212	59	s	

Locality: 4c
GPS Coordinates:

Thrust System: M2
Structural Position: Forlimb
Scanline Number: 05-08
Lithological Unit: Vøringen
Scanline Trend: 130-310
Thickness: 14cm
Date: 25/7-08

UNIT (m)	BED ORIENTATION	DISTANCE	FRACTURE FREQUENCY	STRIKE	DIP	INTER / INTRA	SURFACE	COMMENTS
0-1m	013/33	1	3	245	67	ia	s	
		40		260	78	ir	s	
		80		225	67	ir	s	
1-2m	015/26	17	4	205	65	ia	r	
		33		205	65			
		65		035	79	ir	r	
2-3m	010/26	84	8	262	31	ir	r	
		6		045	82	ir	r	
		25		160	36	ia	r	
		65		155	86	ir	r	
		69		155	86	ir	r	
		70		140	81	ia	r	
3-4m	355/22	78	7	205	45	ir	s	
		82		205	45	ia	r	
		91		125	75	ia		
		7		335	85	ia		
		14		335	85	ir		
		20		255	74	ia	r	
		30		325	79	ia		
		48		280	62	ir		
4-5m	010/22	78	12	240	67	ir		
		92		222	50	ir	r	
		18		070	80	ir		
		22		070	80	ir		

28	165	40	ia
33	260	77	ia
50	113	76	ir
51	140	80	ir
57	170	85	ir
68	100	66	ir
75	340	87	ia
80	304	87	ir
85	265	80	ir
94	265	80	ir

Locality: 4c

GPS Coordinates:

Thrust System: M2

Structural Position: hinge

Scanline Number: 06-08

Lithological Unit: Vøringen

Scanline Trend: 117-297

Thickness: 15cm

Date: 25/7-08

UNIT (m)	BED ORIENTATION	DISTANCE	FRACTURE FREQUENCY	STRIKE	DIP	INTER / INTRA	SURFACE	COMMENTS
0-1m	031/11	1	28	013	85	ir	s	
		3		062	78	ir		
		5		105	81	ir		
		8		180	81	ir	r	
		12		125	89	ir		
		20		095	77	ir		
		20		202	72	ir		
		25		260	78	ir		
		26		260	77	ir		
		28		165	84	ir		
		30		260	78	ir		
		35		165	84	ir		
		37		260	78	ir		
		42		165	84	ir		
		45		260	78	ir		
		47		165	84	ir		
		50		165	84	ir		
		52		260	78	ir		
		55		165	84	ir		
		60		260	78	ir		
		65		145	82	ir		
		72		050	84	ir		
		79		270	78	ir		
		82		175	85	ir		

1-2m	040/12		86	175	85	ir	Lavvikla
			96	270	78	ir	
			97	270	78	ir	
			97	197	83	ir	
			1	165	84	ir	
			5	115	89	ir	
			10	003	72	ir	
			18	003	72	ir	
			20	003	72	ir	
			23	225	23	ir	
			28	225	23	ir	
			34	043	85	ir	
			35	225	23	ir	
			42	003	72	ir	
			45	165	84	ir	
			48	030	40	ir	
			52	030	63	ir	
			55	030	63	ir	
			81	148	79	ir	
			86	040	90	ia	
			89	040	90	ir	
	90	084	80	ia			
	94	145	89	ir			
	96	084	80	ia			
	99	145	89	ir			
2-3m	010/10		1	190	52	ir	
			5	285	86	ir	
			11	190	52	ir	
			12	285	86	ir	
			16	190	52	ir	
			20	285	86	ir	
			27	190	52	ir	
			29	190	52	ir	
			31	325	73	ir	
	33	190	52	ir			
	36	190	52	ir			

3-4m	025/10		40	190	52	ir	
			42	342	52	ir	
			57	214	56	ir	
			90	235	46	ir	
			8	045	50	ir	
			18	130	66	ir	
			22	242	85	ir	
			25	130	66	ir	
			32	355	65	ir	
			40	100	79	ir	
			50	200	55	ir	
			54	100	79	ir	
			66	112	79	ir	
			68	112	79	ir	
			70	112	79	ir	
		4-5m	020/08		75	100	79
	76			048	76	ir	
	76			112	79	ir	
	88			224	87	ir	
	90			105	90	ir	
	5			020	60	ir	
	22			006	30	ia	lavvinkla
	30			100	90	ir	
	53			316	80	ir	
	55			316	80	ir	
	57			316	80	ir	
	64			125	85	ir	
	68			020	82	ir	
	69			335	80	ir	
	70			277	70	ir	
	72			335	80	ir	
	75	003	82	ia			
	78	120	88	ir			
	85	003	82	ir			
	88	220	18	ia	lavvinkla		
	90	325	57	ir			

98

99

220

318

63

81

ir

ir

Locality: 4c

GPS Coordinates:

Thrust System: M2

Structural Position: Backlimb

Scanline Number: 7-08

Lithological Unit: Vøringen

Scanline Trend: 25/205

Thickness: 15cm

Date: 25/7-08

UNIT (m)	BED ORIENTATION	DISTANCE	FRACTURE FREQUENCY	STRIKE	DIP	INTER / INTRA	SURFACE	COMMENTS
0-1m	186/55	1	13	313	60	ia		
		4		106	63	ir		
		20		106	63	ia		
		35		104	75	ia		
		47		097	60	ir		
		49		106	63	ir		
		52		106	63	ir		
		55		097	60	ir		
		73		097	60	ir		
		76		323	60	ir		
		90		326	45	ir		
		95		286	90	ir		
		99		350	44	ir		
1-2m	190/60	25	10	350	44	ir		
		35		350	44	ir		
		37		273	90	ir		
		37		047	55	ir		
		57		318	56	ir		
		70		318	56	ir		
		80		318	56	ir		
		83		318	56	ir		
		88		318	56	ir		
90	040	47	ir					
2-3m	176/54	13	20	145	55	ir		

20	047	70	ir
21	145	55	ir
30	047	70	ir
30	050	73	ir
46	276	75	ir
55	300	45	ir
55	276	75	ir
61	300	45	ir
67	300	45	ir
70	276	75	ir
74	300	45	ir
78	300	45	ir
83	300	45	ir
88	300	45	ir
90	240	82	ir
91	300	45	ir
95	300	45	ir
99	300	45	ir
99	276	75	ir

Locality: 4c

GPS Coordinates:

Thrust System: M2

Structural Position: Backlimb above thrust

Scanline Number: 7-08b

Lithological Unit: Vøringen

Scanline Trend: 357-177

Thickness: 15cm

Date: 25/7-08

UNIT (m)	BED ORIENTATION	DISTANCE	FRACTURE FREQUENCY	STRIKE	DIP	INTER / INTRA	SURFACE	COMMENTS
0-1m	171/23	1	10	274	80	ir		
		5		274	80	ir		
		13		274	80	ia		
		13		355	73	ia		
		20		274	80	ir		
		26		235	67	ir		
		63		274	80	ir		
		75		274	80	ia		
		85		274	80	ir		
		97		250	63	ir		
1-2m	180/25	1	8	276	79	ir		
		44		274	81	ir		
		59		274	80	ir		
		59		350	66	ir		
		63		275	76	ir		
		73		275	76	ir		
		92		295	79	ir		
2-3m	185/26	92	7	005	71	ir		
		1		279	76	ir		
		2		353	68	ir		
		13		279	76	ir		
		25		279	76	ir		
		64		279	76	ir		
	90	279	76	ia				

3-4m	195/30	94	8	279	76	ir
		15		279	76	ir
		15		349	67	ir
		37		279	76	ir
		61		279	76	ir
		69		279	76	ir
		77		279	76	ir
		85		279	76	ir
4-5m	210/30	90	6	345	65	ir
		30		150	81	ir
		35		203	42	ir
		45		279	76	ir
		53		279	76	ir
		98		000	68	ir
	99	279	76	ir		

lavvinkla

Locality: 4c
GPS Coordinates: (58) 0482434 8717568

Thrust System: M2
Structural Position: Backlimb above thrust
Scanline Number: 08-08
Lithological Unit: Vøringen
Scanline Trend: 205-25
Thickness: 15cm
Date: 25/-08

UNIT (m)	BED ORIENTATION	DISTANCE	FRACTURE FREQUENCY	STRIKE	DIP	INTER / INTRA	SURFACE	COMMENTS
0-1m	180/39	5	7	170	85	ia		
		10		265	90	ir		
		23		265	90	ir		
		63		120	88	ir		
		73		090	88	ir		
		83		090	88	ir		
		87		004	60	ir		
1-2m	174/45	1	8	265	85	ir		
		14		265	85	ir		
		35		331	69	ir		
		41		265	85	ir		
		60		265	90	ia		
		70		160	88	ir		
		75		160	88	ir		
	83	355	60	ir				

Locality: 3g
 GPS Coordinates: (060) 0482029 8715430

Thrust System: M3
 Structural Position: Hinge
 Scanline Number: 9-08
 Lithological Unit: unit 3
 Scanline Trend: 220-40
 Thickness: 53cm
 Date: 26/7-08

UNIT (m)	BED ORIENTATION	DISTANCE	FRACTURE FREQUENCY	STRIKE	DIP	INTER / INTRA	SURFACE	COMMENTS
0-1m	164/42	5	18	310	67	ir		backlimb
		8		325	60	ir		
		9		290	78	ir		
		11		325	60	ir		
		13		325	60	ir		
		25		065	85	ir		
		26		335	74	ir		
		30		285	86	ir		
		39		285	86	ir		
		54		315	86	ir		
		60		315	86	ir		
		62		315	86	ir		
		70		325	80	ir	ss:(TP) 230/20	
		75		325	80	ir		
		77		325	80	ir		
		85		327	88	ir		
85	060	81	ir					
96	320	72	ir					
1-2m	153/03	1	19	323	86	ir		hinge
		5		080	45	ir	Lavvinkla	
		10		328	90	ir		
		11		328	90	ir		
		20		334	90	ir		
		30		300	25	ir	Lavvinkla	

		32		323	74	ir	
		37		323	74	ir	
		48		332	90	ir	
		57		328	90	ir	ss:(TP) 230/20
		64		328	90	ir	
		72		155	75	ir	
		73		155	75	ir	
		81		155	75	ir	
		82		173	36	ir	Lavvinkla
		87		148	80	ir	
		94		150	85	ir	
		98		333	85	ir	
		99		053	70	ir	
2-3m	328/30	3	10	340	90	ir	forlimb
		12		165	70	ir	
		30		165	70	ir	
		35		150	90	ir	
		40		150	90	ir	
		50		150	90	ir	
		50		045	85	ir	
		60		150	90	ir	
		80		150	90	ir	
		99		163	85	ir	